УДК 53

ББК 22.3

Д25

The 9th International Scientific Conference on Physics and Control
Proceedings of The 9th International Scientific Conference on Physics and Control – Moscow: LLC "Publishing House" Pero "", – 2019, – 328 p.

ISBN 978-5-00150-470-2

Proceedings of The 9th International Scientific Conference on Physics and Control contain abstracts of reports by scientists and specialists in the field of intelligent technologies, engineering education, research and design of mechatronic and robotic systems, complex networks, nonlinear dynamics, biosystems.

The conference was focused on the multidisciplinary topics of Physics and Control with emphasis on both theory and applications. The event was provided insights into actual problems and scientific issues, which determine the current state and future directions in modern nonlinear dynamics and control theory.

Conference materials are intended for a wide range of scientific and engineering workers, university professors, secondary special educational institutions, graduate students and students.

The conference and this publication have been supported by the Russian Foundation for Basic Research (project № 19-02-20035), City University of Hong Kong.

УДК 004.896
ББК 32.813

ISBN 978-5-00150-470-2

CONFERENCE ORGANISERS

CONFERENCE SPONSORS

Innopolis University, I

Universidad Politécnica de Madrid,
Centre for Biobedical Technology, Spain

ANO "Research Center
"Education. Quality. Industry""

Industry Union Neuronet

International Physics and Control Society (IPACS)

Institute of Problems of Mechanical Engineering,
Russian Academy of Sciences

Russian Foundation for Basic Research City University of Hong Kong

PROGRAMME COMMITTEE

Chair:
Prof. Alexander Hramov, Head of Neuroscience and Cognitive Technology Lab, Professor in Institute of Robotics (Innopolis University, Russia)

Co-Chair:
Prof. Alexander Pisarchik (Innopolis University, Russia; Technical University of Madrid, Spain)

Members:
Prof. Alexander Tormasov (Rector of Innopolis University, Russia)
Prof. Vadim Anishchenko (Saratov State University, Russia)
Prof. Claudio Altafini (Linkoping University, Sweden)
Prof. Fortunato Tito Arecchi (Instituto Nazionale di Ottica – CNR, Università Firenze, Italy)
Prof. Alex Arenas (Universidad Rovira I Virgili, Spain)
Prof. Kazuyuki Aihara (University of Tokyo, Japan)
Prof. Stefano Boccaletti (ISC-Institute for Complex Systems, Italy)
Prof. Igor Belykh (Georgia State University, USA)
Prof. Cyrille Bertelle (University of Le Havre, France)
Prof. Martin Berz (Michigan State University, USA)
Prof. Tommaso Calarco (Universität Ulm, Germany)
Prof. Qing-Jie Cao (Harbin Institute of Technology, China)
Prof. Sergej Celikovsky (Institute of Information Theory and Automation, Czech Republic)
Prof. Ricardo Chacòn (Universidad de Extremadura, Spain)
Prof. Syamal K. Dana (Jadavpur University, India)
Prof. Z.S. Duan (Peking University, China)
Dr. Alejandro Ricardo Femat Flores (IPICYT San Luis Potosì, México)
Prof. Ulrike Feudel (Carl con Ossietzky Universitat Oldenburg, Germany)
Dr. Tatyana Filippova (Russian Academy of Sciences, Russia)
Dr. Mattia Frasca (Università di Catania, Italy)
Prof. Jason Gallas (Universidade Federal da Paraíba, Brazil)
Prof. Maria Isabel Garcia Planas (Universitat Politècnica de Catalunya, Barcelona, Spain)
Prof. Celso Grebogi (University of Aberdeen, UK)
Prof. Jun Jiang (Xi'an Jiaotong University, China)
Prof. Viktor Kazantsev (Nijnij Novgorod State University, Russia)
Prof. Stefano Nolfi (Institute of Cognitive Sciences and Technologies, Italy)
Prof. Alexander Klimchik (Innopolis University, Russia)
Prof. Alexey Koronovskii (Vice-Rector for Research of Saratov State University, Russia)
Dr. Alexandra Kuznetsova (Universitaet Potsdam, Germany)
Prof. Grigory Osipov (Lobachevsky State University of Nizhni Novgorod, Russia)
Prof. Wei Lin (Fudan University, China)
Prof. Jinhu Lu (Chinese Academy of Sciences, China)
Dr. Annika Lüttjohann (Uniresity of Münster, Germany)
Prof. Elbert E. N. Macau (Instituto Nacional de Pesquisas Espaciais, Brazil) **Dr. Riccardo Meucci** (Instituto Nazionale di Ottica – CNR, Università Firenze, Italy) **Prof. Vladimir Nekorkin** (Institute of Applied Physics of Russian Academy of Sciences, Russia)
Prof. Dmitry Ovsyannikov (St. Petersburg State University, Russia)
Prof. Anatoly Pashkevich (Innopolis University, Russia)
Prof. Alexey Pavlov (Yuri Gagarin State Technical University of Saratov, Russia)

Prof. Alexey Porubov (Inst.Probl. Mechanical Engineering, RAS)
Prof. Mikhail Prokhorov (Saratov Branch of the Institute of Radio Engineering and Electronics of Russian Academy of Science, Russia)
Prof. Miguel A. F. Sanjuan (Universidad Rey Huan Carlos, Móstoles, Spain)
Dr. Somdatta Sinha (IISER Mohali, India)
Prof. Giancarlo Succi (Innopolis University, Russia)

Prof. Elena Surovyatkina (Space Research Institute, Russian Academy of Sciences, Moscow, Russia)

ORGANISING COMMITTEE

Chair: Prof. Iskander Bariev (Vice-Rector of Innopolis University, Russia) **Co-Chair:** Prof. Alexander Hramov (Innopolis University, Russia) **Conference secretary**: Prof. Semen Kurkin (Innopolis University, Russia)

Members:

CONTENTS

Andreev Aleksandr, Peregudova Olga, Sutyrkina Katherine ON GLOBAL TRAJECTORY TRACKING CONTROL OF A WHEELED MOBILE ROBOT ……………………………………………………………14

Andreev Aleksandr, Sutyrkina Katherine
ON THE CONTROL PROBLEM OF A TWO-LINK MANIPULATOR………18

Aung Tun Lin, Mikhailov Valeriy, Bazinenkov Alexey, Kazakov Alexander,

Kopylov Alexey, Tovmachenko Dmitry
STUDY OF AN ACTIVE VIBRATION ISOLATION DEVICE FOR THE NANOPOSITIONING BASED ON MAGNETORHEOLOGICAL ELASTOMERS……………………………………………………………………25

Barabash Nikita, Belykh Vladimir
GHOST ATTRACTORS IN THE NON-AUTONOMOUS BLINKING SYSTEMS….……………………………………………………………………2
9

Brister Barrett, Belykh Vladimir N., Belykh Igor
MULTISTABLE CLUSTER RHYTHMS IN NETWORKS OF COUPLED ROTATORS…………………………………………………………………..32

Cheng Yongdong, Jiang Jun
CONTROL METHODS TO ENHANCE POINTING ACCURACY OF AN ANTENNA SERVO SYSTEM ON A CARRIER UNDER LARGE DISTURBANCE.
………………………………………………………………….37

Chertovskih Roman, Khalil Nathalie T., Pereira Fernando Lobo OPTIMAL PATH PLANNING OF AUVS OPERATING IN FLOWS INFLUENCED BY TIDAL CURRENTS……………………………………….40

Chholak Parth, Pisarchik Alexander N., Kurkin Semen A., Maksimenko Vladimir A., Hramov Alexander E.
NEURONAL PATHWAY AND SIGNAL MODULATION FOR MOTOR COMMUNICATION…………………………………………………………….44

Chizhevsky V. N., Kavalenka S. A.
EFFECT OF OPTICAL FEEDBACK ON MULTISTABILITY IN A MULTIMODE VCSEL……………………………………………………...52

D'Huys Otti, Klinshov Vladimir V.
MODE HOPPING IN A PULSE-COUPLED OSCILLATOR WITH DELAYED FEEDBACK……………………………………………………………………57

Demenkov Maxim
ARDUINO-BASED INVESTIGATION OF HYSTERESIS IN POLYMER FLEX
SENSOR……………………………………………………………………….
60

Denisov Igor, Sonin Alexander

SEISMIC-ACOUSTIC SIGNAL GENERATION MODEL FROM FIBEROPTICAL MEASURING LINES FOR NEURAL-LIKE CLASSIFIER…63

Dmitrichev Aleksei, Nekorkin Vladimir
STRUCTURAL STABILITY OF CHIMERA STATES CLONING IN A LARGE NON-STATIONARY COUPLED TWO-LAYER MULTIPLEX NETWORK OF BISTABLE RELAXATION OSCILLATORS…………………………………...66

Eremin E. L., Shelenok E. A.
SIMULATION MODELING OF THE DECENTRALIZED ROBUST-PERIODIC CONTROL SYSTEM FOR MANIPULATOR WITH INPUT CONSTRAINTS…………………………………………………………….72

Erofeeva Victoria, Granichin Oleg, Len Irina
SPARSITY-PROMOTING SENSOR SELECTION IN MULTI-TARGET TRACKING PROBLEM…………………………………………………………78

Erofeeva Victoria, Galyamina Vasilisa, Grani Oleg, Gonta Kseniya, Leonova Anna, Pankov Vikentiy, Tursunova Munira, Ding Mingyue, Yuchi Ming, Fang Xiaoyue
DETECTION OF SPECIFIC AREAS WITH ULTRASOUND TOMOGRAPHY….………………………………………………………………84

Franovi´c Igor, Klinshov Vladimir
EMERGENCE OF COLLECTIVE OSCILLATIONS IN ASSEMBLIES OF STOCHASTIC ACTIVE ELEMENTS WITH COUPLING DELAY…………....90

Gaiko Valery A.
LIMIT CYCLES OF A TOPP SYSTEM…………………………………………96

Garc´ıa-Planas M. Isabel
ANALYZING CONTROLLABILITY AND OBSERVABILITY OF MULTI AGENT LINEAR SYSTEMS…………………………………………………...100

Gordleeva Susan, Kanakov Oleg, Zaikin Alexey

GARBAGE INDUCED MODEL OF INFLAMMAGING

PROPAGATION….104 8

Huerta-Cuellar Guillermo, Echenaus´ıa-Monroy & Jos´e Luis, Jaimes Re´ategui Rider, Garc´ıa-L´opez Juan Hugo, Gilardi-Vel´azquez & H´ector Eduardo
INTERMITTENCY AND HIDDEN FIXED POINTS INDUCED IN A BISTABLE MULTISCROLL ATTRACTOR BY MEANS OF STOCHASTIC MODULATION……………………………………………106

Iluhin Vladimir, Dubovitskih Vladimir, Mezentsev Dmitry WORKSPACE OF MANIPULATOR OF ROBOT AR600E…………………..111

Itami Teturo, Matsui Nobuyuki, Isokawa Teijiro
DISSIPATIVE SYSTEMS AS OPTIMAL CONTROL SYSTEMS WITH INPUT IN SPECIAL FORM OF FEEDBACK LAW…………………………………...115

Ivanchenko Mikhail, Krivonosov Mikhail, Jalan Sarika, Bacallini Maria Giulia, Franceschi Claudio
DOWN SYNDROME: FOOTPRINT IN PARENCLITIC NETWORKS OF DNA METHYLATION.
……………………………………………………………121

Jaimes-Reátegui Rider, Reyes-Estolano Juan M., García-López Juan H., Cuellar Guillermo Huerta, Gallegos Armando, Pisarchik Alexander N.
HINDMARSH-ROSE NEURON RESPONSE TO LASER STIMULATION…124

Kalyakulina Alena, Yusipov Igor, Vershinina Olga, Ivanchenko Mikhail, Franceschi Claudio
NONLINEARITY AND STOCHASTICITY OF AGE-RELATED SEX SPECIFIC METHYLATION CHANGES……………………………………128

Karavaev Anatoly, Kiselev Anton, Borovkova Ekaterina, Ishbulatov Yurii
DYNAMICS OF MATHEMATICAL MODEL OF CARDIO-VASCULAR SYSTEM…………………………………………………………………...

131

Karavaev Anatoly, Borovkova Ekaterina, Kiselev Anton, Runnova Anastasiya, Prokhorov Mikhail, Ponomarenko Vladimir, Hramov Alexander, Gridnev Vladimir, Bezruchko Boris
INTERACTIONS BETWEEN THE PROCESSES OF REGULATION OF THE CARDIOVASCULAR SYSTEM AND THE BRAIN STRUCTURES………...133

Karavaev Anatoly, Kiselev Anton, Borovkova Ekaterina, Popova Yulia, Gridnev Vladimir, Posnenkova Olga
DYNAMICS OF LOW-FREQUENCY COMPONENTS OF PHOTOPLETHYSMOGRAM SIGNALS IN

HYPERTENSION……………...137 9

Kashchenko Alexandra
DEPENDENCE OF DYNAMICS OF TWO DELAYED GENERATORS ON THE STRENGTH OF COUPLING……………………………………………..139

Kashchenko Ilia
THE DYNAMICS OF LOGISTIC EQUATION WITH TWO DELAYS………142

Khantuleva Tatyana A., Shalymov Dmitry S.
SG-PRINCIPLE AND SPECIAL FEATURES OF THE SHORT-DURATION PROCESSES…………………………………………………………….....14
5

Kingston S. Leo, Thamilmaran K., Kapitaniak Tomasz
SUPERTRANSIENT CHAOS IN FORCED LIE´NARD SYSTEM…………...150

Kiselev Oleg
STABILIZATION OF INVERTED WHEELED PENDULUM………………..155

Konyukhov Ivan, Konyukhov Vladimir
CYBER-PHYSICAL SYSTEM FOR CONTROL THE HEAT AND MASS TRANSFER IN THE OIL RESERVOIR AND PRODUCING PUMPING WELL…..……………………………………………………………..…15
6

Krivonosov Mikhail, Ivanchenko Mikhail, Jalan Sarika, Bacallini Maria Giulia, Franceschi Claudio
PARENCLITIC ANALYSIS OF HIGH-DIMENSIONALITY DNA METHYLATION DATA……………………………………………………..164

Kuznetsov Nikolay V., Mokaev Timur N., Prasad Awadhesh, Shrimali Manish Dev, Roy Binoy Krishna
HIDDEN ATTRACTORS AND LYAPUNOV DIMENSION…………………167

Lacerda Juliana, Freitas Celso, Macau Elbert
SECOND ORDER KURAMOTO NETWORKS: TOPOLOGIES THAT FAVOR SYNCHRONIZATION………………………………………………………169

Li Chunbiao, Lu Tianai
A CHAOTIC SYSTEM: FROM CONDITIONAL SYMMETRY TO SYMMETRY……………………………………………………………………172

Lynnyk Volodymyr, Reha´k Branislav, Cˇ elikovsky Sergej ON APPLICABILITY OF AUXILIARY SYSTEM APPROACH IN COMPLEX NETWORK WITH RING
TOPOLOGY_……………………………………176

Makeeva Anastasiya, Dmitrichev Aleksei, Nekorkin Vladimir TORUS CANARDS IN THE ENSEMBLE SYNAPTICALLY RELATED NEURONS FITZHUGH-NAGUMO……………………………………………182

Makovkin Sergey, Ivanchenko Mikhail, Zaikin Alexey, Jalan Sarika
INVESTIGATING MULTIPLEX MODELS OF NEURON-GLIAL SYSTEMS: SMALL-WORLD TOPOLOGY AND INHIBITORY COUPLING……………184

Mari˜no I.P., Lacasa L., M´ıguez J., Nicosia V., Rolda´n E´ ., Lisica A., Grill S.W., G´omez-Garde˜nes J.
IDENTIFYING THE HIDDEN MULTIPLEX ARCHITECTURE OF BIOLOGICAL
PROCESSES……………………………………………………187

Nazarenko Tatiana, Krivonosov Mikhail, Zaikin Alexey
ANALYSIS OF LONGITUDINAL HIGH-DIMENSIONAL MEDICAL DATA WITH PARENCLITIC
NETWORKS………………………………………..192

Oshchepkov Alexander

ROBUST STABILIZATION SYSTEM OF QUBIT BASED ON SPIN ½ IN A MAGNETIC FIELD……………………………………………………………..194

Parsheva Elizaveta, Ternovaja Galina
ROBUST OUTPUT CONTROL OF MULTI-AGENT PLANTS WITH STATE DELAY……………………………………………………………………..200

Petrenko Pavel, Samsonyuk Olga, Staritsyn Maxim
A NOTE ON DIFFERENTIAL-ALGEBRAIC SYSTEMS WITH IMPULSIVE AND HYSTERESIS PHENOMENA……………………………………...204

Petukhov Alexandr
MODELING OF THRESHOLD EFFECTS IN SOCIAL SYSTEMS BASED ON NONLINEAR DYNAMICS………………………………………………….…210

Plotnikov Sergei A., Belov Dmitry R.
SIMULATION OF GAMMA RHYTHM AND ITS CORRELATION WITH LOW-FREQUENCY SIGNALS…………………………………….……..214

Ponomarenko Vladimir I., Karavaev Anatoly S., Ishbulatov Yury M., Kiselev Anton R., Borovkova Ekaterina I., Skazkina Victoriya V., Prokhorov Mikhail D.
INTERACTION OF SLOW OSCILLATORY PROCESSES IN THE HUMAN CARDIOVASCULAR SYSTEM AND THEIR MATHEMATICAL MODELING……………………………………………………………..……219

Prokhorov Mikhail, Kulminskiy Danil, Ponomarenko Vladimir, Hramov Alexander
CONTROL OF SYNCHRONIZATION IN NETWORKS OF NONIDENTICAL NEURONLIKE OSCILLATORS……………………………………….……222

Reh´ak Branisla, Lynnyk Volodymyr
DESIGN OF A NONLINEAR OBSERVER USING THE FINITE ELEMENT METHOD WITH APPLICATION TO A BIOLOGICAL SYSTEM………..…224

Romero-Mel´endez Cutberto, Gonz´alez-Santos Leopoldo
STOCHASTIC OPTIMAL CONTROL APPLIED TO A TWO-LEVEL QUANTUM SYSTEM……………………………………………………….……230

Saha Suman, Bairagi Nandadulal, Dana Syamal Kumar
EMERGENCE OF AMPLITUDE MEDIATED CHIMERA STATES IN ECOLOGICAL NETWORK UNDER WEIGHTED MEAN-FIELD

DISPERSAL……………………………………………………………………236

Sawicki Jakub, Omelchenko Iryna, Zakharova Anna, Sch¨oll Eckehard
DELAY-CONTROLLED RELAY SYNCHRONIZATION IN MULTIPLEX NETWORKS…………………………………………………………………..……24
0

Sedova Natalia
ON UNIFORM ASYMPTOTIC STABILITY FOR NONLINEAR INTEGRO DIFFERENTIAL EQUATIONS OF VOLTERRA TYPE………………………246

Semenova Nadezhda, Zakharova Anna
NOISE INDUCED REGIMES IN NETWORK OF EXCITABLE ELEMENTS. TOPOLOGY, NOISE AND TIME-DELAYED FEEDBACK…………………251

Sergeenko Anna, Yakunina Maria, Granichin Oleg
HAMILTONIAN PATH PROBLEM: THE TIME CONSUMPTION COMPARISON OF DNA COMPUTING AND BRANCH AND BOUND METHOD…………………………………………………………………..256

Shamolin Maxim V.
MATHEMATICAL MODELING OF THE SPATIAL ACTION OF A MEDIUM ON A BODY OF CONICAL FORM……………………………………………261

Simonyan Margarita, Gridnev Vladimir, Karavaev Anatoly, Bezruchko Boris, Ishbulatov Yuri, Kiselev Anton, Skazkina Viktoriia
DIRECTIONAL COUPLING BETWEEN THE LOWFREQUENCY CONTROL OF HEART RATE AND VESSELS TONE IN MYOCARDIAL INFARCTION PATIENTS ……………………………………………………………..….266

Smirnova Vera B., Proskurnikov Anton V., Utina Natalia V. THE PROBLEM OF CYCLE–SLIPPING FOR SYNCHRONIZATION SYSTEMS WITH EXTERNAL DISTURBANCES……………………………270

Sorokin Stepan, Staritsyn Maxim
NUMERICAL ALGORITHMS FOR STATE-LINEAR OPTIMAL IMPULSIVE CONTROL PROBLEMS BASED ON FEEDBACK NECESSARY OPTIMALITY CONDITIONS…………………………………………….………276

Starinova Olga, Chernyakina Irina
THE EFFECTS OF SURFACE DEGRADATION ON BALLISTICS OF SOLAR SAIL'S MISSION TO THE SUN……………………………………….……281

Tomashevich Stanislav
METHOD OF CONTROLS SYNTHESIS FOR MULTIAGENT SYSTEM WITH TIME-VARYING DELAYS IN INFORMATION CHANNELS……………....286

Velmisov Petr A., Ankilov Andrey V.
INVESTIGATION OF DYNAMICS AND STABILITY OF ELASTIC ELEMENTS OF VIBRATION DEVICES……………………………………..292

Vershinina Olga, Denisov Sergey, Ivanchenko Mikhail
QUASI-STATIONARY OSCILLATIONS IN GAME-DRIVEN EVOLUTIONARY DYNAMICS…………………………………………..…298

Vorochaeva Lyudmila, Yatsun Andrey, Savin Sergei, Repkin Anton
DEVELOPMENT OF THE MOTION CORRECTION SYSTEM OF THE CRAWLING ROBOT LINK ON THE SURFACE WITH OBSTACLES……...300

Yusipov Igor, Ivanchenko Mikhail, Denysov Sergiy
NEIMARK-SACKER BIFURCATION IN PERIODICALLY MODULATED OPEN QUANTUM
DIMER…………………………………………………….306

Zakharov Denis, Krupa Martin, Gutkin Boris
MODULATION OF SYNCHRONOUS GAMMA RHYTHM CLUSTERS…...309

Kurkin Semen
INVESTIGATION OF COMPLEX NONLINEAR PROCESSES IN SYSTEMS WITH INTENSE RELATIVISTIC ELECTRON BEAMS.................................313

The program of The 9th International Scientific Conference on Physics and Control (PhysCon2019)

September 9, Monday		
9.00-9.30 – Opening of the Conference **Room 107**		
Time, Room	**Speaker**	**Title of talk**

9.30-10.15, **Room 107**	**Prof. Jürgen Kurths** *Humboldt University, Berlin, Germany*	Predictability of extreme climate events via a complex network approach
10.15-11.00, **Room 107**	**Prof. Claudio Franceschi** *IRCCS Institute of Neurological Sciences Bologna and University of Bologna, Italy*	Systems biology of ageing: dynamics, nonlinearity, and stochasticity
11:00-11:30	*Coffee Break*	
11.30-12.15, **Room 107**	**Prof. Stefano Boccaletti** *ISC-Institute for Complex Systems, Italy*	Collective states of networked phase oscillators: explosive synchronization, dynamically interdependent networks and Bellerophon states
12:15-13:00, Room 307	**Section 1a "Dynamics and Control of Systems with Time Delays"** *Dr. Anna Zakharova; Dr. Vladimir Klinshov*	
12:15-12:30	J. Sawicki, I. Omelchenko, A. Zakharova, E. Schöll	Delay-controlled relay synchronization in multiplex networks
12:30-12:45	S. Yanchuk, S. Ruschel, J. Sieber, M.Wolfrum	Temporal dissipative solitons in time-delay feedback systems
12:45-13:00	S. Tomashevich	**Contributed Talk** Method of controls synthesis for multiagent system with time-varying delays in information channels
12:15-13:15, Room 308	**Section 2a "Synchronization of Regulatory Processes in the Cardiovascular and Neuronal Systems"** *Prof. Mikhail Prokhorov*	
12:15-12:30	M.D. Prokhorov, D.D. Kulminskiy, V.I. Ponomarenko	Controlling synchronization in networks of nonidentical neuronlike oscillators
12:30-12:45	V.I. Ponomarenko, A.S. Karavaev, Yu.M. Ishbulatov, A.R. Kiselev, E.I. Borovkova, V.V. Skazkina, M.D. Prokhorov	Interaction of slow oscillatory processes in the human cardiovascular system and their mathematical modeling
12:45-13:00	A. Karavaev, E. Borovkova, A. Kiselev, A. Runnova, V. Prokhorov,	Interactions between the processes of regulation of the cardiovascular system and

	V. Ponomarenko, A. Hramov,	the brain structures

	V. Gridnev, B. Bezruchko	
13:00-13:15	A. Karavaev, A. Kiselev, E. Borovkova, Y. Popova, V. Gridnev, O. Posnenkova	Dynamics of low-frequency components of photoplethysmogram signals in hypertension
12:15-13:30, Room 107	**Section 3a "Chaotic and Complex Dynamics and its Applications"** *Prof. Syamal Dana*	
12:15-12:30	A. Mishra, C. Hens, S. Dana	Chimeralike states in a network of oscillators under attractive and repulsive global coupling
12:30-12:45	S. Saha, N. Bairagi, S.K. Dana	Emergence of amplitude mediated chimera states in ecological network under weighted mean-field dispersal
12:45-13:00	V.A. Gaiko	Limit cycles of a Topp system
13:00-13:15	N.V. Kuznetsov, T.N. Mokaev, A. Prasad, M.D. Shrimali, B.K. Roy	Hidden attractors and Lyapunov dimension
13:15-13:30	V.N. Chizhevsky, S.A. Kavalenka	Effect of optical feedback on multistability in a multimode VCSEL
12:15-13:45, Room 320	**Section 11a "Dynamics of Complex Networks and their Application in Intellectual Robotics" (DCNAIR)** *Dr. Nikita Frolov*	
12:15-12:25	V.V. Skazkina, E.N. Mureeva, A.S. Karavaev, A.R. Kiselev, E.I. Borovkova, O.S. Panina, Yu.M. Ishbulatov, Y.V. Popova	Choosing parameters for the analysis of synchronization of the autonomic regulatory contours of blood circulation in newborns
12:25-12:35	V.V. Skazkina, Yu.M. Ishbulatov, E.I. Borovkova, B.P. Bezruchko, A.R. Kiselev, A.S. Karavaev	Slow trends in the degree of synchronization of the elements of autonomous control of blood circulation in healthy subjects
12:35-12:45	E.I. Borovkova, Yu.M. Ishbulatov, A.R. Kiselev, A.V. Tankanag, G.V. Krasnikov, A.S. Karavaev	Synchronization of the process of autonomous regulation of blood circulation with low-frequency components of the laser Doppler flowmetry signal
12:45-12:55	E.I. Borovkova, E.P. Chernets, Yu.M. Ishbulatov, V.V. Skazkina, A.S. Karavaev	Experimental observation of Arnold tongues in the analysis of the signal from contour of the autonomous regulation of heart rate and respiration

12:55-13:05	Yu.M. Ishbulatov, E.I. Borovkova, A.S. Karavaev, A.R. Kiselev, B.P. Bezruchko	Comparing methods for extraction of autonomic control signals from electrocardiogramm
13:05-13:15	E.V. Navrotskaya, M.V. Sinkin, A.N. Khramkov, D.M. Yezhov, B.P. Bezruchko	Development of a method for coupling detection based on the phase dynamics modeling for analyzing EEG rhythms during an epileptic seizure in patients with a reduced level of consciousness

13:15-13:25	A. Badarin	Development of a digital software platform for the study of nonlinear dynamics of electronic systems
13:25-13:35	S. Kurkin	Investigation of complex nonlinear processes in systems with intense relativistic electron beams
13:35-13:45	V.B. Baiburin, A.S. Rozov	Poisson equation numerical solution method based on bidirectional multiple passage of grid cells and parallel computations
12:15-13:55, Room 305	**Section 11b "Dynamics of Complex Networks and their Application in Intellectual Robotics" (DCNAIR)** *Prof. Semen Kurkin*	
12:15-12:25	A.A. Grishchenko, T.M. Medvedeva, C.M. van Rijn, M.V.Sysoeva, I.V. Sysoev	Application of directed connectivity measures for identifying the evolution of the interaction structure in WAG/Rij rats brain at absence epilepsy
12:25-12:35	V. Khorev, E. Borovkova, Yu. Ishbulatov, V. Gridnev, A. Karavaev	Asymmetry of coupling between the P3 and P4 electroencephalographic leads during the motions
12:35-12:45	A.V. Kochetkov, D.R. Malakhov, O.V. Zakharov	Optimization approach for inverse kinematic problem for manipulator with redundant degrees of freedom
12:45-12:55	A.V. Kochetkov, P.M. Salov, O.V. Zakharov	Route optimization in measuring surfaces on coordinate measuring machines
12:55-13:05	E. Pitsik, N. Frolov	Time-frequency and recurrence quantification analysis detect limb

		movement execution from EEG data
13:05-13:15	A.R. Miftahova, A.E. Hramov	Reccurence plot analysis of functional brain connectivity during bistable visual perception
13:15-13:25	A. Andreev, A. Pisarchik	Modeling of a brain neuronal network under visual stimulation
13:25-13:35	A. Andreev, V. Makarov, A. Balanov, A. Hramov	Chaos and hyperchaos in a chain of coupled Rydberg atoms
13:35-13:45	O.N. Pavlova, N.M. Kupriyashkina, A.N. Pavlov	Characterization of intermittent dynamics from experimental data with DFA
13:45-13:55	A. Kuc, V. Nedaivozov	Influence of the sensory information ambiguity on the brain state during the decision-making task
13.15-14.45	*Lunch*	
14:45-15:45, Room 307	**Section 4a "Interdisciplinary Issues of Control"** *Prof. Alexander Hramov; Prof. Alexander Pisarchik*	
14:45-		**Invited Talk**

15:15	**Prof. Eugene Postnikov** *Kursk State University, Kursk, Russia*	Quantitative thermodynamics of liquids: a fluctuational approach to the practical predicting liquids' properties under high pressures
15:15-15:30	A. Oshchepkov	Robust stabilization system of qubit based on spin ½ in a magnetic field
15:30-15:45	Tun Lin Aung, V. Mikhailov, A. Bazinenkov, A. Kopylov, D. Tovmachenko	Study of an active vibration isolation device for the nanopositioning based on MR elastomers
14:45-15:30, Room 308	**Section 2b "Synchronization of Regulatory Processes in the Cardiovascular and Neuronal Systems"** *Prof. Mikhail Prokhorov*	
14:45-15:00	M.A. Simonyan, A.S. Karavaev, Y.M. Ishbulatov, V.V. Skazkina, V.I. Gridnev, B.P. Bezruchko, A.R. Kiselev	Directional coupling between the low frequency control of heart rate and vessels tone in myocardial infarction patients

15:00- 15:15	S. Salem, V. Tuchin	Theoretical study for a mixture from magnetic microcapsule suspensions and blood under magnetic field effect
15:15- 15:30	S. Salem, V. Tuchin	Numerical simulation for blood flow in a tube under magnetic field effect
14:45- 15:45, Room 320	**Section 5a "Robotics, Mechatronics and Control"** *Dr. Alexandr Klimchik*	
14:45- 15:00	L. Vorochaeva, A. Yatsun, S. Savin, A. Repkin	Development of the motion correction system of the crawling robot link on the surface with obstacles
15:00- 15:15	V. Erofeeva, O. Granichin, I. Len	Sparsity-promoting sensor selection in multi-target tracking problem
15:15- 15:30	E. L. Eremin, E. A. Shelenok	Simulation modeling of the decentralized robust-periodic control system for manipulator with input constraints
15:30- 15:45	A. Andreev, K. Sutyrkina	On the control problem of a two-link manipulator
14:45- 15:45, Room 305	**Section 11c "Dynamics of Complex Networks and their Application in Intellectual Robotics" (DCNAIR)** *Dr. Vladimir Maksimenko*	
14:45- 14:55	N. Frolov, A. Hramov	**Invited Talk** Multilayer perceptron reveals functional connectivity structure in thalamo-cortical brain network
14:55- 15:05	A.K. Alimuradov, A.Yu. Tychkov, P.P. Churakov	A novel approach to speech signal segmentation based on empirical mode decomposition to assess human psycho emotional state
15:05- 15:15	A. Tychkov, A. Alimuradov, P. Churakov	The empirical mode decomposition for ECG signal preprocessing
15:15- 15:25	A. Petukhov	Modeling the distortions of public opinion under conditions of external influence using differential stochastic equations
15:25- 15:35	A.K. Alimuradov, A.Yu. Tychkov, P.P. Churakov	A method for noise-robust speech signal processing to assess human psycho emotional state

15:35-15:45	V. Khorev	Mean phase coherence modified for piecewise constant phase difference data
September 10, Tuesday		
9.00-9.45, **Room 107**	**Prof. Vladimir Nekorkin** *Inst. Of Appl. Phys., Nizhny Novgorod, Russia*	Dynamics of oscillatory networks: from simple to complex links
9.45-10.30, **Room 107**	**Prof. Alexander Fradkov** *Inst. for Problems of Mech. Eng., St. Petersburg, Russia*	Cybernetical physics and cyber-physical systems
10:30-11:00	*Coffee Break*	
11.00-11.45, **Room 107**	**Prof. Ulrike Feudel** *Carl von Ossietzky Universität Oldenburg, Oldenburg, Germany*	Tipping phenomena and resilience: two sides of the same coin?
11:45-12:45, **Room 107**	**Prof. Eugene Postnikov** *Kursk State University, Kursk, Russia*	Spectral and wavelet approaches for revealing state transitions from individual trajectories
12.45-14.00	*Lunch*	
14:00-14:15, **Room 107**	**Dr. Vasiliy Kuznetsov,** *Goethe-Institut, Moscow, Russia*	Philosophical Aspects of Artificial Intelligence
14.15-14.45, **Room 107**	**Prof. Leonid Savin,** **Prof. Alexey Kornaev** *Orel State University, Orel, Russia*	Application of machine learning to modeling of nonlinear hydromechanical systems
14.45-15.15, **Room 107**	**Prof. Yury Poduraev** *Moscow State University of Technology "STANKIN", Moscow, Russia*	Intellectual collaborative robotics in medicine: problems and solutions
September 11, Wednesday		
9.00-9.45, **Room 107**	**Prof. Eckehard Schöll** *Technische Universität, Berlin, Germany*	Partial synchronization patterns in complex networks - interplay of dynamics, time delay, and network topology

9.45- 10.30, **Room 107**	**Dr. Annika Lüttjohann** *University of Münster, Münster, Germany*	Development of brain computer interfaces for the interruption and prevention of epileptic seizures
10:30- 11:00	*Coffee Break*	
11:00- 12:45, Room 307	**Section 1b "Dynamics and Control of Systems with Time Delays"** *Dr. Anna Zakharova; Dr. Vladimir Klinshov*	
11:00- 11:15	I. Franović and V. Klinshov	Emergence of collective oscillations in assemblies of stochastic active elements with coupling delay
11:15- 11:30	O. D'Huys, V.V. Klinshov	Mode hopping in a pulse-coupled oscillator with delayed feedback
11:30- 11:45	A. Karavaev, A. Kiselev, E. Borovkova, Y. Ishbulatov	Dynamics of mathematical model of cardio vascular system
11:45- 12:00	I. Kashchenko	The dynamics of logistic equation with two delays
12:15- 12:30	A. Kashchenko	**Contributed Talk** Dependence of dynamics of two delayed generators on the strength of coupling
12:30- 12:45	N. Semenova, A. Zakharova	Noise induced regimes in network of excitable elements. Topology, noise and time-delayed feedback
11:00- 13:00, Room 308	**Section 3b "Chaotic and Complex Dynamics and its Applications"** *Prof. Syamal Dana*	
11:00- 11:15	R. Jaimes-Reátegui, J.M. Reyes Estolano, J.H. García-López, G. Huerta Cuellar, A. Gallegos, A.N. Pisarchik	Hindmarsh-Rose neuron response to laser stimulation
11:15- 11:30	G. Huerta-Cuellar, J.L. Echenausía Monroy, R. Jaimes-Reátegui, J.H. García-López, H. E. Gilardi Velázquez	Intermittency and hidden fixed points induced in a bistable multiscroll attractor by means of stochastic modulation
11:30-	S.N. Chowdhury, D. Ghosh, C. Hens	Optimal Frustration in complex networks

11:45		
11:45-12:00	A.Y. Petukhov	Modeling of threshold effects in social systems based on nonlinear dynamics
12:00-12:15	P. Khanra, P. Kundu, C. Hens, P. Pal	Explosive synchronization in adaptive complex networks with phase-frustration
12:15-12:30	T. Kapitaniak	Traveling chimera states for coupled
12:30-12:45	S.L. Kingston, K. Thamilmaran, T. Kapitaniak	Supertransient chaos in forced Liénard system
12:45-	J. Lacerda, C. Freitas, E. Macau	Second order Kuramoto networks:

13:00		topologies that favor synchronization
11:00-13:15, Room 421	**Section 6 "Brain-Computer Interfaces"** *Dr. Annika Lütjohann*	
11:00-11:30	**Prof. Mikhail Lebedev** *Higher School of Economics, Moscow, Russia* *Duke University, Durham, USA*	**Invited Talk** Expansion of brain functions and neurorehabilitation using neurocomputer interfaces
11:30-11:45	P. Chholak, A.N. Pisarchik, S.A. Kurkin, V.A. Maksimenko, A.E. Hramov	**Invited Talk** Phase-amplitude coupling between mu- and gamma-waves to carry motor commands
11:45-12:00	V. Maksimenko, V. Grubov	Cognitive interaction during a collaborative attentional task
12:00-12:15	V. Grubov, V. Maksimenko, V. Makarov	Features of brain activity in children during cognitive tasks of different types
12:15-12:30	V. Grubov, N. Frolov, E. Pitsik, A. Badarin	Features of real and imaginary motor activity on EEG and fNIRS signals for neurorehabilitation
12:30-12:45	E. Pitsik, N. Frolov, A. Hramov	Network analysis of brain activity during real motor actions execution using recurrence-based measure of dependence

12:45-13:00	A. Hramov, A. Kiselev, N. Schykovskii	Post-stroke rehabilitation with the help of brain-computer interface
13:00-13:15	A. Hramov, A. Pisarchik	Kinesthetic and visual modes of imaginary movement: MEG studies for BCI development
11:00-12:45, Room 305	**Section 7a "Complex Networks and Biosystems"** *Prof. Mikhail Ivanchenko*	
11:00-11:15	S. Gordleeva, O. Kanakov, A. Zaikin	Garbage induced model of inflammation propagation
11:15-11:30	M. Ivanchenko, C. Franceschi	DNA methylation in aging: a complex system
11:30-11:45	A. Kalyakulina, I. Yusipov, O. Vershinina, M. Ivanchenko, C. Franceschi	Nonlinearity and stochasticity of age related sex-specific methylation changes
11:45-12:00	V. Lynnyk, B. Rehak, S. Celikovsky	On applicability of auxiliary system approach in complex network with ring topology
12:00-12:15	A. Dmitrichev, V. Nekorkin	Structural stability of chimera states cloning in a large non-stationary coupled two-layer multiplex network of bistable relaxation oscillators
12:15-12:30	B. Rehak, V. Lynnyk	Design of a nonlinear observer using the finite element method with application to a biological system

12:30-12:45	B. Brister, V.N. Belykh, I. Belykh	Multistable cluster rhythms in networks of coupled rotators
11:00-13:40, Room 107	**Section 11d "Dynamics of Complex Networks and their Application in Intellectual Robotics" (DCNAIR)** *Prof. Vladimir Ponomarenko*	
11:00-11:10	A. Kornaev, R. Zaretsky, S. Egorov	Simulation of deep learning control systems to reduce energy loses due to vibration and friction in rotor bearings
11:10-11:20	M.V. Bobyr, A.S. Yakushev, N.A. Milostnaya	Three-coordinate definition of color mark and distance to objects according to stereo image

11:20-11:30	N. Fadeeva, A. Gulai, S. Astakhov	Amplitude-phase dynamics of the three mode cross-coupled generator
11:30-11:40	D. Artyukhov, I. Artyukhov, V. Alekseev, I. Burmistrov	Using thermoelectrics for power supplying of wireless sensors network
11:40-11:50	A. Makashov	The network layer model of the wireless sensor network acting under the influence of interferences
11:50-12:00	A. Kirpichnikov, A. Titovtsev	Practical recommendations on the application of Markov queuing models with a restricted queue
12:00-12:10	V.A.-jr. Krysko, T.V. Yakovleva, V.A. Krysko	Theory of contact interaction of inhomogeneous beam-lamellar nanostructures taking into account the connectivity of the temperature and deformation fields
12:10-12:20	I.V. Papkova, A.V. Krysko, E.Yu. Krylova	Mathematical modeling of NEMS elements in the form of flexible round plates under the Casimir's force action
12:20-12:30	E.Yu. Krylova, I.V. Papkova, O.A. Saltykova, V.A. Krysko	Mathematical modeling of the behavior of flexible micropolar mesh cylindrical panels with two sets of mutually orthogonal rods
12:30-12:40	O.A. Saltykova, V.A. Krysko	Nonlinear dynamics of a flexible closed cylindrical size-dependent shell under the action of a band load
12:40-12:50	M. Bolotov, T. Levanova, L. Smirnov, A. Pikovsky	Dynamics of disordered heterogeneous chains of phase oscillators
12:50-13:00	A.M. Vaskovsky, M.S. Chvanova	Designing the neural network for personalization of food products for persons with genetic president of diabetic sugar
13:00-13:10	A. Kuc, V. Maksimenko	Spatio-temporal cortical activity during a visual task accomplishing
13:10-13:20	S. Kurkin, P. Chholak, V. Maksimenko, A. Pisarchik	Machine learning approaches for classification of imaginary movement type by MEG data for neurorehabilitation
13:20-	A. Badarin	The control of the dynamics of intense electron beams coupled through a common

13:30		field
13:30-13:40	S. Kurkin, V. Maksimenko, E. Pitsik	Approaches for the improvement of motor related patterns classification in EEG signals
13.00-14.30	*Lunch*	
14:30-16:15, Room 307	**Section 5b "Robotics, Mechatronics and Control"** *Dr. Alexandr Klimchik*	
14:30-14:45	O. Kiselev	Stabilization of inverted wheeled pendulum
14:45-15:00	Teturo Itami, Nobuyuki Matsui, Teijiro Isokawa	Dissipative systems as optimal control systems with input in special form of feedback law
15:00-15:15	V. Iluhin, V. Dubovitskih, D. Mezentsev	Workspace of manipulator of robot AR600E
15:15-15:30	V.A. Serov, E.M. Voronov, A.B. Borisov, D.A. Kozlov	Multi-criteria neuro-evolutionary synthesis of the combined trajectory parameters adaptation laws for the unmanned aerial vehicle stabilization system
15:30-15:45	S.A. Kochetkov, A.S. Antipov, S.A. Krasnova	Stabilization of the convey-crane position under the conditions of uncertainty
15:45-16:00	E. Parsheva, G. Ternovaja	Robust output control of multi-agent plants with state delay
16:00-16:15	M. Demenkov	Arduino-based investigation of hysteresis in polymer flex sensor
14:30-16:45, Room 107	**Section 3c "Chaotic and Complex Dynamics and its Applications"** *Prof. Syamal Dana*	
14:30-14:45	P. Pal, M. Ghosh	First order transition in rotating magnetoconvection
14:45-15:00	T.A. Khantuleva, D.S. Shalymov	SG-principle and special features of the short-duration processes
15:00-	N. Barabash, V. Belykh	Ghost attractors in the non-autonomous blinking systems

15:15		
15:15-15:30	V.B. Smirnova, A.V. Proskurnikov, N.V. Utina	The problem of cycle-slipping for synchronization systems with external disturbances
15:30-15:45	I. Denisov, A. Sonin	Seismic-acoustic signal generation model from fiber-optical measuring lines for neural-like classifier
15:45-16:00	I. Yusipov, M. Ivanchenko, S. Denysov	Neimark-sacker bifurcation in periodically modulated open quantum dimer
16:00-	Chunbiao Li; Tianai Lu	A chaotic system: from conditional symmetry to symmetry

16:15		
16:15-16:30	P. Petrenko, O. Samsonyuk, M. Staritsyn	A note on differential-algebraic systems with impulsive and hysteresis phenomena
16:30-16:45	M.V. Shamolin	Mathematical modeling of the spatial action of a medium on a body of conical form
14:30-16:30, Room 308	**Section 4b "Interdisciplinary Issues of Control"** *Prof. Alexander Hramov; Prof. Alexander Pisarchik*	
14:30-14:45	Yongdong Cheng, Jun Jiang	Control methods to enhance pointing accuracy of an antenna servo system on a carrier under large disturbance
14:45-15:00	M. Isabel Garcia-Planas	Analyzing controllability and observability of multi-agent linear systems
15:00-15:15	A. Chanes Espigares, M. Isabel Garcia-Planas	Exact controllability of linear Hamiltonian control systems
15:15-15:30	I. Halperin, G. Agranovich, Yu. Ribakov	Implementation of Krotov's method for a type of constrained bilinear quadratic optimization problem
15:30-15:45	V. Serov, E. Voronov, A. Erohin	Coordinated stable-effective compromise based hierarchical game model of system ecological safety level prediction under anthropogenic impact

15:45-16:00	C. Romero-Meléndez, L. González Santos	Stochastic optimal control applied to a two level quantum system
16:00-16:15	S. Sorokin, M. Staritsyn	Numerical algorithms for state-linear optimal impulsive control problems based on feedback necessary optimality conditions
16:15-16:30	S. Haider, U. Saeed	Explosive material detection and security alert system
14:30-16:30, Room 305	**Section 7b "Complex Networks and Biosystems"** *Prof. Mikhail Ivanchenko*	
14:30-14:45	**Prof. Viktor Kazantsev** *Lobachevsky State University of Nizhni Novgorod, Russia*	**Invited Talk** To be announced
14:45-15:00	S. Jalan, V. Rathore, A.D. Kachhvah, A. Yadav	Multiplexing with inhibitory layer leading to explosive synchronization in multiplex networks
15:00-15:15	I.P. Mariño, L. Lacasa, J. Míguez, V. Nicosia, É. Roldán, A. Lisica, S.W. Grill, J. Gómez-Gardeñes	Identifying the hidden multiplex architecture of biological processes
15:15-15:30	S. Makovkin, M. Ivanchenko, A. Zaikin, S. Jalan	Investigating multiplex models of neuron glial systems: small-world topology and inhibitory coupling
15:30-15:45	M. Krivonosov, M. Ivanchenko, S. Jalan, M.G. Bacallini, C. Franceschi	Parenclitic analysis of high-dimensionality DNA methylation data
15:45-16:00	O. Vershinina, S. Denisov, M. Ivanchenko	Quasi-stationary oscillations in game driven evolutionary dynamics
16:00-16:15	A. Makeeva, A. Dmitrichev, V. Nekorkin	Torus canards in the ensemble synaptically related neurons Fitzhugh-Nagumo
16:15-16:30	T. Nazarenko, M. Krivonosov, A. Zaikin	Analysis of longitudinal high-dimensional medical data with parenclitic networks
14:30-16:40, Room 421	**Section 11e "Dynamics of Complex Networks and their Application in Intellectual Robotics" (DCNAIR)** *Dr. Anatoly Karavaev*	

14:30-14:40	M. Rassabin, R. Yagfarov, S. Gafurov	Approaches for road lane detection
14:40-14:50	S. Mikhel	State-based velocity profile for manipulator
14:50-15:00	V. Skvortsova, D. Popov	Design of the parallel spherical manipulator for wrist rehabilitation
15:00-15:10	R. Khusainov, S. Mamedov, P. Dmitry	Trajectory planning for biped walk with non-instantaneous double support phase
15:10-15:20	A. Evlampev, M. Ostanin	Obstacle avoidance for robotic manipulator using mixed reality glasses
15:20-15:30	P. Khakimov, S. Savin, A. Klimchik	Trajectory optimization for underactuated systems using reinforcement learning: cart pole problem
15:30-15:40	I.D. Galushko, G.M. Makaryants, S.A. Gafurov	Mathematical modeling of changes in geometric parameters of pneumatic muscles
15:40-15:50	A. Kurbanov, S. Grebennikov, S. Gafurov, A. Klimchik	Vulnerabilities in the vehicle's electronic network equipped with ADAS system
15:50-16:00	R. Yagfarov, V. Ostankovich, S. Gafurov	Augmentation-based object detection for winter time applications
16:00-16:10	G.Y. Prokudin, N.G. Sharonov, E.S. Briskin	Optimal control of orthogonal-rotary movers of walking robot with an excessive number of drives
16:10-16:20	T.I. Muftakhov, V.M. Giniyatullin, D.V. Shekhovtsov	Interpretation of the results of the neural network after the substitution of continuous activation function on the threshold function
16:20-16:30	N. Stankevich, E. Volkov, E. Hellen	Self-organized quasiperiodicity and multistability in dynamical systems of different nature
16:30-16:40	E. Bagautdinova, S. Kuznetsov, E. Seleznev, N. Stankevich	Circuit simulation of a blue sky catastrophe in the context of bursting dynamics occurrence
16:30-17:00	*Coffee Break*	
17:00-	**Section 8 "Dynamics and Control of Self-Driven Cars"**	

18:00, Room 307	*Dr. Salimzhan Gafurov*	
17:00-17:15	R. Chertovskih, N.T. Khalil, F.L. Pereira	Optimal path planning of AUVs operating in flows influenced by tidal currents
17:15-17:30	A. Andreev, O. Peregudova, K. Sutyrkina	On global trajectory tracking control of a wheeled mobile robot
17:30-17:45	A.V. Utkin, V.A. Utkin	Synthesis of control systems at unilateral limitations on controls and their derivatives
17:45-18:00	A.V. Utkin, J.G. Kokunko, D.V. Krasnov	Synthesis of the subsystem of observation for an unmanned aerial vehicle under uncontrolled disturbances
17:00-17:45, Room 305	**Section 9 "Self-Organization and Complexity in Brain Circuits"** *Prof. Alexander Pisarchik*	
17:00-17:15	D. Zakharov, M. Krupa, B. Gutkin	Modulation of synchronous gamma rhythm clusters
17:15-17:30	A. Sergeenko, O. Granichin, M. Yakunina	Hamiltonian path problem: the time consumption comparison of DNA computing and branch and bound method
17:30-17:45	S.A. Plotnikov, D.R. Belov	Simulation of gamma rhythm and its correlation with low-frequency signals
17:00-17:45, Room 308	**Section 4c "Interdisciplinary Issues of Control"** *Prof. Alexander Hramov; Prof. Alexander Pisarchik*	
17:00-17:15	O. Starinova, I. Chernyakina	The effects of surface degradation on ballistics of Solar sail mission to the Sun
17:15-17:30	P.A. Velmisov, A.V. Ankilov	Investigation of dynamics and stability of elastic elements of vibration devices
17:30-17:45	V. Erofeeva, V. Galyamina, K. Gonta, O. Granichin, A. Leonova, V. Pankov, M. Tursunova, Mingyue Ding, Ming Yuchi, Xiaoyue Fang	Detection of specific areas with ultrasound tomography

17:00-18:00, <u>Room 107</u>	**Section 10 “Emerging Challenges in Autonomous Cyber-Physical Systems”** *Dr. Allahyar Montazeri; Dr. Alexandr Klimchik; Dr Mohammad Reza Bahrami*	
17:00-17:15	M. Reza Bahrami, M.R. Wasilewski	Performance analysis of dynamic vibration absorber using semi-active control system for skidding tractor with an operator
17:15-17:30	A. Montazeri, Weiling Zheng	Multi-objective particle swarm optimization algorithm approach for parameter optimization of a 7 DOF robotic manipulator
17:30-17:45	H. Ahmadian, M.M. Arefi, A. Khayatian, A. Montazeri	L1 adaptive controller design for nuclear robots in the presence of loss data, time delay and uncertainty

17:45-18:00	I.V. Konyukhov, V.M. Konyukhov	Cyber-physical system for control the heat and mass transfer in the oil reservoir and producing pumping well
17:00-18:00, Room 421	**Section 11f “Dynamics of Complex Networks and their Application in Intellectual Robotics” (DCNAIR)** *Dr. Vadim Grubov*	
17:00-17:10	S. Savin	Detecting changes in contact interaction regime with a reaction predictor and a linear contact model
17:10-17:20	D. Popov, A. Klimchik	Identification stiffness model parameter for bipedal robots
17:20-17:30	D. Popov, A. Klimchik	Multiple collision detection for a collaborative robot
17:30-17:40	P. Kozlov, A. Klimchik	Automated robotic assembly of complex workpieces from regular components
17:40-17:50	E.A. Marchuk, A.P. Fedin, Ya.V. Kalinin	Neuro-fuzzy anti-block braking system of the vehicle
17:50-18:00	T.A. Tarasova, I.A. Tarasova, A.V. Maloletov, Ya.V. Kalinin	Application of systems of stochastic differential equations for modeling transport processes

18.00-18.30, **Room 107**	**Closing ceremony**

PHYSCON 2019, Innopolis, Russia, 8–11 September, 2019

ON GLOBAL TRAJECTORY TRACKING CONTROL OF A WHEELED MOBILE ROBOT

Aleksandr Andreev
Department of Information Security and Control Theory
Ulyanovsk State University Russia
asa5208@mail.ru

Olga Peregudova
Department of Information Security and Control Theory
Ulyanovsk State University Russia
peregudovaoa@gmail.com

Katherine Sutyrkina
Department of Information Security and Control Theory
Ulyanovsk State University Russia
kea-ul@yandex.ru

Abstract

In the paper, the global trajectory tracking control problem of a wheeled mobile robot is considered. We use the dynamical model of the mobile robot which has one castor front wheel and two rear wheels controlled by two independent electric motors. A feedback con troller has been constructed using a backstepping de sign procedure and Lyapunov approach.

Key words

Mobile wheeled robot, global trajectory tracking, Lya punov function, backstepping method.

1 Introduction

Many approaches exist to trajectory tracking and set point stabilizing of a nonholonomic wheeled mobile robot. In [Gao, Lee, and Chong, 2008] the trajectory tracking control problem has been solved using only kinematical system which is linearized at the equilib rium point. A global tracking control law has been pro posed in [Blazic, 2011] for a kinematical model of the robot using a Lyapunov approach.

An idea to integrate a velocity control for the kine matical system into a torque controller for the physical vehicle has been proposed in [Fierro and Lewis, 1997] on the backstepping method. The global exponential setpoint controller has been proposed in [Dixon, Jiang, and Dawson, 2000] via backstepping design technique and Lyapunov approach. A three level control algo rithm has been proposed in [Kozlowski and Majchrzak, 2002] on the base of a backstepping procedure for the trajectory tracking and setpoint stabilization. In [Hou, Zou, Chen, and Tan, 2009] the trajectory tracking con trol problem has been solved for a wheeled mobile robot with model uncertainties and the wheel actua tor dynamics using backstepping and fuzzy logic tech niques. has been solved by integrating a neural network into the backstepping technique.

In this paper, we consider the global trajectory track ing control problem of a wheeled mobile robot. The motion equations of such a robot model were obtained by [Martynenko, 2007]. Dynamics of the robot are de scribed by differential equations with an angular coor dinate. The phase space of such systems is a cylin drical space. We propose a novel control scheme to solve a global trajectory tracking control problem for a wheeled mobile robot in a cylindrical phase space.

2 Problem Statement

Consider the model of a wheeled mobile robot that moves on the horizontal plane. The robot consists of a platform, two driving wheels and a front free wheel. The robot moves under the action of two independent electric motors. The dynamics equations of a robot are given by [Martynenko, 2007]

$$
\begin{cases}
m\dot{V} - m_1 a\Omega^2 - \frac{nc}{r}(i_1 + i_2) = 0 \\
J\dot{\Omega} + m_1 a V \Omega - \frac{ncl}{r}(i_1 - i_2) = 0 \\
L\frac{di_1}{dt} + Ri_1 + \frac{nc}{r}(V + l\Omega) = U_1 \\
L\frac{di_2}{dt} + Ri_2 + \frac{nc}{r}(V - l\Omega) = U_2
\end{cases}
\qquad (1)
$$

In [Chwa, 2010] a tracking controller has been

where V is the velocity of the point A; Ω is the angu lar velocity of the platform; i_1 and i_2 are the currents in the external circuits of electric motors; r is the radius of rear wheels; m_1 is the platform mass; L is the general ized inductance of the

proposed by using a backstepping-like feedback lin earization. In [Ye, 2008] the tracking control problem

(2)

14

$m = m_1 + 2m_k + 2\,\frac{J_y}{}$

motor circuit; c is the coefficient of electromechanical interaction; R is the ohmic resis tance of the rotor circuit; n is the gear ratio; $a = AC$;

}

r^2

$J = J_1 + 2J_{kz} + (m - m_1)l^2 + m_1a^2$

where $U_3 = U_1 + U_2$ and $U_4 = U_1 - U_2$. The aim of this paper is to find the output feedback controller

$U_i = U_i(t, x_e, y_e, \psi_e, \Omega)$ $i = 1, 2, \forall t \geq 0$ } (8)

which insures the global uniform asymptotical stability of zero solution of the system (1).

3 Problem Solution

Let us make the change of variables as follows

wheel and the motor

Figure 1. Model of a wheeled mobile robot.

$\eta_1 = y_e,\ \eta_2 = x_e - \gamma y_e$

$\eta_3 = \psi_e,\ \xi_1 = V,\ \xi_2 = \Omega$

where γ is some positive constant.

} (9)

m_k is the total mass of the driving

center of mass

Then the system (7) can be written in the following form:

rotor, J_1 is the inertia moment of the platform relative to the vertical axis passing through the

C; J_{kz} is the inertia moment of the driving wheel with respect to the vertical axis; J_y is the reduced inertia moment of the wheel.

The kinematic equations of the robot are given by $\dot{x} = V\cos\psi,\ \dot{y} = V\sin\psi,\ \dot{\psi} = \Omega$ (3)

$\dot{\eta}_1 = -\gamma\xi_2\eta_1 - \xi_2\eta_2 + V_r(t)\sin\eta_3$

$\dot{\eta}_2 = (\gamma^2 + 1)\xi_2\eta_1 + \gamma\xi_2\eta_2 - \xi_1 + V_r(t)(\cos\eta_3 - \gamma\sin\eta_3)$

$\dot{\eta}_3 = \Omega_r(t) - \xi_2$

$\dot{\xi}_1 = -\frac{2n^2c^2}{r^2Rm}\xi_1 + \frac{m_1a}{m}\xi_2^2 + \frac{nc}{rRm}U_3$

$\dot{\xi}_2 = -\frac{m_1a}{}\xi_1\xi_2 - \frac{2n^2c^2l^2}{r^2RJ}\xi_2 + \frac{ncl}{rRJ}U_4$ (10)

The robot is required to follow a desired trajectory $x = x_r(t)$, $y = y_r(t)$ and $\psi = \psi_r(t)$, i.e.

$\dot{x}_r(t) = V_r(t)\cos(\psi_r(t))$ $\dot{y}_r(t) = V_r(t)\sin(\psi_r(t))$ $\dot{\psi}_r(t) = \Omega_r(t)$ (4)

The system (10) consists of two subsystems with the state vectors $\eta = (\eta_1, \eta_2, \eta_3)^T$ and $\xi = (\xi_1, \xi_2)^T$ re spectively. Note that the input signal of the first sub system is the state vector of the second one. In order to construct the stabilizing control inputs U_3 and U_4 for

where the smooth bounded functions $V_r(t)$ and $\Omega_r(t)$ are the corresponding desired velocities satisfying the following inequalities

}

$|V_r(t)| \leq v_{rmax},\ |\dot{V}_r(t)| \leq v_{r1max}$

$0 < \omega_{rmin} \le \Omega_r(t) \le \omega_{rmax}, \ |\dot{\Omega}_r(t)| \le \omega_{r1max}$ (5)

where v_{rmax}, v_{r1max}, ω_{rmin}, ω_{rmax} and ω_{r1max} are some positive constants.

Let us define the tracking errors of the robot as follows

the whole system (10), we use a recursive procedure of a backstepping method [Kokotovic, 1992]. Namely, at first we find the control law $\xi = (\varphi_1, \varphi_2)^T$ with the smooth functions $\varphi_1 = \varphi_1(t, \eta)$ and $\varphi_2 = \varphi_2(t, \eta)$, which stabilizes the zero position $\eta = 0$ of the first subsystem (10). We also find a Lyapunov function for the first subsystem. Then we find the control law of the whole system (10) by constructing a composite Lya punov function.

Choose the functions φ_1 and φ_2 as follows

$x_e = \cos\psi(x_r(t) - x) + \sin\psi(y_r(t) - y)$ $y_e = -\sin\psi(x_r(t) - x) + \cos\psi(y_r(t) - y)$ (6)

$\psi_e = \psi_r(t) - \psi.$

$\varphi_1 = V_r(t) + v\eta_2$

$\varphi_2 = \Omega_r(t) + \mu \sin(\frac{\eta_3}{2})$ } (11)

where v and μ are some positive constants.

Assuming that $L = 0$ in (1), one can obtain the error dynamics for the robot as

$\dot{x}_e = \Omega y_e - V + V_r(t)\cos\psi_e$ $\dot{y}_e = -\Omega x_e + V_r(t)\sin\psi_e$ (7) $\dot{\psi}_e = \Omega_r(t) - \Omega$

$m\dot{V} - m_1 a\Omega^2 + \frac{2n^2c^2}{r^2R} V = \frac{nc}{rR} U_3$

$J\dot{\Omega} + m_1 a V\Omega + \frac{2n^2c^2l^2}{r^2R}\Omega = \frac{ncl}{rR} U_4$

Applying the virtual controller $\xi = (\varphi_1, \varphi_2)^T$ with the functions (11) to the kinematical part of (10), we obtain the system

$\dot{\eta}_1 = -\gamma(\Omega_r(t) + \mu\sin(\frac{\eta_3}{2}))\eta_1 - (\Omega_r(t) + \mu\sin(\frac{\eta_3}{2}))\eta_2 + V_r(t)\sin\eta_3$

$\dot{\eta}_2 = (\gamma^2 + 1)(\Omega_r(t) + \mu\sin(\frac{\eta_3}{2}))\eta_1 + (\gamma(\Omega_r(t) + \mu\sin(\frac{\eta_3}{2})) - v)\eta_2 + V_r(t)(\cos\eta_3 - \gamma\sin\eta_3 - 1)$ (12)

$\dot{\eta}_3 = -\mu\sin(\frac{\eta_3}{2})$

15

Choose the Lyapunov function candidate $V = V(t, \eta)$ for the system (12) such as

$$V = \frac{1}{2}((\gamma^2 + 1)\eta_1^2 + \eta_2^2) + 2\left(1 - \cos\left(\frac{\eta_3}{2}\right)\right) \quad (13)$$

The time derivative of V is given by

$$\dot{V} = -\gamma(\gamma^2 + 1)\left(\Omega_r(t) + \mu\sin\left(\frac{\eta_3}{2}\right)\right)\eta_1^2 - \left(v - \gamma\left(\Omega_r(t) + \mu\sin\left(\frac{\eta_3}{2}\right)\right)\right)\eta_2^2 + (\gamma^2 + 1)\eta_1 V_r(t)\sin\eta_3 + \eta_2 V_r(t)(\cos\eta_3 - \gamma\sin\eta_3 - 1) - \mu\sin^2\left(\frac{\eta_3}{2}\right) \quad (14)$$

8

6

xe (m)

4

0

0 2 4 6 8 12 14 16 18 22 24 10 20 t (sec)

Figure 2. Time evolution of the tracking error x_e.

Let rewrite the time derivative of V as follows

$$\dot{V} = -\gamma(\gamma^2 + 1)\left(\Omega_r(t) + \mu\sin\left(\frac{\eta_3}{2}\right)\right)\eta_1^2 - \left(v - \gamma\left(\Omega_r(t) + \mu\sin\left(\frac{\eta_3}{2}\right)\right)\right)\eta_2^2 + 2(\gamma^2 + 1)V_r(t)\cos\frac{\eta_3}{2}\eta_1\sin\frac{\eta_3}{2} - 2V_r(t)\left(\gamma\cos\frac{\eta_3}{2} + \sin\frac{\eta_3}{2}\right)\eta_2\sin\left(\frac{\eta_3}{2}\right) - \mu\sin^2\left(\frac{\eta_3}{2}\right) \quad (15)$$

4 Numerical Simulation

In this section, the performance of the proposed con troller is illustrated.

The robot parameters are given as

$m = 30$ kg, $m_1 = 25$ kg

Note that $\dot{V}$ is negative definite quadratic form of the variables η_1, η_2 and sin $\eta_3/2$, if the following inequal ities hold

}

$r = 0.2$ m, $a = 0.5$ m, $l = 0.3$ m $c_v = 6 * 10^{-5}$ N · m · sec

$n = 0.8$, $c = 0.6$, $R = 1.7$

nc $(2n^2c^2l^2$ $m\xi_2\varphi_2 + \dot{\varphi}_1$) (17)

$U_4 = rRJ$ ncl

$r^2RJ\varphi_2 + m_1a$

$J\xi_2\varphi_1 + \dot{\varphi}_2$

In order to check the property of global tracking we consider the

The desired velocities are chosen as

(19)

$v > \gamma(\omega_{rmax} + \mu)$

$v^2_{rmax} < \frac{\gamma\mu}{2}$

$1+\gamma^2 (\omega_{rmin} - \mu)$

Now consider the whole system (10). We use the following output feedback controller:

(16)

$V_r(t) = 0.4 \cos t$ m/sec

$\Omega_r(t) = 3.5 + 2 \sin t$ rad/sec (20)

The control parameters were

chosen such that

$U_3 = rRm$

$(2n^2c^2$

$r^2Rm\varphi_1 - m_1a$

)

$\gamma = 0.7$, $\mu = 1$, $v = 5$ (21)

simulations results using the initial condi tions for the robot such as

Choose the composite Lyapunov vector-function can didate as follows

$$V_c = (V, W)^T \quad (18)$$

where $W = z^2_1/J + z^2_2/m$, $z_1 = \xi_1 - \varphi_1$ and $z_2 = \xi_2 - \varphi_2$.

Using the comparison lemma [Khalil, 2002], it is easy to get that the closed-loop system (10), (17) is exponen tially stable. Consequently, the controller (17) provides the global exponential stability of the system (7).

Note that the proposed controller (17) has a more sim ple structure with respect to one obtained in [Andreev and Peregudova, 2017].

$x_e(0) = 6.5$ m, $y_e(0) = 15$ m, $\psi_e(0) = 3$ rad $V(0) = 25$ m/sec, $\Omega(0) = 4$ rad/sec

(22)

In Figures 2, 3, and 4 we show the tracking perfor mance of the controller (17) within the time interval $t = 25$ sec. From these results, it can be seen that con troller (17) provides smooth fast convergence to the ref erence trajectory of the robot. From Figure 4 it can be seen that controller (17) provides smooth fast conver gence to the reference angle plus $2\pi k$, where $k = 10$.

5 Conclusion

We have addressed the global trajectory tracking con trol problem for a wheeled mobile robot controlled by

16 14 12 10

tional Journal of Systems Science, 48(9), pp. 2003–2012.

Blazic, S. (2011) A novel trajectory tracking control law for wheeled mobile robots. *IEEE Robotics and Autonomous Systems*, 59, pp. 1001–1007. Chwa, D. (2010) Tracking control of differential

ye (m)

drive wheeled mobile robots using a backstepping

8

like feedback linearization. *IEEE Transactions on*

6

Systems, Man and Cybernetics. Part A: Systems and

4

Humans, 40(6), pp. 1285–1295.

Dixon, W.E., Jiang, Z.P., and Dawson, D.M. (2000)

2

Global exponential setpoint control of wheeled mo

0

−2

0 2 4 6 8 12 14 16 18 22 24 10 20 t (sec)

Figure 3. Time evolution of the tracking error y_e.

70

60

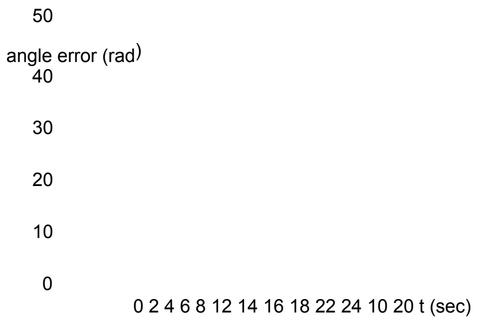

Figure 4. Time evolution of the tracking error ψ_e.

two DC motors. By employing the backstepping design procedure and constructing a Lyapunov vector func tion, a novel nonlinear control scheme is obtained. We exploit a new analysis framework where the behaviour of the mechanical system with an angular coordinate is considered in a cylindrical phase space.

Acknowledgements

This work is financially supported in part by the Rus sian Foundation for Basic Research (project no. 19-01- 00791) and Ministry of Science and High Education of Russia within the framework of the State task under Grant (9.5994.2017/BP).

References

Andreev, A. and Peregudova, O. (2017) Lyapunov vector function method in the motion stabilisation problem for nonholonomic mobile robot. *Interna*

bile robots: a Lyapunov approach. *Automatica*, 36, pp. 1741–1746.

Fierro, R., and Lewis, F.L. (1997) Control of a non holonomic mobile robot: backstepping kinematics into dynamics. *Journal of Robotic Systems*, 14(3), pp. 149–163.

Hou, Z.-G., Zou, A.-M., Chen, L., and Tan, M. (2009) Adaptive control of an electrically driven nonholo nomic mobile robot via backstepping and fuzzy ap proach. *IEEE Transactions on Control Systems Tech nology*, 7(4), pp. 803–815.

Gao, Y., Lee, C.-G., and Chong, K.T. (2008) Receding horizon tracking control for wheeled mobile robots with time dealy. *Journal of Mechanical Science and Technology*, 22, pp. 2403–2416.

Khalil, H. K. (2002). *Nonlinear systems (3rd ed.)*. Up per Saddle River, NJ: Prentice Hall.

Kokotovic, P.V. (1992). The joy of feedback: Non linear and adaptive. *IEEE Control Systems Magazine*, 12, pp. 7-17.

Kozlowski, K.R., and Majchrzak, J. (2002) A back stepping approach to control a nonholonomic mobile robot. *Proceedings of the 2002 IEEE International Conference on Robotics and Automation, Washington, DC, May 2002*, pp. 3972–3977.

Martynenko, Yu. G. (2007) Motion control of mobile wheeled robots. *Journal of Mathematical Sciences*, 147, pp. 6569-6606.

Ye, J. (2008) Tracking control for nonholonomic mo bile wheeled robots: integrating the analog neural net work into the backstepping technique. *Neurocomput ing*, 71, pp. 3373-3378.

ON THE CONTROL PROBLEM OF A TWO-LINK MANIPULATOR

Aleksandr Andreev
Department of Inform. Security and Contr. Theory Ulyanovsk State University
Russia
asa5208@mail.ru

Abstract

Robotic arms are included in a large number of robotic systems. The study of control problem of such robots has been the subject of numerous researches in the lat est 70 years. One of the simple but effective common robot manipulators is a two-link robotic arm. There fore, the problem of control synthesis for such manip ulators is one

of the base questions in identifying the effectiveness of the developed methods in control study of robotic systems. In this paper we propose a nonlin ear PID controller which solves the stability problem for stationary motions of such manipulators as well as the problem of trajectory tracking control.

Key words
Two-link manipulator, trajectory tracking, PID and PD controllers, control synthesis.

1 Introduction

The study of the problem of manipulating manipula tors, robotic systems was started in the 50s of the last century, and by now a large number of works have been devoted to it. Nevertheless, the urgency of the problem is only constantly growing due to the inten sive automation of technologies and production with increasing complexity, increasing requirements for ac curacy, reliability, energy consumption and other fac tors controlling equipment. Most of the research in this area is limited to studying the established control modes, linearizing model equations, using the classi cal type of controls, and making other simplifications in modeling the system. Often use standard links de veloped for linear models. For the construction of non linear models of manipulation control systems, linear and nonlinear proportional-differential type controllers (PD regulators) are widely used. A large number of works including [Wen, and Bayard, 1988], [Kelly and Salgado, 1994], [Andreev and Peregudova, 2015], [An dreev and Peregudova, 2016], [Andreev, and Peregu dova, 2019] are devoted to the use of continuous PD

Katherine Sutyrkina
Department of Inform. Security and Contr.
Theory Ulyanovsk State University
Russia
kea-ul@yandex.ru

[Meza, Santibanez, and Campa, 2007], [Meza, Santibanez, and Hernandez, 2005], [Meza, Santibanez, Soto, and Perez, 2010], [Ortega, Loria, and Kelly, 1995], [Qu and Dorsey, 1991], [Rocco, 1996], [Santibanez, Ca marillo, Moreno-Valenzuela, and Campa, 2010], [San tibanez and Kelly, 1998], [Santibanez, Kelly, Zavala Rio, and Parada, 2008], [Sun, Hu, Shao, and Liu, 2009], [Wen, and Murphy, 1990] is presented in the publications [Andreev and Peregudova, 2017a], [An dreev, and Peregudova, 2018a]. Studies on the use of proportional-integral (PI-) regulators have so far not been available. The results obtained in [Andreev and Peregudova, 2017a], [Andreev, and Peregudova, 2018a], [Andreev, 2018], [Andreev, and Peregudova, 2018b] made it possible to significantly expand the methods for constructing structures for controlling me chanical systems without measuring velocities. A dif ferent approach to solving this problem is based on ap plying a filter by coordinates with an estimate of the speeds in the hinges and their interval values [Andreev, and Peregudova, 2017b], [Andreev, and Peregudova, 2017d], [Andreev, and Peregudova, 2018c], [Andreev, Peregudova, and Makarov, 2016], [Andreev, 2018], [Burkov, 1998], [Burkov, 2009], [Chaouki, Dawson,

Dorato, and Jamshidi, 1991], [Peregudova, 2018]. Widespread use of both independently in the technique, and as a composite link in robotic systems, has a two

coordinates and let

$$X = \{(q^0(t), \dot{q}^0(t)) : [t_0, +\infty) \to R^4$$

stage manipulator. Therefore, his model is widely used

to identify the effectiveness of the developed meth ods and algorithms for constructing robot control struc

regulators in the task of tracking the trajectory of a robotic arm. Note that this problem remains open to date in terms of the lack of common methods and al gorithms for its solution. Since the beginning of the 80s of the last century, intensive research has been con ducted on the use of proportional-integro-differential (PID) regulators in the control of robots, mechanical systems. It is believed that such regulators have cer tain advantages over PD regulators. A detailed analysis of the known works in this field [Alvarez, Cervantes, and Kelly, 2000], [Alvarez, Kelly, and Cervantes, 2003], [Arimoto, 1994], [Arimoto, 1995], [Arimoto, 1996], [Arimoto, Naniwa, and Suzuki, 1990], [Cer vantes and Alvarez-Ramirez, 2001], [Gorez, 1999], [Jafarov, Parlakci, and Istefanopulos, 2005], [Kelly, 1995], [Kelly, 1998], [Kelly, Santibanez, and Loria, 2005], [Loria, Lefeber, and Nijmeijer, 2000],

$$q^0(t) \le g_0, \dot{q}^0(t) \le g_1, \ddot{q}^0(t) \le g_2\} \quad (2)$$

tures [Alvarez, Cervantes, and Kelly, 2000], [Alvarez, Kelly, and Cervantes, 2003], [Meza, Santibanez, and Campa, 2007], [Meza, Santibanez, Soto, and Perez, 2010], [Rocco, 1996], [Santibanez, Kelly, Zavala-Rio, and Parada, 2008]. The purpose of this work is to de velop a control structure for a two-stage manipulator based on [Andreev, and Peregudova, 2018b], [Andreev, and Peregudova, 2019].

be the set of desired trajectories $q = q^0(t)$ which are chosen bounded and twice continuously differentiable functions with both of these derivatives bounded for all $t \in [t_0, +\infty)$.

Let $(q^0(t), \dot{q}^0(t)) \in X$ denote the chosen desired tra jectory of the manipulator, which is provided by con troller $U = U^0(t)$. Thus, to ensure such a trajectory, the following controller takes place:

$$U^0{}_1(t) = a_{11}(q^0{}_2(t))\ddot{q}^0{}_1(t) + a_{12}(q^0{}_2(t))\ddot{q}^0{}_2(t) - -2m_2 l l_2 \sin q^0{}_2(t)\ \dot{q}^0{}_1(t)\ \dot{q}^0{}_2(t) - -m_2 l l_2 \sin q^0{}_2(t)\ \dot{q}^0{}_2(t)^2 - M^0{}_1(t)$$

$$U^0{}_2(t) = a^0{}_{12}(t)\ddot{q}^0{}_1(t) + I_2\ddot{q}^0{}_2(t) - M^0{}_2(t) \quad (3)$$

2 Formulation of the problem

Let us consider the mathematical model of a two-link manipulator (Fig. 1).

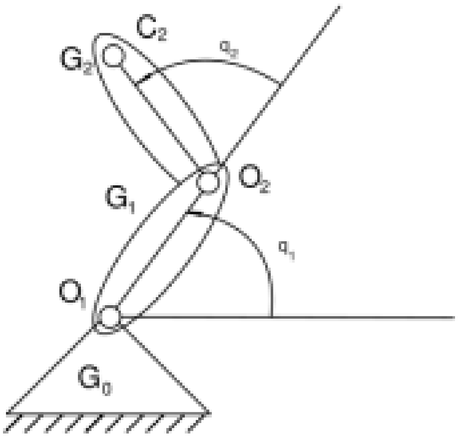

Figure 1. Model of two-way manipulator.

The manipulator consists of a fixed base and two ab

where we have $M^0{}_1(t) = M^0{}_2(t) = 0$ for a horizon

solutely rigid links G_1 and G_2. The structural elements are interconnected by two ideal cylindrical hinges O_1 and O_2 in such a way that both links can move in a hor izontal or a vertical plane only. The center of mass C_1 of the link G_1 lies on the ray O_1O_2. The position of the center of mass C_2 of the link G_2 doesn't coincide with the position of the hinge O_2.

Then, the Lagrange equations of the second kind could be written as:

$$\frac{d}{dt}\frac{\partial T}{\partial \dot{q}_1} - \frac{\partial T}{\partial q_1} = M_1 + U_1$$
$$\frac{d}{dt}\frac{\partial T}{\partial \dot{q}_2} - \frac{\partial T}{\partial q_2} = M_2 + U_2 \quad (1)$$

Let $q = q(q_1, q_2)$be the vector of the generalized

tally moving manipulator. And for a vertically moving robotic two-link manipulator we'll get:

$$M^0{}_1(t) = (m_1 l_1 + m_2 l)g \cos q^0{}_1(t)$$
$$M^0{}_2(t) = m_2 l_2 g \cos(q^0{}_1(t) + q^0{}_2(t)) \quad (4)$$

Let us introduce the following perturbations $x_k = q_k - q^0{}_k(t)$, $\dot{x}_k = \dot{q}_k - \dot{q}^0{}_k(t)$, $k = 1, 2$.

Then, the dynamic model of a two-link robot manipu lator is described by the matrix equation:

$$A^{(1)}(t, x)\ddot{x} = \dot{x}C^{(1)}(t, x)\dot{x} + Q^{(1)}(t, x) + Q^{(2)}(t, x, \dot{x}) + U^{(1)} \quad (5)$$

where U represents the vector of the input control, A is the positive definite inertia matrix:

$$A^{(1)}(t, x) = \begin{pmatrix} a_{11}(q^0{}_2(t) + x_2) & a_{12}(q^0{}_2(t) + x_2) \\ a_{12}(q^0{}_2(t) + x_2) & I_2 \end{pmatrix} \quad (6)$$

Q is the vector of the generalized uncontrolled forces:

$$Q^{(1)}(t, x) = F(t, x)p(x),\ Q^{(2)}(t, x, \dot{x}) = D(t, x)\dot{x} \quad (7)$$

$p(x) = (\sin(x_1/2), \sin(x_2/2))$

$$D(t, x) = \begin{pmatrix} d_{11}(t, x) & d_{12}(t, x) \\ d_{21}(t, x) & d_{22}(t, x) \end{pmatrix} \quad F(t, x) = \begin{pmatrix} f_{11}(t, x) & f_{12}(t, x) \\ f_{21}(t, x) & f_{22}(t, x) \end{pmatrix} \quad (8)$$

with the matrices of coefficients for $D(t, x)$ and $F(t, x)$ correspondingly

$$d_{11}(t, x) = 2m_2 l l_2 \sin(q^0{}_2(t + x_1)\ \dot{q}^0{}_2(t))\quad d_{12}(t, x) = 2m_2 l l_2 \sin(q^0{}_2(t + x_1)\ \dot{q}^0{}_1(t)) + +2m_2 l l_2 \sin(q^0{}_1(t) + x_2)\ \dot{q}^0{}_2(t)$$
$$d_{21}(t, x) = -2m_2 l l_2 \sin(q^0{}_2(t) + x_2)\ \dot{q}^0{}_1(t)\quad d_{22}(t, x) = 0 \quad (9)$$

3 Stabilization of positions and stationary move ments of a two-link manipulator without mea suring speeds

Let us start with solving the stability problem for a horizontally moving two-link manipulator with only

$\{+(-2m_1l_1 - 2m_2l)g \sin(q^0{}_1(t) + x_1/2)\}$ $f_{12}(t, x) = 4m_2gll_2\ddot{q}^0{}_1(t) \sin(q^0{}_2(t) + x_2/2)+$

$q^0{}_1(t) = q^0{}_1 = const,\ q^0{}_2(t) = q^0{}_2 = const$ (16)

position measurement with desired trajectory for the first and the second link correspondingly:

Such a problem could be solved by the controller of a proportional-integral type:

where the terms enclosed in braces are added in the case of a vertical manipulator:

$_1(x_1) = -k_1 \sin x_1(t)$

$f_{11}(t, x) = 0$

$+2m_2ll_2\ddot{q}^0{}_2(t) \sin(q^0{}_2(t) +$ $\dot{q}^0{}_1(t)\ \dot{q}^0{}_2(t)+$

$x_2/2)+ +4m_2ll_2 \cos(q_2(t) + x_2/2)\ U^{(1)}\ _t$

2^-

$- \cos^{x}{}_{1(t)}$ $_2 - \sin\ ^{x}{}_{1(\tau)}$

$_0p^0{}_1e^{s_0{}_1(\tau-t)}(\sin\ ^{x}{}_{1(t)}$

$_2)d\tau,$

2

$+2m_2ll_2 \cos(q^0{}_2(t) + x_2/2)(\ \dot{q}^0{}_2)^2$

$_1(x_2) = -k_2 \sin x_2(t)$

$- \cos^{x}{}_{1(t)}$

$U^{(2)}\ _t$

$f_{21}(t, x) = 0\{+(-4m_2l_2g$ (10)

$\sin(q^0{}_1(t) + q^0{}_2(t)+$ 2^-

$+x_1/2 + x_2/2 \cos x_2/2))\}$

generalized forces:

2

$f_{22}(t, x) = 2m_2ll_2\ddot{q}^0{}_2(t) \sin(q^0{}_2(t) + x_2/2)+$

$_0p^0{}_2e^{s_0{}_2(\tau-t)}(\sin\ ^{x}{}_{2(t)}$

$_2 - \sin\ ^{x}{}_{2(\tau)}$

$_2)d\tau$ (17)

$+2m_2ll_2 \cos(q^0{}_2(t) + x_2/2)(q^0{}_1(t))^2+$

$\{+(-4m_2l_2 \sin(q^0{}_1(t) + q^0{}_2(t)+$

$+x_1/2 + x_2/2) \cos x_1/2)\}$

where $k_1, k_2, p^0{}_1, p^0{}_2, s^0{}_1, s^0{}_2$ are some positive con stants. Wherein each non-stationary trajectory of the system (1) will be unlimitedly approaching to the equilibrium point

$_2 = 0 \sin\ ^{x}{}_{2(t)}$

C is the matrix of centrifugal and Coriolis

$\sin\ ^{x}{}_{1(t)}$

$_2 = 0$ *or*

$C^{(1)}(t, x) = C^{(1)}{}_1(t, x) + C^{(1)}{}_2(t, x)$ (11)

with $k \in Z$ and $t \to \infty$. Let's now demonstrate the nu merical results for solving problem of trajectory track

$x_1(t) = 2\pi k,\ x_{2(t)} = 2\pi k$ (18)

ing control with proposed controller (17) for the de scribed model (1) of plane two-link manipulator where the initial and system parameters are given as:

$C^{(1)}{}_1(t, x) = m_2ll_2 \sin(q^0{}_2(t) + x_2)$ 1 1 (12)

0 1

$C^{(1)}{}_2(t, x) = -m_2ll_2 \sin(q^0{}_2(t) + x_2)$ 0 0 (13)

1 0

$p^0{}_1 = p^0{}_2 = 90$

$m_1 = 5$ kg, $m_2 = 5$ kg $l = 1$ m, $l_1 = l_2 = 0,5$ m $I_1 = I_2 = 3,33$ kg $\cdot$ m^2 $k_1 = k_2 = 1,$ (19)

$s^0{}_1 = s^0{}_2 = 10$

To solve the uniform asymptotic stability problem for the described system we'll construct regulator of a kind:

$U^{(1)} = U - U^0(t)$ (14)

such that $U^{(1)} = U^{(1)}(t, x, \dot{x})$, $U^{(1)}(t, 0, 0) \equiv 0$, provides not perturbed trajectory $\dot{x} = x = 0$ of (5) to be uniformly asymptotically stable.

In other words, we will find the controller $U =$

$U^0(t) + U^{(1)}(t, q - q^0(t), \dot{q} - \dot{q}^0(t))$ (15)

where $U^0(t)$ is from (3)-(4) to stabilize the reference trajectory $(q^0(t), \dot{q}^0(t)) \in X$ of the system (1).

where m_i denotes the mass of link i (i = 1, 2), l_i is the length of link i, l is the distance, I_i is the moment of inertia about the center of mass of the link i.

We have for a state variables q_1, q_2 and for each non stationary trajectory $q_1(t)$, $q_2(t)$ of the system (1) the following

$$q_1(t) \to q^0_1 + 2\pi k,\ q_2(t) \to q^0_2 + 2\pi k,\ t \to +\infty. \quad (20)$$

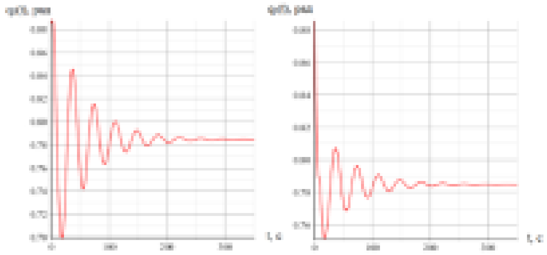

Figure 2. Coordinates of the links of the manipulator with the pa rameters (19) under the control (17)

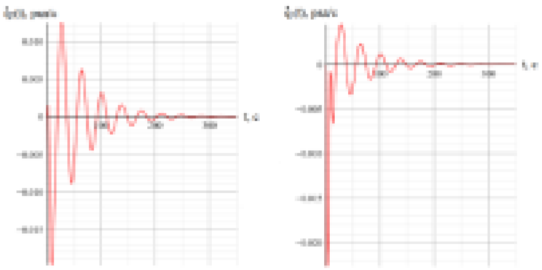

Figure 3. Velocities of the links of the manipulator with the param eters (19) under the control (17)

obtain a cyclic pulse of a type:

$$\frac{\partial T}{\partial \dot q_1} = a_{11}\dot q_1 + a_{12}\dot q_2 = v \quad (21)$$

Consider the Routh function with $\dot q_1 = (v - a_{12}\dot q_2)/a_{11}$, that will have form

$$R = \frac{1}{2}\frac{(v - a_{12}\dot q_2)^2}{a_{11}} + \frac{1}{2}a_{22}\dot q^2_2 - v\frac{(v-a_{12}\dot q_2)}{a_{11}} = \frac{1}{2}\left(a_{22} - \frac{a^2_{12}}{a_{11}}\right)\dot q^2_2 - \frac{1}{2}\frac{v^2}{a_{11}} \quad (22)$$

Since the position of the manipulator could be com puted with the accuracy of up to 2π, the controller of a type (17) provides the uniform asymptotic stability for the program trajectory (16). As the equation for the ki netic energy doesn't include the state q_1 explicitly, we

Thus, the control problem for a motion (25) of a holonomic mechanical system with a cyclic coordinate could be solved by the following controller:

$$U_2 = U^0_2 - k_2 \sin x_2(t) - \frac{-\cos x_2(t)}{2 - \cos x_2(t)} \int_0^t p^0_2 e^{s^0_2(\tau - t)} \frac{(\cos x_2(\tau))}{2 - \cos x_2(\tau)} d\tau \quad (26)$$

$$a_{11} + a_{22}(v - a_{12}\dot q_2)\ \dot q_2$$

where $k_2 = \frac{m_2 l l_2 \cos q^0_2 v^2_0}{(ml^2 + I_1 + I_2 + 2m_2 l l_2 \cos q^0_2)^2}$; $p^0_2 > 0$, $s^0_2 > 0$ are some constants.

The results of numerical experiment for the controller (26) and parameters denoted in (19) represents that mentioned position-feedback controller solves the tra jectory tracking control problem for a cyclic coordinate q_2 (as shown in the Fig. 4 — Fig. 5).

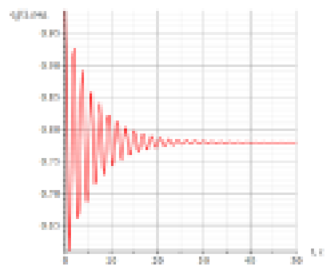

Figure 4. Trajectory of the manipulator's 2-nd link with the param eters (19) under the control (26)

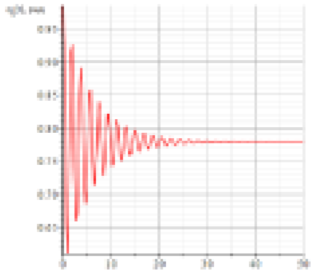

$a_{11}+a_{12}v$

$a_{11}\dot{q}_2$

From here we can easily get the motion equations de pend only on the variables q_2, $\dot{q}_2$, v:

Figure 5. Velocity of the manipulator's 2-nd link with the parame

v^2_0

$dt\ a_{22} - a^2_{12}$

d

$a_{11}\dot{q}_2 - \frac{1}{2}\partial a_{11}\ \partial q_2\ a^2_{11} = M_1$ (23)

control (26)

ters (19) under the

control problem for a vertically moving two-link manipulator. As it's shown (16) is provided by the controller:

If one determines the controller of the following

form $U^0_1 = m_2 l l_2 \sin q^0_2 v^2_0$

$$U^0_1 = -(m_1 l_1 + m_2 l_2) g \cos q^0_1,$$

$$U^0_2 = -m_2 l_2 g \cos(q^0_1 + q^0_2).$$

Therefore, the trajectory tracking control problem with unmeasurable link's velocities for non-local motion

$(m_2 l^2 + I_1 + I_2 + 2m_2 l l_2 \cos q^0_2)^2$ (24)

then the reference trajectory of the equation (23) admits the representation:

21

$v = v_0 = const,\ \dot{q}_2 = 0,\ q_2 = q^0_2 = const$ (25)

Let us now consider the trajectory tracking (16) could be solved with the

$k_1(q_1(t) - q^0_1) -$

following controller: $U_1 = U^0_1 -$ where

2

x_i

$-\cos^{x}{}_{1(t)\ 2}$

t

$_0p^0_1 e^{s_{0_1}(\tau - t)}(\sin(q_1(t))$ $- \sin(q_1(\tau)))d\tau$

$S = diag(s_1, s_2),\ \Pi(x)\ (b_{2i} + s_i b_{1i})\ 0$ $=\ {}_{i=1}$ $p_i(x_i)dx_i$

(30)

$U_2 = U^0_2 - k_2(q_2(t) - q^0_2) -$

$-\cos^{x}{}_{2(t)\ 2}$

t

$_0p^0_2 e^{s_{0_2}(\tau - t)}(\sin(q_2(t)) - \sin(q_2(\tau)))d\tau$

(27)

$U^{(1)}(x, \dot{x}) = B\ sign(\dot{x} + p(x))$ (31)

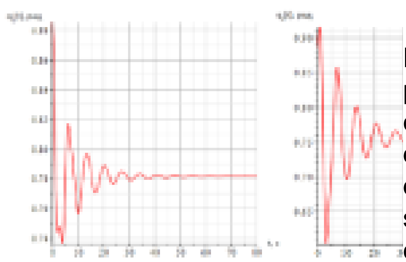

In the Fig. 8 - Fig. 9 the possibilities of the proposed controllers are illustrated, where dotted lines corre spond the desired program trajectories and solid lines - stabilized components. We demonstrate the results of numerical tests with the parameters (19), where the de sired trajectory of the two-link manipulator is taken as

Lets point out that if there is no practical opportunity to realize the described controller of a type (17), (26) or (27), the following robust program controller should be used

Figure 6. Coordinates of the vertical's manipulator links with the parameters (19) under the control (27)

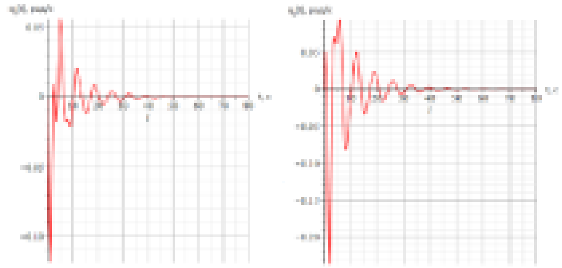

Figure 7. Velocities of the vertical's manipulator links with the pa rameters (19) under the control (27)

In the Fig. 6, 7 the simulation results for a vertical robotic manipulator are presented.

4 On stabilization of motions of a two-link manip ulator

To solve the stability problem for the system (1) and motion $(q_0(t), \dot{q}_0(t))$ we'll construct controller of a type:

$$U^{(1)}(x, \dot{x}) = -B_1\dot{x} - B_2 p(x)) \quad (28)$$

where $B \in R^{2\times2}$ is a gain matrix that should be de fined. For the further assumption we'll consider, that there is a Lyapunov function of a kind:

$$V = \frac{1}{2}(\dot{x} + Sp(x))^T A^{(1)}(t, x)(\dot{x} + Sp(x)) + \Pi(x) \quad (29)$$

$q^0_1(t) = \sin(0, 5t)$, $q^0_1(t) = \cos(0, 5t) + \frac{\pi}{2}$ and initial conditions are: $q_{10} = 0.5$, $\dot{q}_{10} = -0.5$, $q_{20} = 2.1$, $\dot{q}_{20} = 0.3$.

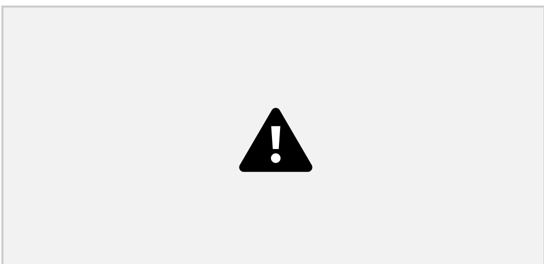

Figure 8. Coordinates of the vertical's manipulator links with the parameters (19) under the control (28)

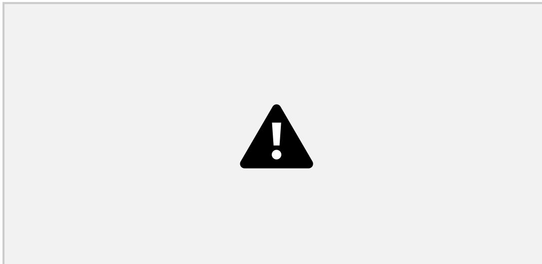

Figure 9. Velocities of the vertical's manipulator links with the pa rameters (19) under the control (31)

5 Conclusion

The main purpose of this article is to show how PI and PID controllers for a two-link planar robotic ma nipulator could be constructed. The proposed ap proach of controllers building develops the theoretical

results from [Andreev and Peregudova, 2016], [An dreev, Peregudova, and Sutyrkina, 2018], [Andreev, and Peregudova, 2019] and is based of the compar ison principle with construction of Lyapunov vector functions. The first section of the paper is devoted to the main idea how the tracking control problem of a two-link manipulator could be solved by the con troller of the general kind with stabilizing and program components, moreover, here we describe the model of a two-link manipulator and define the forms of sys tem's matrices. In the second section the controller of proportional-integral type is proposed and the re sults of numerical experiment for the trajectory track ing problem for manipulators of horizontal and vertical movement are represented. The last section presents the procedure of how the system's gain matrices could be chosen accordingly to the Lyapunov vector-function which provides the uniform asymptotic stability of the described system. In order to verify the proposed tech nique we construct two types of controller: continuous and robust ones with the corresponding numerical ex periment. In conclusion we note that the designed dy namic feedback controllers solve the trajectory tracking control problem for a large class of robotic manipula tors in condition of parameters' uncertainness.

Acknowledgements

This work was supported by Russian Foundation for Basic Research under Grants (19-01-00791, 18-41- 730022).

References

Alvarez, J., Cervantes, I., Kelly, R. (2000) PID regula tion of robot manipulators: stability and performance. *Systems and Control Letters*, 41, pp. 73–83.

Alvarez, J., Kelly, R., and Cervantes, I. (2003) Semiglobal stability of saturated linear PID control for robot manipulators. *Automatica*, 39, pp. 989–995.

Alvarez, J., Santibanez, V. and Campa, R. (2008) Sta bility of robot manipulators under saturated PID com pensation. *IEEE Transactions on Control Systems Technology*, 16(6), pp. 1333–1341.

Andreev, A.S. (2018) On Motion Stabilization of a Me chanical System with Cyclic Coordinates. *Proceed ings of 2018 14th International Conference "Stability and Oscillations of Nonlinear Control Systems" (Py atnitskiy's Conference) (STAB). 2018. IEEE Xlpore*.

Andreev, A. and Peregudova, O. (2015) On control for double-link manipulator with elastic joints. *Nelinein. Din.*, 11(2), pp. 267–278.

Andreev, A. and Peregudova, O. (2016) On stabi lization of program motions of holonomic mechan ical system. *Automation and Remote Control*, 77(3), pp. 416–427.

Andreev, A.S., and Peregudova, O.A. (2017) Stabiliza tion of the preset motions of a holonomic mechani cal system without velocity measurement. *Journal of Applied Mathematics and Mechanics*, 81(2), pp. 95– 105.

Andreev, A.S., Peregudova, O.A., and Makarov, D.S. (2016) Motion control of multilink manipulators without velocity measurement. *Proc. 2016 Intern. Conf. Stability Oscill. Nonlin. Control Syst. (Pyatnit skiy's Conf.). 2016*.

Andreev, A., Peregudova, O., and Sutyrkina, K. (2018) Trajectory Tracking Control of Robot Manipulators with Revolute Joints using Only Position Measure ments. *Proceedings of the 2018 18th International Conference on Mechatronics - Mechatronika (ME) 2018. Brno, Czech Republic, December 5-7, 2018. IEEE Xplore*.

Arimoto, S. (1994) A class of quasi-natural poten tials and hyper-stable PID servo-loops for nonlinear robotic systems. *Trans. of the Society of Instrument and Control Engineers*, 30(9), pp. 1005–1012.

Arimoto, S. (1995) Fundamental problems of robot control: Part I, Innovation in the realm of robot servo loops. *Robotica*, 13, pp. 19–27.

Arimoto, S. (1996) Control Theory of Non-Linear Me chanical Systems: A Passivity-Based and Circuit Theoretic Approach. *Oxford, U.K.: Clarendon Press*.

Arimoto, S., and Miyazaki, F. (1984) Stability and ro bustness of PID feedback control for robot manipu lators of sensory capability. In *In M. Brady and R.P. Paul (Ed.), Robotics Researches: First International Symposium MIT press, Cambridge, MA*, pp. 783–799.

Andreev, A.S., and Peregudova, O.A. (2017) Trajec tory tracking control for robot manipulators using only position measurements. *International Journal of Control*.

Andreev, A.S., and Peregudova, O.A. (2017) Stabiliza tion of the preset motions of a holonomic mechani cal system without velocity measurement. *Journal of Applied Mathematics and Mechanics*, 81(2), pp. 95– 105.

Andreev, A.S., and Peregudova, O.A. (2017) On Posi tion Stabilization and Trajectory Tracking Control for Robot Manipulators with Flexible Joints. *8th ECCO MAS Thematic Conference on Multibody Dynamics. Prague - Czech Republic, 19-22 June 2017*, pp. 501– 510.

Andreev, A.S., and Peregudova, O.A. (2018) Non linear PI regulators in control problems for holo nomic mechanical systems. *Systems Science and Control Engineering*, 6(1), pp. 12–19.

Andreev, A.S., and Peregudova, O.A. (2018) Nonlinear regulators in position stabilization problem of holo nomic mechanical system. *Mechanics of Solids*, (3), pp. S22–S38.

Andreev, A.S., and Peregudova, O.A. (2018) Nonlinear Controllers in the Regulation Problem of the Robots. *IFAC-PapersOnLine*, 51(4), pp. 7–12.

Andreev, A.S., and Peregudova, O.A. (2019) On Global Trajectory Tracking Control of Robot Ma nipulators in Cylindrical Phase Space. *International Journal of Control*.

Arimoto, S., Naniwa, T., and Suzuki, H. (1990) Asymptotic stability and robustness of PID local feedback for position control of robot manipulators. *Proc. ICARCV. Singapore*, pp. 382–386.

Berghuis, H., and Nijmeijer, H. (1993) A passivity ap proach to controller-observer design for robots. *IEEE Trans. Robotics Autom.*, 9(6), pp. 740–754.

Burkov, I.V. (1998) Stabilization of a natural mechan ical system without measuring its velocities with ap plication to the control of a rigid body. *Journal of Applied Mathematics and Mechanics*, 62(6), pp. 853- 862.

Burkov, I.V. (2009) Stabilization of position of uniform motion of mechanical systems via bounded control and without velocity measurements. *3-rd IEEE Multi conf. Systems Control. St Petersburg. 2009*, pp. 400– 405.

Cervantes, I., Alvarez-Ramirez, J. (2001) On the PID tracking control of robot manipulators. *Systems and Control Letters*, 42, pp. 37–46.

Chaouki, A.T., Dawson, D., Dorato, P., and Jamshidi, M. (1991) Survey of robust control for rigid robots. *Control Systems Magazine*, 11(2), pp. 24–30.

Gorez, R. (1999) Globally stable PID-like control of mechanical systems. *Systems and Control Letters*, 38, pp. 61–72.

Jafarov, E.M., Parlakci, M.N.A., and

Istefanopulos, Y. (2005) A new variable structure PID-controller de sign for robot manipulators. *IEEE Trans. Contr. Syst. Technol.*, 13(1), pp. 122–130.

Kelly, R. (1995) A tuning procedure for stable PID con trol of robot manipulators. *Robotica*, 13(2), pp. 141– 148.

Kelly, R. (1998) Global positioning of robot manipula tors via PD control plus a class of nonlinear integral actions. *IEEE Trans. Automat. Contr.*, 43(4), pp. 934– 937.

Kelly, R., and Salgado, R. (1994) PD Control with Computed Feedforward of Robot Manipulators: A Design Procedure. *IEEE Transactions on Robotics and Automation*, 10(4), pp. 566–571.

Kelly, R., Santibanez, V., and Loria, A. (2005) Con trol of Robot Manipulators in Joint Space. *Berlin: Springer- Verlag*

Loria, A., Lefeber, E., and Nijmeijer, H. (2000) Global asymptotic stability of robot manipulators with lin ear PID and PI2D control. *Stability Control: Theory Appl.*, 3(2), pp. 138–149.

Meza, J.L., Santibanez, V., and Campa, R. (2007) An Estimate of the Domain of Attraction for the PID Regulator of Manipulators. *International Journal of Robotics and Automation*, 22(3), pp. 187–195.

Meza, J.I., Santibanez, V., and Hernandez, V. (2005) Saturated nonlinear PID global regulator for robot manipulators: Passivity based analysis. *Proceedings of the 16th IFAC World Congress, Prague, Czech Re public. 2005*.

Meza, J.L., Santibanez, V., Soto, R., and Perez, J. (2011) Analysis via passivity theory of a class of nonlinear PID global regulators for robot manipula tors. *Advances in PID Control. Chapter 3. Edited by Valery D. Yurkevich, InTech, 2011*, pp. 45–64.

Orrante, J., Santibanez, V., Campa, R. (2010) On Satu rated PID Controllers for Industrial Robots: the PA10 Robot Arm as Case of Study, Advanced Strategies for Robot Manipulators. *S. Ehsan Shafiei (Ed.), InTech*.

Ortega, R., Loria, A., and Kelly, R. (1995) A semiglob ally stable output feedback PI2D regulator for robot manipulators. *IEEE Transactions on Automatic Con trol*, 40(8), pp. 1432–1436.

Peregudova, O.A. (2018) Robust Trajectory Track ing Control for Robot Manipulators without Veloc ity Measurements. *Proceedings of 2018 14th Interna tional Conference "Stability and Oscillations of Non linear Control Systems" (Pyatnitskiy's Conference) (STAB). 2018. IEEE Xlpore*.

Qu, Z., and Dorsey, J. (1991) Robust PID control of robots. *Int. Journal of Robotics and Automation*, 6(4), pp. 228–235.

Rocco, P. (1996) Stability of PID control for industrial robot arms. *IEEE Transactions on Robotics and Au tomation*, 12(4), pp. 606–614.

Santibanez, V., Camarillo, K., Moreno-Valenzuela, J., and Campa, R. (2010) A practical PID regulator with bounded torques for robot manipulators. *Inter national Journal of Control, Automation and Sys tems*, 8(3), pp. 544–555.

Santibanez, V., and Kelly, R. (1998) A class of non linear PID global regulators for robot manipulators. *Proceedings of the IEEE international conference on robotics and automation, Leuven, Belgium. 1998*, pp. 3601–3606.

Santibanez, V., Kelly, R., Zavala-Rio, A., Parada, P. (2008) A new saturated nonlinear PID global regu lator for robot manipulators. *Proceedings of the 17th IFAC World Congress, Seul, Korea. 2008.*.

Slotine, J-J. E. (1985) The Robust Control of Robot Manipulators. *The International Journal of Robotics Research*, 4, pp. 49–64.

Sun, D., Hu, S., Shao, X., and Liu, C. (2009) Global stability of a saturated nonlinear PID controller for robot manipulators. *IEEE Transactions on Control Systems Technology*, 17(4), pp. 892–899.

Wen, J.T., and Bayard, D.S. (1988) New class of control laws for robotic manipulators. Part 1. Non adaptive case. *International Journal of Control*, 47(5), pp. 1361–1385.

Wen, J.T., and Murphy, S. (1990) PID control for robot manipulators. *CIRSSE Document 54, Rensse laer Polytechnic Institute, Troy, NY.*

STUDY OF AN ACTIVE VIBRATION ISOLATION DEVICE FOR THE NANOPOSITIONING BASED ON MAGNETORHEOLOGICAL ELASTOMERS

Tun Lin Aung[1*], Valeriy Mikhailov[1*], Alexey Bazinenkov[1*], Alexander Kazakov[1*], Alexey Kopylov[1*], Dmitry Tovmachenko[1*]

[1]Department of Electronic Technologies in Mechanical Engineering

*Bauman Moscow State Technical University (BMSTU)

Moscow, Russia

tunlinaung52salay@gmail.com

Abstract

In this paper, we described the study of an active damper and platform for active vibration isolation system based on magnetorheological elastomers and developed a calculation method of the elastic suspension with mass corrector, which allows adjusting the platform to the desired resonant frequency and the mass of the vibration-proof object. MR elastomers based on silicone and magnetoactive micron-sized particles can be reversibly deformed and changed the modulus of elasticity under the action of the magnetic field. Devices based on them have the ability to work in all vibration isolation modes (passive, semi-active and active modes) and presented the analysis of experimental research of the active damper.

Key words

vibration isolation system, precision equipment, magneto-rheological elastomer, damper.

1 Introduction

One of the most effective ways to protect against vibration is active vibration isolation. It is widely known that the production of micro - and nanoelectronic devices are impossible without the protection of technological and research equipment operating in a vacuum and atmospheric pressure, vibration disturbing effects. Vibration isolation systems based on magnetorheological elastomers (MRE) have high vibration isolation efficiency in comparison with other existing systems by combining semi-active and active vibration isolation in one device. In the production of nano - and microelectronics products, precision analytical equipment is used: scanning probe (tunnel, atomic force, etc.) microscopes, optical microscopes, control, and measuring machines, etc. [1-3]. The external disturbances (vibrations), that reduces the degree of control and, especially, increase the error of scanning probes. To protect the equipment from vibration, the most effective way is the active vibration isolation [4,5]. In this project, we developed and presented the active damper based on magneto rheological elastomers, which allows for solving this problem. MRE are composite materials based on silicone and magnetoactive micron-sized particles. Such materials under the action of the magnetic field can be reversibly deformed and changed the modulus of its elasticity. These properties allow improving the damping in comparison with conventional viscoelastic systems. Besides, thanks to their dynamic characteristics of the active damper that operates as nano-precision actuator, determined by the time of transient processes when it is moved in different modes: step-by-step, continuous tracking or mode stabilizing the situation. The properties of MRE can be used to control the accuracy, dynamics, and amplitude frequency characteristics of the active damper. In developed countries, the systems of active vibration isolation and, in particular, a number of vibration tables based on piezoelectric transducers, which are characterized by an active frequency range from 5-13 Hz [4]. The viscoelastic vibration-insulating tables with negative stiffness [5] are also developed, which have the following characteristics: resonance frequency - 0.5 Hz; the transmission coefficient of the amplitude of vibration - 0.05; operating frequency range: 4-60 Hz; maximum load - 25 kg. The disadvantage of these tables is the low efficiency of vibration suppression (transmission coefficient of more than 0.1) at frequencies less than 4-5 Hz. Thus, the problem of creating an active vibration isolation system for operation in the low-frequency range from 0.5 to 200 Hz with a high degree of vibration suppression for precision equipment is extremely relevant. The advantages of active vibration isolation system using magnetorheological elastomers are a large range of displacements (up to 1 mm) compared to piezoelectric transducers and a more effective absorption of vibration energy, the capabilities of active control of amplitude-frequency characteristics with millisecond speed and nano-meter accuracy of displacements.

2 Fundamentals of MRE

To solve the technical problems in the modern highly organized technology such as robotics, mechanical engineering, medical technology, space technology and etc., required materials with a set of fundamentally new properties, which could be

controlled by the external influences of magnetic fields. To such class of materials, which received the name of "smart" or "intelligent" materials, which refers to the magneto-rheological elastomers, which are produced at the State Research Institute for Chemistry and Technology of Organoelement Compounds, GNIIKhTEOS. Using the dependence of the elastic, rheological, electrical and other properties from an external magnetic field, could be created sensors of magnetic and electric fields, controlled damping devices, car bumpers and so on.

2.1 Organization

In Bauman Moscow State Technical University at the Department "Electronic Technologies in Mechanical Engineering" is designed and manufactured experimental samples of active dampers and positioning and vibration isolation platform based on MRE.

The system based on the MRE investigated in this work is much easier and cheaper in the manufacture and maintenance of all of the aforementioned, contains fewer complex mechanical and electrical elements. The platform of active vibration isolation system consists of the lower and upper plates, four active dampers and four elastic suspension units with a mass corrector located at the corners of the platform as shown in Fig. 1. The key sign of the platform is the reduction of vibrations caused by external disturbances and coming from the environment. This equipment can operate in three modes of vibration isolation, active, semi-active and passive.

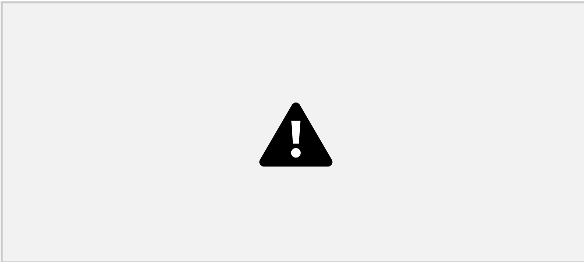

Passive vibration isolation is provided by a system with quasi-zero stiffness. The nodes of the elastic suspension with quasi-zero stiffness is a kind of pendulum, with a mass corrector and an elastic element. The system is based on the absorption of vibrations due to the fact that when forced vibrations appear, they are transmitted to the pendulum system located in the area of the quasi-zero stiffness of the previously selected spring, where the elastic force is close to zero with some movement of the object. The elements of the system support the platform at four points symmetrically with respect to the center of the moveable platform. This mechanism allows not only to reduce the amplitude of external influences due to the dynamic deformation of the spring elements, but also allows the working plane of the platform to isolate the object of greater mass. Semi-active and active vibration isolation is provided by a set of four damping elements (MR dampers), located symmetrically relative to the center of the platform and controlled by electromagnetic coil.

The main elements for the active damper include membrane 1 of MR elastomer with the movable rigid center 2, housing 3, electromagnetic coil 4, the core 5, the base 6. The core forms an air gap with a movable rigid center as shown in Fig. 2. When applying the external magnetic field, the membrane with the core is moved in the axial direction within the air gap.

In addition, the membrane is deformed and changes

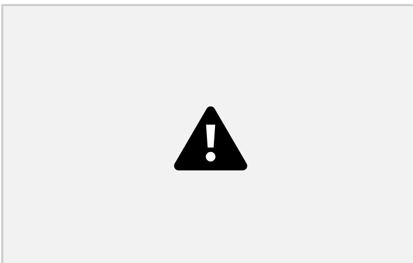

its stiffness and elastic modulus depending on the applied external magnetic field. So that, the active damper can work in the mode of active and semi-active vibration isolation. Without supplying a control current the active damper can be performed as a passive system of vibration isolation. MR elastomer absorbs the vibration energy due to its elastic properties.

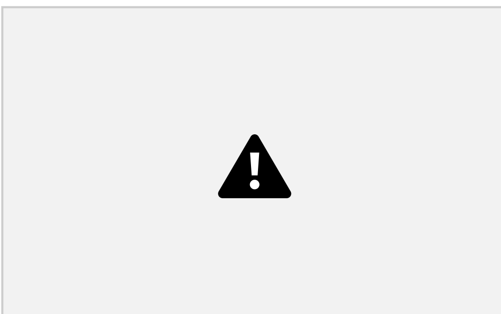

$$��_0 = 2 \cdot �� \cdot \sqrt{��}\ ��_1 \quad (1)$$

Where *J* - moment of inertia of the pendulum mass:

$$�� = �� \cdot ��^2 \quad (2)$$

From equation (1) we define:

$$��_1(��_0) = 4 \cdot ��^{2 \cdot ��}\ ��_{02} \quad (3)$$

For a pendulum with corrector:

$$��_0 = 2 \cdot �� \cdot \sqrt{��}\ ��_{1-��\cdot��\cdot��} \quad (4)$$

Where *R* – the distance from the center of mass $��_{��}$ to the axis.

From equations (1) and (3) we find:

$$��_{��} = {}^{4\cdot��2\cdot��}\ {}_{��\cdot��}\cdot\left({}^1��_{02} - {}^1��^2\right) \quad (5)$$

The adduced length of the pendulum will be equal to:

$$�� = ��_0 \cdot (1 + {}^{��\underline{��}}{}_{��}) \quad (6)$$

Angular stiffness:

$$��_1 = �� \cdot ��^2 \quad (7)$$

Spring stiffness from equations (3) and (7):

$$�� = {}^{4\cdot��\cdot��}\ ��^2 \cdot ��_{02} \quad (8)$$

Thus, the elastic suspension units allow to adjust the platform for active vibration isolation to the required mass of the object by the use of a spring with a stiffness *C* and a resonant frequency through the use of a mass corrector with a mass $��_{��}$.

3 The Results of Studies

The purpose of this work was studying of MR damper transition process quality, which involves determining parameters of the transition processes. Investigations of the damper were carried out for displacements of 50, 100 and 200μm.

For movement of the dampers in a closed control system is developed the control algorithm in the LabVIEW environment, which implemented the control algorithm according to the law of the integral controller (I-controller). During the experimental study, the position of the rigid center of the damper's membrane was measured depending on the time. According to the results of measurements, the parameters of transients are determined – the time of the transition process, the value of overshoot in the table. 1. Transient graphs were also plotted as shown in Fig. 4, 5, 6.

Table 1. Parameters of properties of transients

Transmission coefficient ��, V/μm	Displacement, μm	Transition time *t*, s	Deregulation%
0,002	50	0,20	2,7
	100	0,38	7,0
	200	0,31	11,5
0,005	50	0,16	15,5
	100	0,17	25,3
	200	0,24	42,8

0,010	50	0,19	35,4
	100	0,20	53,8
	200	0,26	107,0

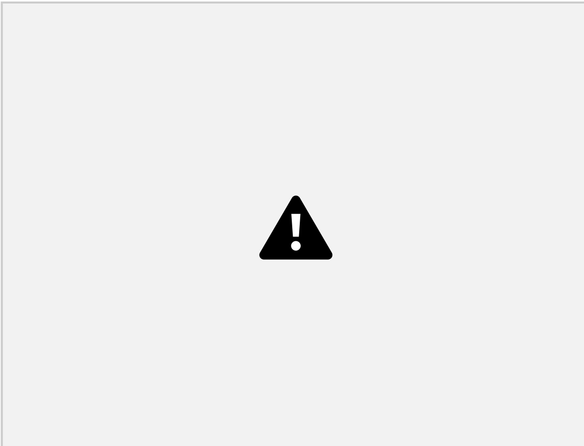

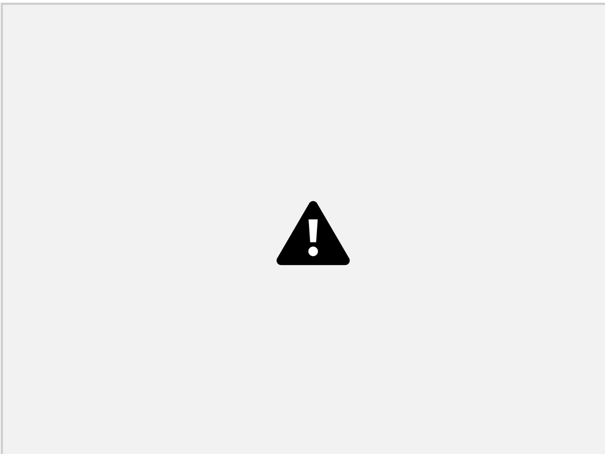

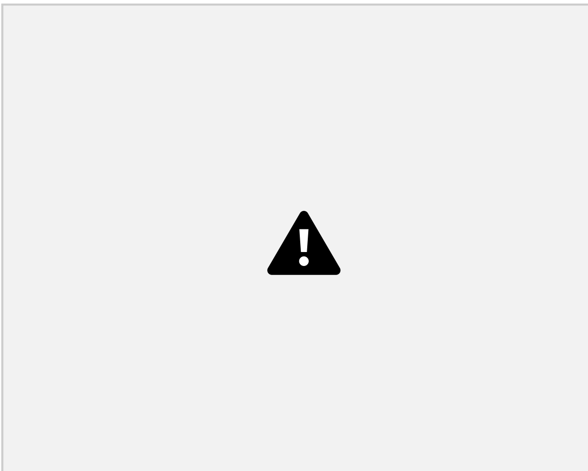

This study was performed within the framework of implementing the base part of the State project no. 9.8503.2017/8.9 of the Russian Ministry of Education and Science in the field of research.

References

Bykov, V.A. (2010). Tools of Nanotechnology Today and Tomorrow. Nano-industry. Special issue, pp. 10-14.

Borisenko, V.E., Vorobyeva, A.I., Utkin, E.A. (2009) Nanoelectronics. BEAN. Laboratory of knowledge. Moscow.

Popov, V.V., Saletsky, A.M. (2008). Nanomachinery, Possibilities and Prospects," Nanotechnologies in

4 Conclusion

As a result for this work, transient characteristics of MR damper were acquired for different displacements and control system parameters.

To reduce overshoot during positioning, the value of transmission coefficient can be decreased, but in this case transition time increases. If the value of transmission coefficient is too high, both transition time and overshoot increase. To minimize transition time, optimal value of transmission coefficient can be found.

The conducted study shows that the performance of the system can be enhanced by the improvement of the law of control system. To achieve the best performance when stabilizing the platform, it is also necessary to ensure the sufficient performance of the hardware part of the platform's control system.

Acknowledgements

Firstly, I would like to thank my supervisor Professor Valeriy Pavlovich Mikhailov for his advice, great encouragement, unselfish help and suggestions throughout this research. I am thankful to Associate Prof. Bazinenkov for the valuable advice and providing me with experimental facilities in laboratories for my research work. I am indebted to my many of my Russian friends and colleagues in the University BMSTU to support me.

Russia, no. 9-10, pp. 32-35.
Workstation Series, Active Vibration Isolation, Accurion. [Accessed: 02- Jun- 2017] [Online].Available: http://www.accurion.com/active vibration-isolation-products/workstations-series.
Minus K® Technology-Vibration Isolation. [Accessed: 09- Jun- 2017]. [Online].Available:http://www.minusk.com/products /bm8-vibration-isolation-platforms-bench-tops isolators.html.
Alabuzhev, P.M., Gritchin, A.A., Kim, L.I. (1986) Vibration-Protection System with Quasi-Zero Stiffness. K.M. Ragulskis (ed.), Mashinostroenie, Leningrad, p. 96, 1986.
Mikhailov, V.P., Tun Lin Aung, Kopylov, A.A., Tovmachenko, D.K. (2018) Platform for active vibration isolation of the precision equipment based on magnetorheological elastomers," 2018 IEEE Conference of Russian Young Researchers in Electrical and Electronic Engineering (EIConRus) pp. 1992-1995.
Mikhailov, V.P., Tovmachenko, D.K.,Bazinenkov, A.M., Stepanov, G.V. (2016) The Characteristics of the Platform for Active Vibration Isolation Based on Magnetorheological Elastomers," Proceedings of higher educational institutions, Mechanical Engineering, no. 12, pp. 51-57. [In Russian]

PHYSCON 2019, Innopolis, Russia, 8–11 September, 2019

GHOST ATTRACTORS IN THE NON-AUTONOMOUS BLINKING SYSTEMS

Nikita Barabash
Volga State University of Water Transport Nizhny Novgorod State University
Russia
barabash@itmm.unn.ru

Vladimir Belykh
Volga State University of Water Transport Nizhny Novgorod State University Russia
belykh@unn.ru

Abstract

2 The blinking model

Definitions of blinking systems and ghost attrac tor are given. As examples of such systems, the rotator-oscillator with switching torque and blinking piecewise-linear Lorenz model are considered. The pa rameter ranges of the ghost attractor existence for both examples are derived.

Key words

Blinking systems, a ghost attractor, stochastic switch ing, averaging

1 Introduction

The behaviour of a large number of living and tech nical systems can be represented as a process with instantaneous random changes in their structures. In networks of neurons and technical devices, interac tion between nodes may be a subject for such changes [Parastesh, Azarnoush, Jafari, et al.; Mills, 1991]. The behaviour of pulse power converters can be mod elled by a dynamical system, which parameters ran domly and independently change their values in a piecewise-constant manner implying switching [Tse and Di Bernardo, 2002]. In literature such random and independent switching have been called *blinking* by analogy to blinking of an eye [Belykh, Belykh and Hasler, 2004], and systems with such o sort of switch ing got the name *blinking systems*.

Later it turned out that the blinking systems may ex hibit non-trivial unexpected behaviour, which means, for example, the emergence of dynamics which is not met in each of the composing systems [Hasler, Belykh and Belykh, 2013b; Belykh, Belykh, Jeter et al., 2013; Belykh and Barabash, 2018]. The attracting set cor responding to this behaviour has been called *a ghost attractor*.

In this talk we give examples of such systems in which we managed to find ghost attractors, and also offer ways to find them in the general case.

We consider the blinking system [Hasler, Belykh and Belykh, 2013a; Barabash and Belykh, 2018]

$$\dot{x} = F(x, s(t)), \quad (1)$$

where $x \in \mathbb{R}^N$, $s(t)$ is a random discrete scalar value equalled a constant s_i, $i = 1, 2, \dots, M$ with the prob ability p_i at each k-th time interval $t \in [k\tau, (k+1)\tau)$, $k \in \mathbb{Z}^+$. Here $\tau = const$ is a switching period.

The trajectories of the system (1) are glued at $t = k\tau$ from the trajectories of M autonomous systems

$$\dot{x} = F(x, s_i), \; i = 1, 2, \dots, M, \quad (2)$$

given at each interval $t \in [k\tau, (k+1)\tau)$ with the prob ability p_i. We assume that each i-th N-dimensional system (2) considered at the whole interval of time has an attractor A_i.

We assume that the autonomous N-dimensional aver aged system of the form

$$\dot{x} = \sum_{i=1}^{M} p_i F(x, s_i), \quad (3)$$

has an attractor $\bar{A}$. (Note that averaging is correct for sufficiently small switching period τ 1 [Hasler, Be lykh and Belykh, 2013a].)

The problem of the interrelation between attractors A_i, $i = 1, 2, \dots, M$, and the attractor $\bar{A}$ we widely discussed in [Hasler, Belykh and Belykh, 2013b]. Here we consider a particular case of the *ghost attractor* [Be lykh, Belykh, Jeter et al., 2013; Belykh and Barabash, 2018].

Definition. If the averaged system (3) is not topologi cally conjugated to any i-th autonomous system (2) and the attractor $\bar{A}$ is missing among A_i, then $\bar{A}$ we call the ghost attractor.

In this talk we consider different examples of blinking systems including for example Lorenz system. More over we formulate the rule how to obtain different ghost attractors.

3 Blinking rotator-oscillator

Here as an example we consider the equation of blink ing nonlinear rotator-oscillator

$$\ddot{\phi} + (\lambda - a\cos\phi)\dot{\phi} + \sin\phi = s(t), \quad (4)$$

where ϕ is the phase of oscillator, λ and a are positive parameters and $s(t)$ is a randomly switching function which is chosen as $s_1 = \gamma$, $s_2 = -\gamma$ with probabilities $p_1 = p_2 = \frac{1}{2}$. Here γ is a positive constant.

We consider the small switching period τ 1. In this case the system (4) can be averaged over a fast time $t = \frac{t}{\tau}$ and the random function $s(t)$ can be replaced by its average time value $s(t)_t = 0$. Thus, the averaged system corresponds to the case of the system (4) with $s(t) \equiv 0$.

4 Autonomous oscillator

Consider the case of fixed values of the switching function $s(t) \equiv \gamma$. The system (4) gets the form of the autonomous modified non-linear oscillator

$$\ddot{\phi} + (\lambda - a \cos \phi) \dot{\phi} + \sin \phi = \gamma. \quad (5)$$

This system is invariant under involution $\phi \to -\phi$, $\dot{\phi} \to -\dot{\phi}$, $\gamma \to -\gamma$, that allows us to consider only upper phase semi-cylinder $\dot{\phi} > 0$ without loss of gen erality.

The partition of the parameter space $D : \gamma, \lambda, a$, whose domains correspond to different partitions of the phase space, was considered in [Belyustina and Be lykh, 1973].

The system (5) has two equilibria: the fixed point $O_e(\arcsin \gamma, 0)$

For $\gamma = 0$ and $\lambda_h < \lambda < a$, where λ_h is the sym metrical homoclinic bifurcation, the system (5) has the globally stable oscillating limit cycle O_c (Fig. 1, up per).

For $|\gamma| > 1$ the system has no equilibrium, no oscil lating cycles and has the globally stable rotating cycle O_r (Fig. 1, bottom).

Hence, the attractor A_1 is the globally stable rotating cycle O^+_r in the region $\dot{\phi} > 0$ ($\gamma > 1$), the attractor A_2 is the globally stable rotating cycle O^-_r in the region $\dot{\phi} < 0$ ($\gamma < -1$), and the attractor $\bar{A}$ is the globally stable oscillating limit cycle O_c ($\gamma = 0$).

Hence, according to definition $\bar{A}$ is the ghost attractor of the blinking system (4).

The interesting question on the system (4) behaviour for non-small period τ arises. In order to obtain an an swer to this question we present the result of numerical

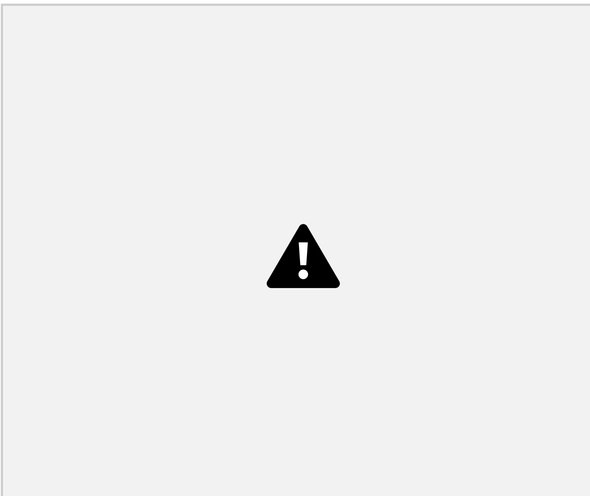

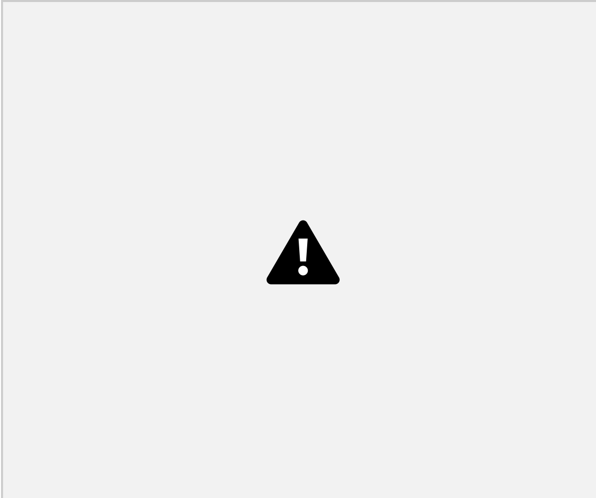

Figure 1. Phase pictures of the autonomous system (5). (Upper) The globally stable oscillating cycle O_c for $\gamma = 0$. (Bottom) The globally stable rotating cycle O^+_r for $\gamma = 1.2$. Note, that for $\gamma = -1.2$, the stable rotating cycle O^-_r is odd symmetric to O^+_r and lies in the bottom phase semi-cylinder $\dot{\phi} < 0$. The parameters: $\lambda = 0.75$, $a = 1$.

modelling. In Fig. 2 the phase pictures of the blink ing system (4) for two periods $\tau = 0.01$ (upper) and $\tau = 0.07$ are shown. The globally sable limit cycle O_c (red in Fig. 2) of the averaged system (the system (5) for $\gamma = 0$) acts like a ghost attractor of the blink ing system (4), and the non-wandering trajectory of the stochastic dynamical process (blue in Fig. 2) lies in the neighbourhood of O_c. The size of this neighbourhood tends to zero with decreasing $\tau \to 0$ and vice versa: for some threshold switching period's value $\tau > \tau^*$ the probability of leaving of the blinking system's trajec tory to one of the rotational cycles $O^{\pm}_r$ becomes suffi ciently large.

5 Conclusion

In our talk, certain blinking systems with ghost attrac tors are presented. For this systems, we analytically obtained conditions for the ghost attractor existence.

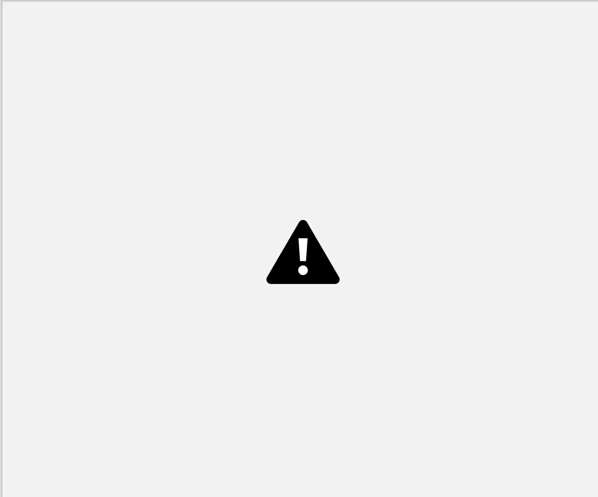

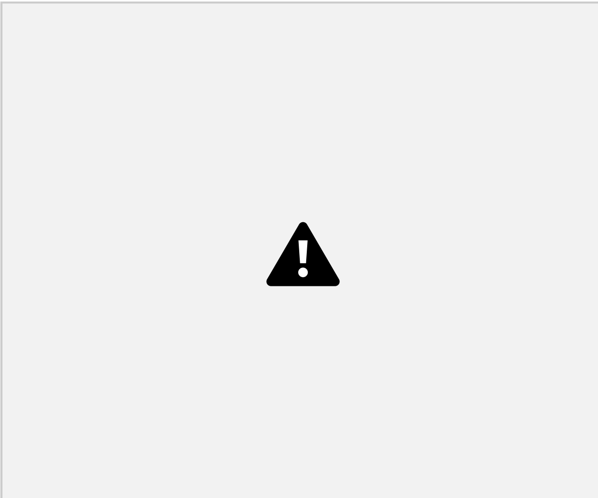

Figure 2. Non-wandering trajectories of the blinking system (4). Blue is the shift mapping along trajectories of the system (4) in pe riod τ . Red is the stable limit cycle O_c of the averaged system (the system (5) for $\gamma = 0$) which acts like a ghost attractor of the blinking system. Switching periods are $\tau = 0.01$ (upper) and $\tau = 0.07$ (bottom). A longer switching period τ corresponds to a larger neighbourhood of the ghost attractor O_c, in which the non stationary attracting set of the blinking system lies. The parameters: $\lambda = 0.75$, $a = 1$.

The open question about the nature of the system's behaviour under slow switching is discussed.

Acknowledgements

This work was supported by the Russian Foundation for Basic Research (the project No. 18-01-00556, ana lytical results) and the Russian Science Foundation (the project No. 19-12-00367, numerical results).

References

Parastesh, F., Azarnoush, H., Jafari, S., Hatef, B., Perc, M. and Repnik, R. (2019). Synchronizability of two neurons with switching in the coupling. *Applied Mathematics and Computation*, Vol. 350, pp. 217- 223.

Mills, D. L. (1991) Internet time synchronization: the network time protocol.*IEEE Transactions on Commu nications*, Vol. 39, No. 10, pp. 1482-1493.

Tse, C. and Di Bernardo, M. (2002) Complex behav ior in switching power converters. *Proc. IEEE*, Vol. 90, No. 5, pp. 768-781.

Belykh, I., Belykh, V. and Hasler, M. (2004) Blinking model and synchronization in small-world networks with a time-varying coupling. *Physica D*, V. 195/1-2, pp. 188–206.

Hasler, M., Belykh, V. and Belykh, I. (2013a) Dynam ics of stochastically blinking systems. Part I: Finite time properties. *SIAM Journal on Applied Dynamical Systems*, Vol. 12, No. 2, pp. 1007–1030.

Hasler, M., Belykh, V. and Belykh, I. (2013b) Dynam ics of stochastically blinking systems. Part II: Asymp totic properties. *SIAM Journal on Applied Dynamical Systems*, Vol. 12, No. 2, pp. 1031–1084.

Barabash, N. V. and Belykh, V. N. (2018) Synchro nization Thresholds in an Ensemble of Kuramoto Phase Oscillators with Randomly Blinking Cou plings. *Radiophysics and Quantum Electronics*. Vol. 60, No. 9, pp. 761–768.

Belyustina, L. N. and Belykh, V. N. (1973) Qualitative analysis of dynamic systems in a cylinder, *J. Differen tial Equations* (in Russian) Vol. 9, pp. 403–415. Belykh, I., Belykh, V., Jeter, R. et al. (2013) Multi stable randomly switching oscillators: The odds of meeting a ghost. *Eur. Phys. J. Spec. Top.*, Volume 222, Issue 10, pp. 2497–2507.

Belykh, V. and Barabash, N. (2018) Ghost attractor in randomly blinking phase system. *Proc. 20th Int. Scientific and Industrial Forum "Great Rivers 2018"* Nizhny Novgorod, Russia, May 15-18.

MULTISTABLE CLUSTER RHYTHMS IN NETWORKS OF COUPLED ROTATORS

Barrett Brister
Department of Mathematics and Statistics Georgia State University
Atlanta, USA
bbrister1@student.gsu.edu

Vladimir N. Belykh
Department of Mathematics
Volga University of Water Transport Nizhny Novgorod, Russia
belykh@unn.ru

Igor Belykh
Department of Mathematics and Statistics
Georgia State University
Atlanta, USA
ibelykh@gsu.edu

Abstract

In this paper, we study the co-existence of stable pat terns of synchrony in two coupled populations of iden tical rotators which are represented by Kuramoto oscil lators with inertia. The two populations have different sizes and can split into two clusters where the oscilla tors synchronize within a cluster while there is a phase shift between the dynamics of the two clusters. Due to the presence of inertia, which increases the dimension ality of the oscillator dynamics, this phase shift can os cillate, inducing a breathing cluster pattern. We review our recent analytical results on the co-existence of sta ble two-cluster patterns with constant and oscillating phase shifts. We demonstrate that the dynamics, that governs the bistability of the phase shifts, is described by a driven pendulum equation. We also demonstrate how inertia affects the hysteretic transitions between the patterns.

Key words
Synchronization, clusters, Kuramoto model, inertia, multistability.

1 Introduction

Patterns of synchronized clusters are observed in many networks, ranging from neuronal populations to power grids. Two important cooperative rhythms of pattern dynamics are complete and cluster synchro nization. Complete synchronization, in which all os cillators evolve in unison, and its dependence on net work structure have received a great deal of atten tion in the literature [Pecora and Carroll, 1998; Boc caletti, Kurths, Osipov, Valladares, and Zhou, 2002; Belykh, Belykh, Hasler, 2004]. Cluster synchroniza tion is observed when the network splits into groups of coherent oscillators but the dynamics between the groups is asynchronous [Belykh, Belykh, Hasler, 2000; Pogromsky, Santoboni, and Nijmeijer, 2002; Pecora, Sorrentino, Hagerstrom, Murphy, and Roy, 2014].

Despite significant interest among physicists and ap plied mathematicians, the emergence and hysteretic transitions between stable clusters in a network of iden tical oscillators have still not been fully understood. In particular, the celebrated Kuramoto model of iden tical phase oscillators is known to exhibit multiple spatio-temporal patterns, including co-existing clusters of synchrony and chimera states in which some oscil lators form a synchronous cluster, while the others os cillate asynchronously. Rigorous analysis of the stabil ity of clusters and chimeras in the finite-size Kuramoto model has proven to be challenging, and most existing results are numerical.

The classical Kuramoto model is a network of 1-D phase oscillators with mean-field coupling [Kuramoto, 1975; Pikovsky, Rosenblum, and Kurths, 2001]. The oscillators are assumed to be non-identical with differ ent natural frequencies, whose distribution is defined by a given probability density function. The model has a coupling threshold such that the oscillators, evolving incoherently for a weak coupling, synchronize when the coupling exceeds the threshold. Transitions from the incoherent state to various forms of partial fre quency synchronization, measured by an order parame ter, have been studied in the Kuramoto model with dif ferent regular and random coupling configurations (see a review paper [Acebron, Bonilla, Perez Vicente, Ri tort, and Spigler, 2005] for more details).

Inspired by the adaptive frequency model of firefly synchronization [Ermentrout, 1991] where the oscilla

32

tors are capable of adjusting their natural frequencies, the classical Kuramoto model of 1-D phase oscillators was extended to a model of 2-D oscillators with inertia [Tanaka, Lichtenberg, and Oishi, 1997] also known as *rotators*. This Kuramoto model with inertia was shown to exhibit various synchronization transitions [Tanaka, Lichtenberg, and Oishi, 1997; Li, Peron, Ridrigues, and Kurth, 2014] and hysteristic phenomena [Olmi, Navas, Boccaletti, and Torcini, 2014], including inter mittent chaotic chimeras [Olmi, 2015]. Existing an alytical studies of the collective dynamics of the Ku ramoto model with inertia mainly aim at (i) the stability of complete synchronization [Dorfler and Bullo, 2011] and (ii) bifurcations leading to its loss [Belykh, Bolo tov, and Osipov, 2015].

In this paper, we go further to analyze the co-existence of stable patterns of synchrony in two symmetrically coupled populations of identical Kuramoto oscillators with inertia. We derive exact results on the stability of a two-cluster synchronous state in which the popula tion splits into two clusters of synchronized oscillators, but there is no synchrony between the clusters. We re duce the system, governing the dynamics of the phase shift between the clusters, to the pendulum equation. As a result, the phase shift between the clusters can remain constant or can periodically rotate its phase, de pending on the choice of initial conditions. This yields the bistability of patterns of synchrony where a pattern with a constant inter-cluster phase shift stably co-exists with a breathing pattern when the inter-cluster phase shift evolves in time.

2 The model

Following previous studies in networks of Kuramoto models without [Panaggio, Abrams, Ashwin, and Laing, 2016] and with inertia [Olmi, 2015], we con sider a two-group network of 2-D rotators

$$m\ddot{\theta}_i + \dot{\theta}_i = \omega + \frac{\mu}{N+M}\sum_{j=1}^{N}\sin(\theta_j - \theta_i - \alpha) + \frac{\nu}{N+M}\sum_{j=1}^{M}\sin(\phi_j - \theta_i - \alpha),\ i = 1, ..., N$$

$$m\ddot{\phi}_k + \dot{\phi}_k = \omega + \frac{\mu}{N+M}\sum_{j=1}^{M}\sin(\phi_j - \phi_k - \alpha) + \frac{\nu}{N+M}\sum_{j=1}^{N}\sin(\theta_j - \phi_k - \alpha),\ k = 1, ..., M. \quad (1)$$

Here, the network is divided into two groups of oscil lators of sizes N and M, with all-to-all

inertia as the individual cell model and consider non equal group sizes. These two properties will allow for deriving analytical conditions on the stability of clus ters of synchrony, exhibiting two types of co-existing behavior where (i) the phase between the synchronized clusters remains fixed and (ii) the phase between the clusters oscillates.

Figure 1. The network (1) is composed of two uneven groups of sizes M and N. Oscillators within each population group are glob ally connected to each other through intra coupling μ. Inter-group coupling ν provides global connections between the oscillators from the two groups. $\gamma = \nu/\mu \le 1$.

By rescaling time $\tau = \mu t/(N + M)$ and parameter $\beta = \mu m/(N + M)$, and using a rotating frame of ref erence $\Theta_i = \theta_i - \omega t + c$, $\Phi_k = \phi_k - \omega t + c$, where c is a constant, we can cast the model (1) into a more compact form

$$\beta\ddot{\Theta}_i + \dot{\Theta}_i = \sum_{j=1}^{N}\sin(\Theta_j - \Theta_i - \alpha) + \gamma\sum_{j=1}^{M}\sin(\Phi_j - \Theta_i - \alpha),\ i = 1, ..., N$$

$$\beta\ddot{\Phi}_k + \dot{\Phi}_k = \sum_{j=1}^{M}\sin(\Phi_j - \Phi_k - \alpha) + \gamma\sum_{j=1}^{N}\sin(\Theta_j - \Phi_k - \alpha),\ k = 1, ..., M, \quad (2)$$

where $\gamma = \nu/\mu$ represents the ratio between the intra and intergroup couplings such that $\gamma \in (0, 1)$.

3 Existence of synchronous clusters

In general, clusters of perfect synchrony are deter symmetrical coupling within and between the two groups, such that the intragroup coupling strength, μ, is stronger than or equal to the intergroup coupling strength, v (see Fig. 1). Variables θ_i and ϕ_k represent the phases of oscillators in the first and second groups, respectively. The oscil lators are assumed to be identical, with identical fre quency ω, phase lag $\alpha \in [0, \pi/2)$ and inertia m. In the model (1), we use the 2-D Kuramoto oscillator with

mined by a network decomposition into the disjoint subsets of oscillators $V = V_1 \cup ... \cup V_d$, $V_p \cap V_q = \varnothing$ defined by the equalities of the oscillator states. If this cluster decomposition is flow-invariant with respect to the vector field of the network system, then the corre sponding manifold $D(d)$ is invariant and defines d syn chronous clusters. In the context of the network (2), a necessary condition for oscillators to form a cluster is the equal row sum constraint. As a result, the mini mal cluster partition has two colors. The corresponding

cluster synchronization manifold

$$D(2) = \{\Theta_1 = ... = \Theta_N = \Theta, \dot\Theta_1 = ...\dot\Theta_N = \dot\Theta, \Phi_1 = ... = \Phi_M = \Phi, \dot\Phi_1 = ...\dot\Phi_M = \dot\Phi\} \quad (3)$$

defines two clusters of synchrony. As the two groups of oscillators are formed by all symmetrical all-to-all networks, all other combinations of cluster partitions within the two clusters are also possible. Note that complete synchronization is impossible in the network (2) as $N = M$ and the equal row sum constraint is not respected. In the following, we will focus on the dynamics on the two-cluster synchronization manifold $D(2)$ and the conditions of its transversal stability.

obtained from the system (2) by omitting the subscripts i, j and k.

cos $\alpha^N{}_{j=1}$

We introduce the difference variable $x = \Phi - \Theta$ and subtract the first from the second equation in (4) and use simple trigonometric formulas to obtain the differ ence variable system

$$\beta\ddot{x} + \dot{x} = \Omega - R\sin(x + \delta), \quad (5)$$

where $\Omega = (N - M)\sin\alpha$, $\Omega = \tilde{}\ \frac{N^2 + M^2}{N}$, and $\delta = \arctan \frac{1-\kappa}{1+\kappa}\tan\alpha$, with $\kappa = M/N$. The shift $x + \delta \to x$ transforms the system (5) into the equation

$$\beta\ddot{x} + \dot{x} + R\sin(x) = \Omega \quad (6)$$

which governs the difference dynamics between the cluster. The equation (6) happens to be the

4 Dynamics on the cluster manifold

The dynamics on the manifold $D(2)$ is defined by the following 4-D system

$$\beta\ddot\Theta + \dot\Theta = -N\sin\alpha + \gamma M\sin(\Phi - \Theta - \alpha)\ \beta\ddot\Phi + \dot\Phi = -M\sin\alpha + \gamma N\sin(\Theta - \Phi - \alpha) \quad (4)$$

$T(h)$ as an approximation of the Tricomi

curve: $T(h) = \frac{4}{\pi}h - 0.305h^3 = \frac{4}{\pi}\sqrt{\beta R} - 0.305(\beta R)^{-3/2}$. (7)

In terms of the intercluster dynamics, the stable equi librium $x_e = \arcsin\frac{\Omega}{R} - \delta$ and a stable limit cycle $x_c(t)$ yields two cluster regimes with a constant phase shift between the clusters $x_e = \arcsin\frac{\Omega}{R} - \delta$ and an oscillating shift $x_c(t)$, respectively. The conditions on their stable co-existence can be found in [Belykh, Bris ter, Belykh, 2016].

5 Stability of clusters

To demonstrate that the synchronous clusters can sta bly appear in the network (2), we will prove the transversal stability of the cluster manifold $D(2)$. Lin earizing the network system (2) about the synchronous cluster solution (3) $(\Theta, \dot\Theta, \Phi, \dot\Phi)$, we obtain the vari ational equations for the local stability of the cluster manifold $D(2)$

$$\beta\ddot\xi_i + \dot\xi_i = -(N\cos\alpha + \gamma M\cos(x_s - \alpha))\,\xi_i + \cos\alpha\sum_{j=1}^{N}\xi_j + \gamma\cos(x_s - \alpha)\sum_{j=1}^{M}\eta_j,\ i = 1, .., N$$

$$\beta\ddot\eta_k + \dot\eta_k = -(M\cos\alpha + \gamma N\cos(x_s + \alpha))\,\eta_k + \cos\alpha\sum_{j=1}^{M}\eta_j + \gamma\cos(x_s + \alpha)\sum_{j=1}^{N}\xi_j,\ k = 1, .., M. \quad (8)$$

Here, ξ_i is an infinitesimal perturbation of the i-th os cillator's synchronous solution in the larger N-cluster, and η_k corresponds to the smaller M-cluster. x_s is the cluster phase shift as defined above.

We then introduce the difference variables

$$u_i = \xi_i - \xi_{i+1},\ i = 1, ..., N - 1$$

equation of a pendulum, with a constant torque Ω, [Andronov, Vitt, and Khaikin, 1966]. Its dynamics on the cylinder (x mod2π, $\dot{x} = v$) are known to exhibit various inter esting dynamical regimes, including bistability where the stable equilibrium $x_e = \arcsin \frac{\Omega}{R} - \delta$ co-exists with a stable limit cycle $x_c(t)$. The curve $\Omega/R = 1$ corre sponds to a saddle-node bifurcation of equilibria. The

curve $\Omega/R = T(h)$ with $h = 1/\sqrt{\beta R}$ is the Tricomi curve that indicates a homoclinic bifurcation of the sad dle where the homoclinic orbit encircles the cylinder and forms a saddle connection. The two curves meet at $h^* \approx 1.22$ [Andronov, Vitt, and Khaikin, 1966]. While the closed-form derivation of the Tricomi curve is not available, we suggest the following nonlinear function

$$w_k = \eta_k - \eta_{k+1},\ k = 1, .., M - 1 \quad (9)$$

whose convergence to zero will imply the transversal stability of $D(2)$. Subtracting the $(i+1)$-th [$(k+1)$- th] equation from the i-th [k-th] equation in system (8), we obtain the variational equations for the transversal stability:

$$\beta \ddot{u}_i + \dot{u}_i + q_1 u_i = 0,\ i = 1, ..., N - 1 \quad (10a)$$
$$\beta \ddot{w}_i + \dot{w}_i + q_2 w_i = 0,\ i = 1, ..., M - 1, \quad (10b)$$

where $q_1 = N c + M c^- = N \cos\alpha + \gamma M \cos(x_s - \alpha)$ and $q_2 = N c^+ + M c = N \gamma \cos(x_s + \alpha) + M \cos\alpha$. Note that the equations (10a) and (10b) are uncoupled. The analysis of the stability equations (10a)-(10b) leads to the following assertions.

Theorem 1. [Belykh, Brister, Belykh, 2016]. *Let the parameters satisfy the condition $\Omega/R < 1$, then the cluster solution (3) $(\Theta, \dot{\Theta}, \Phi, \dot{\Phi})$ with the constant*

phase shift x_e is locally stable iff

$$\alpha < \alpha^{cr}, \quad (11)$$

where the critical value α^{cr} is the solution of the equa tion

$$q_2 = \gamma \cos(x_e + \alpha) + \kappa \cos\alpha = 0. \quad (12)$$

Here, $\gamma \in (0, 1)$ is the coupling ratio, $x_e = \arcsin \frac{\Omega}{R} - \delta$, $\kappa = M/N$, and $\alpha \in [0, \alpha^*)$, where $\alpha^* = \arctan \frac{1-\kappa}{1+\kappa}\frac{\sqrt{1-\gamma^2}}{\gamma}$. Positive values of q_2 correspond to $\alpha < \alpha^{cr}$ and define the stability of the cluster solution. The conditions of Theorem 1 for $q_2 > 0$ demon strate that the stable cluster with a constant shift ex ists in a wide region of parameters *α, γ, κ.* For exam ple, in the region of $\kappa = 0.8$, $\alpha \in [0, 1.26056)$ and $\gamma \in [0, 0.3275)$, the cluster with a constant shift re mains stable as long as it exists.

Theorem 2. [Stability of the breathing cluster solu tion] (sufficient conditions). *Let the parameters sat isfy the condition: $\Omega/R > T(h)$ (see Fig. 1) such that the system (5) has a stable limit cycle which de termines the oscillating phase shift $x_c(t)$ between two clusters. Then, the cluster solution (3) $(\Theta, \dot{\Theta}, \Phi, \dot{\Phi})$ with the phase shift x_c in the network system (2) is lo cally stable to transversal perturbations if*

$$\kappa \cos\alpha > \gamma,\ 1 - 4\beta N(k \cos\alpha - \gamma) > 0. \quad (13)$$

Proof. The proof is given in [Belykh, Brister, Belykh, 2016].

6 Bistability and histeretic transitions

As the emergence of stable clusters and chimeras is easier to demonstrate in large Kuramoto networks with out [Panaggio, Abrams, Ashwin, and Laing, 2016] and with inertia [Olmi, 2015], where the dynamics is close to its mean-field approximation, we knowingly choose the harder case of a small network (2) with $N = 5$ and $M = 4$ as our numerical example. Figure 2 demon strates co-existing stable clusters with a constant and periodically oscillating phase shifts for $\alpha = \pi/3$ and $\beta = 20$. In Fig. 2(top), we present a snapshot of the established cluster pattern. The oscillators in the first five- and second four-oscillator groups synchro nize within the two clusters, and there is always a phase shift between the two synchronized groups. Depending on the initial conditions, the network exhibits either the two-cluster pattern with a constant inter-cluster phase shift or a breathing two-cluster pattern where the phase shift oscillates. While the static snapshot of Fig. 2(top) does not allow for identifying the dynamics of the phase shift, it actually corresponds to the breathing cluster with the oscillating phase shift x_c, (red wave form depicted in Fig. 2(middle)). Figure 2(middle) in dicates the bistability of the two patterns of synchrony starting from random non-equal initial conditions close to the cluster solution. Figure 2(bottom) shows the co existence of the two dynamics for the phase shifts. To explicitly define the phase shift x between the clusters, in Fig. 2(bottom), we set all initial conditions for the oscillators in the first five-oscillator cluster to zero, and for the oscillators in the second four-oscillator cluster to the same set of values $x, \dot{x}$. Thus, the initial differ ence between the cluster variable determines the ini tial phase shift x. Note that different initial conditions (points A and B) induce different phase shifts.

7 Conclusion

In this paper, we have discussed the stability of clus ters in two coupled populations of identical rotators. This network is essentially the two-population Ku ramoto model[Panaggio, Abrams, Ashwin, and Laing, 2016], proposed as a simple model of chimeras. The new important modifications, which are vital for bista bility of cluster patterns in our network, are (i) non equal population sizes and (ii) the addition of inertia to the oscillator equation. Property (i) makes the exis tence of complete synchronization impossible such that a two-cluster pattern is the minimal cluster partition in this two-population network, although other multi cluster partitions are also possible. Property (ii) in creases the dimensionality of the intrinsic oscillator dy namics and creates a possibility for bistability of cluster patterns.

We have rigorously analyzed the dynamical properties and stability of the two-cluster pattern where the pop ulation splits into two synchronized groups, but there is always a phase shift between the groups. We have explicitly demonstrated that the dynamics of the phase shift can be bistable such that a constant phase shift co-exists with a time-varying shift which periodically changes from 0 to 2π. As a result, a two-cluster pat tern with a constant shift co-exists with a breathing two-cluster pattern with an oscillating phase shift. We have derived the stability conditions for the stability of the cluster patterns. Due to the simple structure of the two-population network, the stability conditions for the variables, corresponding to the first and sec ond populations, are independent. Therefore, the in stability of synchrony within one group does not im mediately imply the instability within the other group. In more rigorous terms, the cluster solution becomes a saddle such that stable transversal directions corre spond to the first (larger) group of oscillators whereas unstable transversal directions correspond to the oscil lators from the second (smaller) group. The stabil ity result can be interpreted in terms of multidimen sional clusters and chimeras. It can lead to the emer gence of stable multi-cluster states, where the oscilla tors in the smaller population split into subgroups. Rig orous study of the transition from lower dimensional to high-dimensional cluster regimes, governed by the symmetry-induced embedding hierarchy [Belykh, Be

π

π

π

π

π

π

π

π

Acknowledgements
The part of the work related to the constant phase shift was supported by the Russian Foundation for Basic Re search under Grant No. 18-01-00556 (to V.B.); the part related to the

oscillating phase shift was supported by the Russian Science Foundation under Grant No. 19- 12-00367 (to V.B.). This work was also partially sup ported by the National Science Foundation (USA) un der Grant No. DMS-1616345 (to B.B. and I.B.).

References

Pecora, L.M. and Carroll, T.L. (1998) *Phys. Rev. Lett.*, 80, 2109.
Boccaletti, S., Kurths, J., Osipov, G., Valladares, D.L., and Zhou, C.S. (2002) *Phys. Reports*, 366,
1. Belykh, V.N., Belykh, I.V., and Hasler, M. (2004) *Physica (Amsterdam)*, 195D, 159.
Belykh, V.N., Belykh, I.V., and Hasler, M. (2000) *Phys. Rev. E*, 62, 6332.
Pogromsky, A.Yu., Santoboni, G., and Nijmeijer, H. (2002) *Physica (Amsterdam)*, 172D, 65.
Belykh, I., Belykh, V., Nevidin, K., and Hasler, M. (2003) *Chaos*, 13, 165.
Pecora, L.M., Sorrentino, F., Hagerstrom, A.M., Mur phy, T.E., and Roy, R. (2014) *Nature Commun.*, 5, 4079.
Kuramoto, K. in Araki, H. (Editor) (1975) *Interna tional Symposium on Mathematical Problems in The oretical Physics, Lecture Notes in Physics*, 39, 420. Springer-Verlag, Berlin.
– –
Pikovsky, A., Rosenblum, M., and Kurths, J. (2001). *Synchronization, A Universal Concept in Nonlinear Sciences*. Cambridge University Press, Cambridge. Acebron, J.A., Bonilla, L.L., Perez Vicente, C.J., Ri

−π −π π π

Figure 2. (Top). Snapshot of the synchronized two-cluster pattern in the network (2) for $\alpha = \pi/3$ and $\beta = 20$. Initial condi tions are chosen close to the cluster manifold and correspond to the breathing cluster pattern. (Middle). Corresponding time series of the co-existing phase shifts x_e and $x_c(t)$, robustly appearing from non identical random initiation conditions, close to the cluster manifold. (Bottom). Co-existence of the constant (x_e) and oscillating phase shifts ($x_c(t)$), determined by the fixed point (depicted in white) and the stable limit cycle (depicted in red), respectively. Initial conditions are chosen on the cluster manifold. Trajectories starting from initial conditions A and B converge to different attractors (the fixed point and limit cycle). Basins of attraction of the fixed point and the limit cycle are shown in black and white, respectively.

Ermentrout, B. (1991) *J. Math. Biol.*, 29, 571.
Tanaka, H.-A., Lichtenberg, A.J., and Oishi, S. (1997) *Phys. Rev. Lett.*, 78, 2104.
Li, P., Peron, T.K.D.M., Ridrigues, F.A., and Kurths, J. (2014) *Scientific Reports*, 4, 4783.
Olmi, S., Navas, A., Boccaletti, S., and Torcini, A. (2014) *Phys. Rev. E*, 90, 042905.
Olmi, S. (2015) *Chaos*, 25, 123125.
Dorfler, F. and Bullo, F. (2011) *SIAM J. Appl. Dynam. Sys.*, 10, 1070.
Belykh, V.N., Bolotov, M.I., and Osipov, G.V. (2015) *Modeling and Analysis of Information Systems*, 22, 595.
Panaggio, M.J., Abrams, D.M., Ashwin, P., and Laing, C.R. (2016) *Phys. Rev. E*, 93, 012218.
Andronov, A.A., Vitt, A.A. and Khaikin, S.E. (1966). *Theory of Oscillations*. Pergamon, New York. Belykh, I., Brister, B., and Belykh, V.N. (2016) *Chaos*, 26, 094822.

lykh, Hasler, 2000] and accompanied by multistability of patterns of synchrony is a subject of future study.

tort, F., and Spigler, R. (2005) *Rev. Mod. Phys.*, 77, 137.

Control methods to enhance pointing accuracy of an antenna servo system on a carrier under large disturbance

Yongdong Cheng
State Key Laboratory for Strength and Vibration Xi'an Jiaotong University
China
cheng.yong.dong@stu.xjtu.edu.cn

Abstract

In this paper, control strategies and vibration isolation methods are investigated in order to enhance the attitude control accuracy of an antenna servo system on a carrier under large disturbance. First, the multi body dynamical equations of the antenna servo system on a carrier incorporated with six wire-cable vibration isolators with hysteretic characteristics of restoring forces are derived. Then, an improved adaptive variable-rated exponential reaching law is proposed, and the non-singular terminal sliding mode control is designed. Finally, simulations are carried out and results show that excellent control accuracies for both

the azimuth and the pitch of the antenna can be achieved by the proposed control method.

Keywords

Antenna servo system, adaptive reaching law, non singular terminal sliding mode control

1 Objectives

Communication in motion is a kind of communication technology that transmits information uninterruptedly in real-time on moving vehicles (carriers). The key point to realize a stable and accurate communication is to control the attitude angles of the antenna accurately through the antenna servo system. Since it is free from dynamical models of antenna servo systems, the main control method

Jun Jiang
State Key Laboratory for Strength and Vibration Xi'an Jiaotong University
China
jun.jiang@xjtu.edu.cn

A A A A A M t q M R - ( )sin

⌈ ⌉ ⌈ ⌉ ⌈ + ⌉ ⌈ ⌉ α

| | | | | | +

α α α α α α α 1 2 3 4 5 3 2

A A A A A M t q M R ( )cos

adopted by now is the traditional PID method [Debruin, 2008; Fan and Wang, 2015]. However, PID is difficult to always achieve the required accuracy, especially when the carrier is under large outside disturbance. In this paper, the multi-body dynamical

| | | | | | |||||⌋

β

β β β β β β β 1 2 3 4 5 3 2

| | | | | = + + + | | A A A q F m m m g R

0 0 - ( )

| | | | | |

11 12 13 1 1 2 3 1 A A A q M t R

0 0 ( )

| | | | | | 21 22 24 2 2 2 | | | | | | ⌊ ⌋ ⌊ ⌋ ⌊ ⌋ ⌊

A A A q M t R

0 0 ( )

31 32 35 3 3 3

equations of an antenna servo system on a carrier under disturbance are build. An improved adaptive variable-rated exponential reaching law is proposed, and the non-singular terminal sliding mode control is designed. These works contribute to enhance pointing accuracy of the antenna servo system

2 Methods

The system is shown in Figure 1. The whole system is simplified into four rigid bodies ( ).

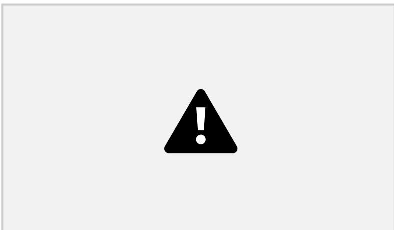

Figure 1. The antenna servo system.

represents the carrier, not depicted in Figure. 1. is the vibration isolation equipment that consists of six wire-cable vibration isolators. The isolators own the hysteretic characteristic of resilience-displacement. There are three degrees of freedom for : is the vertical translation displacement of to , while and are the horizontal rotation displacements.

is the servo system and performs azimuth motion ( ). is the antenna and undergoes pitch motion ( ). The Robertson-Wittenburg method [Roberson and Schwertassek, 1989] is adopted and the equation of the antenna servo system can be derived as follows

(1)

where is the external control torque on , while on . The system is strongly nonlinear. One effective and powerful control method for nonlinear systems is the sliding mode control (SMC). The exponential approach law [Gao, 1989] of SMC is

37

s s ks k = − − > > ε ε sgn( ) , 0, 0 (2)

= + < < > ⎤⎤⎫

γ

s e e e

β γ β

sgn( ),1 2, 0 2

2 2 2 2 2 2 2

= + < < > ⎤⌋ (5)

γ

s e e e

β γ β

3

To reject disturbances and shorten reaching time, an

sgn( ),1 2, 0

adaptive variable speed exponential reaching law [Xu et al., 2016] is given as follows

s s k cx s k c = −ε ε − + > > >

3 3 3 3 3 3 3

where and are the control errors of and respectively. According to (1), the control inputs and using the proposed improved

1 sgn( ) ( ) , 0, 0, 0 + (3) 1

cx

variable-rated exponential reaching law are as follows

= − − + + | +|

M t R A s k c e s ( ) (sgn( ) (sgn( ))

ε

1 sgn( )

The reaching law has two parts: is the exponential reaching item, which can adjust the

β γ

reaching time to the equilibrium point. The constant reaching rate is far less than when c is

M t R A s k c e s ( ) (sgn( ) (sgn( )) = − − + +

ε

1 sgn( )

increased, so the chattering can be weakened.

\+ 31 3

In this paper, an improved adaptive variable speed

− + > > > > *q e k c c*

β γ

exponential reaching law is given by

1 sgn( ) (sgn( ))

s s k x c x s

= −ε − +

\+ (4)

1 sgn( )

x c x 1

where and .

3 Results

In simulations below, it is assumed that the initial

Remark 1. The instant answer of the exponential reaching term in (3) is . When the system converges to the equilibrium point, x cannot keep positive definitely. If x has a negative value at some moments, the coefficient c must be changed to a negative value to keep a shorter reaching time and a smaller chattering. By introducing to the reaching law, this problem can be solved.

Remark 2. Coefficient c in (3) should be chosen as a large value in order to keep the system converging to the equilibrium state more rapidly. But a large value of c will reduce the constant reaching item, that may increase the reaching time again especially under a high precision control situation. On the other hand, a small value of c in (3) cannot achieve good effectiveness to shorten reaching time as well. So two different coefficients and are proposed in the improvement adaptive variable speed exponential reaching law in (4). can be chosen with a large value while a relatively small value. By choosing and appropriately, the system can converge to the equilibrium state rapidly.

c e

2 2 24 2 2 22 2 2

21 2 2

reaching speed according to the value of and shorten

− + > > > > ||

q e k c c

1) (0, 0, 0, 0)

2 γ −

20 2 2 21 22 2 ε

2

2 2

c e

3 3 35 3 3 32 3 3 3

1) (0, 0, 0, 0)

2 γ −

30 3 3 31 32 3 ε

3

3 3

(6)

2

The targeted azimuth and angle of the antenna in the inertia space can be transformed into the targeted relative angles (,) by coordinate transformation. Therefore, the goal of control in this paper is to minimize the tracking error of and . The terminal sliding mode control (TSMC) was proposed [Zak, 1988], which has the advantage of finite convergence time. And the non-singular TSM control (NTSMC) was developed to overcome the problem of singularity. The non-singular terminal sliding mode variables for and can be designed [Yu et al., 2005] respectively as

values of and are zero. The carrier moves in an angular velocity of sinusoidal form with the amplitude of 60 degrees and period of 2 seconds about all three directions. The performance of the proposed control method is tested by realizing two control objectives: one is to hold the antenna attitude in a fixed angle of 30 degrees for both and ; another is to make
and track a sinusoidal motion with the amplitude of 30 degrees and period of 5 seconds.

Considering the limited capability of the control power in realistic situations, the control parameters are chosen following a muti-objective optimization program using the cell mapping method [Qin et al., 2015] in order to guarantee a relatively higher control accuracy under the constraint on and . With same design of sliding variables as (5), four different control methods, namely traditional PID control method, NTSMC with exponential approach law in (2), NTSMC with adaptive variable speed exponential reaching law in (3), and NTSMC with the proposed improved adaptive reaching law in (4), are adopted to realize the attitude control of the antenna.

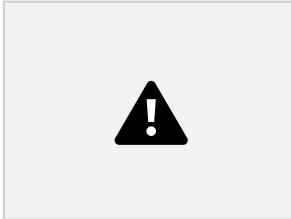

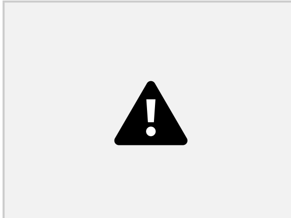

(a) (b)

Figure 2. The control by the proposed method to realize a fixed angle control for (a) ; (b) . The solid line represents the targeted trajectory and the dotted line the controlled trajectory.

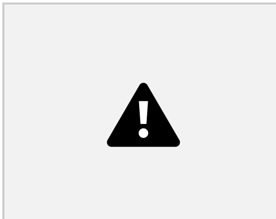

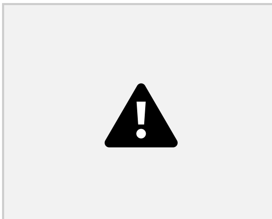

(a) (b)

Figure 3. The control error in the case to hold a fixed angle for (a) ; (b) .

Figure 2 shows the control results of the proposed method to hold a fixed angle. The proposed method performs a remarkable control on the system with high control accuracies for both and . Comparison of control errors using four control methods are given in Figure 3. Compared with PID controller, the proposed method has obvious smaller static error and higher robustness. Compared with NTSMC, both of the proposed method and the existing adaptive NTSMC can shorten the convergence time of and . The existing adaptive NTSMC still performs well in the case to realize a fixed angle control because and
are always positive in the control process. So control trajectories of the proposed method and the adaptive NTSMC come closest to coinciding in shape.

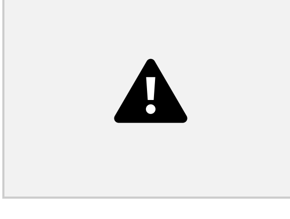

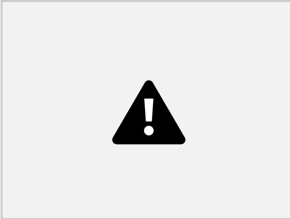
(a) (b)

Figure 4. The control by the proposed method to track a sinusoidal motion for (a) ; (b) . The solid line represents the targeted trajectory and the dotted line the controlled trajectory.

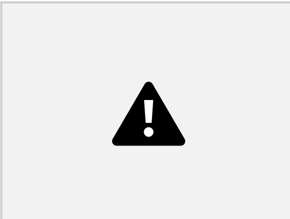

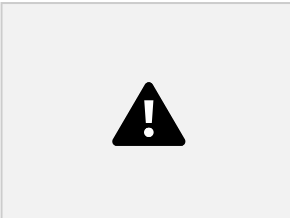
(a) (b)

Figure 5. The control error in the case to track a sinusoidal motion for (a) ; (b) .

Figure 4 shows the control results of the proposed method in the case to track a sinusoidal motion for and . The control errors using four control methods are presented in Figure 5. It is easy to find that the PID controller is not satisfactory. The existing adaptive NTSMC loses its strength with the increasings of reaching time and overshoot for both and , because and are not always positive and the constant reaching time increases. But the proposed method shows a remarkable control performance for both and that has obvious tiny static error and high robustness and a great effect of shortening the reaching time and reducing the overshoot.

4 Conclusions

In order to achieve better attitude control accuracy of an antenna servo system on a carrier subjected to large disturbance, this paper investigates the modelling, and the design of the controller for the nonlinear multi-body system. An improved adaptive variable speed exponential reaching law is proposed and the non-singular terminal sliding mode controller is designed based on the multi-body dynamical equations. Through simulations it is found that the proposed control method provides high accuracy and robustness to realize the attitude control targets of holding fixed angles and tracking sinusoidal motions. Compared with the traditional NTSMC, the existing adaptive NTSMC causes the increasing of reaching time and overshoot in the case to track a sinusoidal motion. In contrast, the proposed control method can shorten the reaching time and reduce the overshoot for both the two control objectives.

Acknowledgements

This work was supported by the National Natural Science Foundation of China (Grant Nos. 11332008 and 11772243).

References

Debruin J (2008). Control systems for mobile satcom antennas. Control Systems IEEE 28(1): 86–101. Fan Q and Wang Y (2015) Design of vehicle antenna servo tracking system controller. In: Proceeding of the International Conference on Advances in Mechanical Engineering and Industrial Informatics, Zhengzhou, China, 11–12 April 2015, pp.887–892. Gao W (1989). Variable structure control to nonlinear systems. Acta Automatica Sinica 15(5): 408–415.

Qin, Z. C., et al. (2015). Multi-objective optimal design of sliding mode control with parallel simple cell mapping method. Journal of Vibration and Control:1077546315574948.

Roberson RE and Schwertassek R (1989). Dynamics of multibody systems 108(2): 167–175.

Xu B, Shi G, Ji W, et al. (2016). Design of an adaptive nonsingular terminal sliding model control method for a bearingless permanent magnet synchronous motor. Transactions of the Institute of Measurement & Control 39(12): 1821–1828.

Yu S, Yu X, Shirinzadeh B and Man Z (2005). Continuous finite-time control for robotic manipulators with terminal sliding mode. Automatica 41(11): 1957–1964.

Zak M (1988). Terminal attractors for addressable memory in neural networks. Physics Letters A, 133(1): 18–22.

OPTIMAL PATH PLANNING OF AUVS OPERATING IN FLOWS INFLUENCED BY TIDAL CURRENTS

Roman Chertovskih
Research Center for Systems and Technologies, Electrical and Computer Engineering Department, Faculdade de Engenharia, Universidade do Porto Porto, Portugal
roman@fe.up.pt
Federal Research Center "Computer Science and Control", Russian Academy of Sciences Moscow, Russia

Nathalie T. Khalil
Research Center for Systems and Technologies, Electrical and Computer

Engineering Department, Faculdade de Engenharia, Universidade do Porto Porto, Portugal
khalil.t.nathalie@gmail.com

Abstract

Fernando Lobo Pereira
Research Center for Systems and Technologies,
Electrical and Computer Engineering Department,
Faculdade de Engenharia, Universidade do Porto
Porto, Portugal
flp@fe.up.pt

estuaries or straits of tidal rivers, such time-periodic os

We propose an algorithm to compute the time-optimal path of an autonomous underwater vehicle (AUV) con necting two given points in a time-periodic flow. The considered problem is an optimal control problem with state constraints, which is numerically solved using the Pontryagin maximum principle and a variation of the shooting method. The proposed solution method is based on a rigorous mathematical analysis of the opti mal control problem, which is proved to be regular, and the developed algorithm essentially uses the continuity of the measure Lagrange multiplier.

Key words
Motion planning; tidal currents; time-optimal control problem; Pontryagin maximum principle; state con straints; shooting method.

1 Introduction

Periodically induced forces of astronomical origin generate horizontal water flows called tidal currents (also periodic in time). They belong to the most intense flows near the sea and ocean coasts [Joseph, 2013]. Tidal currents in rivers act alternately in approximately opposite directions, introducing time-periodic pertur bations of relatively steady river flows. Also, flows in some coastal conditions are fully driven by the tidal cir cle, leading to reversals of currents directions several times a day. Planning activities of AUVs, operating in cillations should be taken into account.

The paper is organized as follows. In section 2 the statement of the optimal control problem describing the path planning problem is given. In section 3 the solution method based on the Pontryagin maximum principle is presented. In section 4 the optimal solu tions found numerically for some sample flows are de scribed. In the last section brief conclusions are given.

2 Statement of the problem

Focusing on mathematical properties of the control problem in hands, we consider the following statement of the path planning problem: to find the fastest path connecting two given points on a surface of a tidal river, where the river flow is assumed to be a prescribed time periodic two-dimensional field in the presence of state constraints represented by the river banks.

In mathematical terms, the following time-optimal control problem is studied:

Minimize T subject to

$$\dot{x} = u + v, \quad (1)$$

$$x(0) = A, \ x(T) = B, \quad (2)$$

$$-1 \leq x_1 \leq 1, \quad (3)$$

$$u^2_1 + u^2_2 \leq 1. \quad (4)$$

Here $x = (x_1(t), x_2(t))$ and $u = (u_1(t), u_2(t))$

A

stand for the state and control variables, respectively;

0

$\dot{x} = dx/dt$ and $t \in [0, T]$ is time. Points A and B de fine the given initial and terminal positions of the AUV. Prescribed field $v = (v_1(x, t), v_2(x, t))$ describes mo tion of a time-dependent fluid flow where the AUV op erates.

-1

-2

3 Solution method

It can be proved, that if $|v_1(x, t)| < 1$ for all x and t, then any feasible process (x, u) in this problem is reg ular with respect to the state constraints. Application

x^2 4.30 4.30 -3

of the Pontryagin maximum principle (see [Pontrya -4 gin, Boltyanskii, Gamkrelidze and Mishchenko, 1962; Arutyunov and Karamzin, 2016] for more details) re sults in the following two-points boundary value prob -5 lem (BVP):

$\dot{x} = u + v,$ (5a)

-6

$\dot{\psi} = -\psi v + \mu \nabla v_1,$ (5b)

$x(0) = A,$ (5c)

$x(T) = B.$ (5d)

5.58 5.58 6.00

B

-1 -0.5 0 0.5 1 x_1

Here $\psi = (\psi_1(t), \psi_2(t))$ is the adjoint func tion, $\mu = \mu(t)$ the measure Lagrange multiplier and $v = (v)_{ij} = \{\partial v_i/\partial x_j\}$, $i, j = 1, 2$ the Jacobian ma trix for the flow $v(x, t)$. The control variables are given by

$u_1 = \psi_1 - \mu$

Figure 1. Field of extremals (solid lines) for the steady flow $v(x) = (0, -x_1^2)$ (arrows), $A = (0, 0)$ and $B = (0, -6)$. Inscribed numbers stand for travelling time along the corresponding trajectories. The optimal (minimal time) trajectories are shown by red lines.

$(\psi_1 - \mu)^2 + \psi_2^2,$ (6a)

$u_2 = \psi_2$

$(\psi_1 - \mu)^2 + \psi_2^2,$ (6b)

the measure Lagrange multiplier is constant for trajec tories not meeting the boundary and is

$\mu = \psi_1 + |\psi_2||v_1|$

$1 - v_1^2.$ (7)

along the boundary of the state constraint (i.e. for $|x_1| = 1$). Note, that boundary conditions (at 0 and T) for the adjoint variable, $\psi(t)$, are absent.

The BVP problem (5) is solved by the shooting method (see, e.g., [Asher, Mattheij and Russell, 1988]), where the shooting parameter is the angle θ parametriz ing the initial boundary condition for ψ:

$\psi(0) = (\cos(\theta), \sin(\theta)).$ (8)

Starting from the initial conditions (5c) and (8) for a given value of θ, the Cauchy problem for the system of ordinary differential equations (5a)–(5b) is solved by the classical 4th order Runge-Kutta method with the constant time step $\tau = 10^{-4}$. Solutions to the BVP (5) constitute the field of extremals.

Integrating the system (5a)–(5b) forward in time start ing from $t = 0$, the measure Lagrange multiplier μ in (5b) and (6) is set to zero while the trajectory is inside the domain (i.e. $|x_1| < 1$). If it reaches the boundary, $|x_1| = 1$, at, say, $t = t^*$, then $\mu^* = \mu(t^*)$ is computed by (7). Using continuity of the measure Lagrange mul tiplier [Arutyunov and Karamzin, 2015], we conclude, that if $|\mu^*| < 10^{-3}$, the point is a junction point of an (potential) extremal and integration of the system is continued along the boundary. Following the boundary, at each time step, the trajectories leaving the bound ary (with constant values of μ) are computed in order to find another junction point or a segment joining the boundary with the terminal point B. If at a certain time the terminal boundary condition (5d) is satisfied to the accuracy 10^{-3}, the corresponding trajectory represents an extremal. To find such trajectories, the parameter θ is varied from 0 to 2π in (8) with a constant step of $10^{-2}$and bisection is used if the required accuracy is not achieved. Once all extremals are computed, the one possessing minimal travelling time among all the ex tremals is the optimal solution to the original control problem (1)–(4).

0

-1 -2

5.92 5.92

0

-1 -2

A

A

5.18

x^2 4.95 3.57 -3

x^2 4.15 4.15 -3

-4 -5 -6

-4 -5 -6

-1 -0.5 0 0.5 1 x_1

5.57 5.57

6.00

B

-1 -0.5 0 0.5 1 x_1

B

Figure 2. Field of extremals for the time-periodic flow (9), $A = (0, 0)$ and $B = (0, -6)$. Inscribed numbers stand for trav elling time along the corresponding trajectories. The minimal time trajectories are shown by red lines.

4 Numerical results

In order to demonstrate solutions to the optimal con trol problem (1)–(4) for some sample flows, we start from considering a steady flow, $v(x) = (0, -x^2_1)$ (shown by arrows in Fig. 1). It mimics a simple river flow, flowing predominately down (see Fig. 1, the fluid is at rest along the vertical mid-line, $x_1 = 0$) and being faster near the boundaries. Initial and terminal posi tions of the AUV are $A = (0, 0)$ and $B = (0, -6)$, respectively. The field of extremals is constituted by 5 extremals shown in Fig. 1: four of them (represented by red and green lines) are two pairs of trajectories re lated by the reflection symmetry about the vertical axis, $x_1 = 0$; the black trajectory corresponds to travelling along this symmetry axis where the flow is absent.

The optimal trajectories (shown in red) are the ones possessing boundary segments, travelling along them takes 4.3 time units, while travelling along other ex tremals takes 5.58 (green) and 6 (black) time units. It is not surprising that the boundary trajectories are fa vorable, since the flow is faster on the boundary.

Next, we consider the previous flow modulated peri odically in time,

$$v(x, t) = (0, -x^2_1(1 - \cos(\pi t)), \quad (9)$$

and the same positions for the initial and terminal points. The corresponding field of extremals is shown

Figure 3. Field of extremals for the time-periodic flow (9), $A = (0.5, 0)$ and $B = (0.25, -6)$. Inscribed numbers stand for travelling time along the corresponding trajectories. The minimal time trajectory is shown by red line.

in Fig. 2. As in the steady case, all of extremals are represented by pairs of trajectories related by the re flectional symmetry (the straight line is its own sym metrical counterpart), however, in contrast to the steady case, there are three pairs of trajectories (note the blue trajectories in Fig. 2). The minimal time trajectories, are again the ones containing boundary segments, the optimal travelling time is 4.15 time units.

Finally, we consider the time-periodic flow from the previous example, but with “non-symmetric” configu ration of the initial and terminal points: $A = (0.5, 0)$ and $B = (0.25, -6)$. The field of extremals, display ing the absence of reflectional symmetry, is presented in Fig. 3. One of the extremals (green) does not meet the boundary and has the longest travelling time – 5.18 time units, two other extremals include boundary seg ments. The extremal possessing a segment of the left boundary (blue) demonstrates longer travelling time, 4.95, in comparison to the travelling time, 3.57, for the extremal involving an interval of the right bound ary (red). This agrees with the observation, that out of the two boundary extremals, the optimal trajectory (red) is “closer” to the points *A* and *B*.

In this work we developed a new algorithm for so lution of the path planning problem for an AUV in a

5 Conclusions

river flow varying periodically in time. For two sample flows and for two configurations of the initial and ter minal points, we computed optimal paths minimizing the travelling time between two given locations.

Although, from practical point of view, the statement of the path planning problem considered here may look to be too simple, the main ingredient – state con straints, making such optimal control problems difficult to solve, is present and successfully treated here. In or der to show the ability of the method to treat extremals involving boundary segments, in all examples above, the flows were chosen to make the boundary active.

Acknowledgements

This investigation was supported by FCT (Portu gal): support of FCT R&D Unit SYSTEC – POCI 01-0145-FEDER-006933/SYSTEC funded by ERDF | COMPETE2020 | FCT/MEC | PT2020 extension to 2018, and NORTE-01-0145-FEDER-000033, by ERDF | NORTE 2020. The first author (results ob tained in Chapters 3 and 4) was supported by the Rus sian Science Foundation (project no. 19-11-00258) during his research visits to the Federal Research Cen ter “Computer Science and Control” of the Russian Academy of Sciences.

References

Joseph, A. (2013). *Measuring Ocean Currents: Tools, Technologies, and Data*. Elsevier Science.

Pontryagin, L.S., Boltyanskii, V.G., Gamkrelidze, R.V. and Mishchenko, E.F. (1962) *The Mathematical The ory of Optimal Processes*, Interscience, New York.

Arutyunov, A.V. and Karamzin, D.Yu. (2016) Proper ties of extremals in optimal control problems with state constraints. *Differential Equations*, 52(11), pp. 1411–1422.

Ascher, U.M., Mattheij, R.M.M. and Russell, R.D. (1995) *Numerical Solution of Boundary Value Prob lems for Ordinary Differential Equations*. Classics in Applied Mathematics (Vol. 13), SIAM, Philadelphia.

Arutyunov, A.V. and Karamzin, D.Yu. (2015) On some continuity properties of the measure Lagrange mul tiplier from the maximum principle for state con strained problems. *SIAM Journal on Control and Op timization*, 53(4), pp. 2514–2540.

PHYSCON 2019, Innopolis, Russia, 8–11 September, 2019

NEURONAL PATHWAY AND SIGNAL MODULATION FOR MOTOR COMMUNICATION

Parth Chholak
Center for Biomedical Technology Technical University of Madrid Spain
parth.chholak@ctb.upm.es

Alexander N. Pisarchik
Center for Biomedical Technology Technical University of Madrid Spain
alexander.pisarchik@ctb.upm.es

Semen A. Kurkin, Vladimir A. Maksimenko, Alexander E. Hramov
Research and Educational Center ’Artificial Intelligence Systems and Neurotechnology’ Yuri Gagarin State Technical University of Saratov
Russia
kurkinsa@gmail.com, maximenkovl@gmail.com, hramovae@gmail.com

Abstract

The knowledge of the mechanisms of imaginary mo tion or motor imagery (MI) is very important for the development of brain-computer interfaces. Depend ing on neurophysiological cortical activity, MI can be divided into two categories: visual imagery (VI) and kinesthetic imagery (KI). Our magnetoencephalogra phy (MEG) experiments with ten untrained subjects provided evidences that inhibitory control plays a dom inant role in KI. We found that communication be tween inferior parietal cortex and prefrontal cortex is realised in the mu-frequency range. We also pinpointed three gamma frequencies to be used for motor com mand communication. The use of artificial intelli gence allowed us to classify MI of left and right hands with maximal accuracy of the artificial neural network in classification between MI of hands obtained using the brain activity encoded in these gamma frequencies which was then proposed to be used for communica tion of specifics. Mu-activity was identified as the car rier of gamma-activity between these areas by means of phase-amplitude coupling.

Key words

Brain-computer interface, motor imagery, inhibition, neural communication, phase-amplitude coupling.

1 Introduction

Brain-computer interfaces (BCI) aim to control exter nal devices as per the interpretation of the operator’s brain activity [Abiri et al., 2019]. BCI systems can be classified into two general categories [Abiri et al., 2019]. In the first category, feedforward brain activity is used to control external devices, and in the second category, closed-loop brain activity with feedback de vice(s) is used for neural rehabilitation.

The important task of BCI applications is the recogni tion of the patterns of neurophysiological brain activity associated with motor imagery (MI) which is defined as a mental simulation of overt actions in the absence of any muscle movements. This bears crucial importance for both brain-controlled exoskeletons or bioprosthesis and neurorehabilitation of amputee and stroke patients. MI can be classified into two categories, namely, vi sual imagery (VI) and kinesthetic imagery (KI) [Chho lak et al., 2019]. While in VI subjects MI activates visual cortex, in KI subjects the activity is detected in the same motor areas as in the case of real move ments [Pfurtscheller and Neuper, 1997] with an addi tional mechanism for inhibiting motor commands to avoid overt actions [Solodkin et al., 2004, Hanakawa et al., 2008, Guillot et al., 2012, Abiri et al., 2019]. Functional magnetic resonance imaging (fMRI) stud ies evidence the involvement of motor associated areas and inferior parietal (IP) cortex for KI subjects, in con trast to VI subjects who exhibit the involvement of vi sual and superior parietal cortices [Guillot et al., 2009]. Moreover, transcranial magnetic stimulation (TMS) ex periments suggest that the IP area participates in the in hibitory control of the primary motor cortex (M1) dur ing KI-dominated MI [Lebon et al., 2012]. However, despite extensive research on MI, no clear experimen tal evidence of the underlying KI mechanism has yet been provided.

One of the most popular experimental paradigms for MI studies is based on sensorimotor rhythms (SMR) [Abiri et al., 2019], which involves KI of large body parts, such as whole limbs, to obtain modulations of neuronal activity [Morash et al., 2008]. At the same

time, alpha- and beta-rhythms are crucial and ubiq uitous in most studies on MI [Craik et al., 2019]. For example, in 1991 [Wolpaw et al., 1991] used the alpha-rhythm to control the cursor position on a com puter screen in one-dimensional space. Later, more ad vanced and sophisticated methods, such as linear re gression, logistic regression, and artificial neural net works (ANNs), were applied to control the cursor po sition in three-dimensional space [Wolpaw and McFar land, 2004, Wolpaw and McFarland, 1994, McFarland et al., 2010], prosthetics [Murguialday et al., 2007, Chen et al., 2008, Ramos-Murguialday et al., 2013], robots [Muller-Putz et al., 2005, Kai Keng Ang et al., ¨ 2009, Sarac et al., 2013, Baxter et al., 2013, LaFleur et al., 2013], and for stroke rehabilitation [Ramos Murguialday et al., 2013, Ono et al., 2014, Rayegani et al., 2014] (for review see [Abiri et al., 2019,Ang and Guan, 2017]).

Among the massive amounts of literature on the BCI development using MI, electroencephalography (EEG) is found to be the most popular noninvasive technique [Bi et al., 2013, Machado et al., 2013, Moghimi et al., 2013, Vaughan et al., 1996, Hwang et al., 2013, Lotte et al., 2007, Pfu, 2006, Machado et al., 2010] for controlling wheelchairs [Bi et al., 2013], communi cation aid systems [Birbaumer et al., 1999], assistive and rehabilitative devices for healthy [Meng et al., 2016] and disabled people, stroke patients and peo ple with other neurological deficits [Daly and Wol paw, 2008,Birbaumer and Cohen, 2007,Machado et al., 2013, Moghimi et al., 2013, Birbaumer, 2006]. In ad dition, a fair amount of papers were devoted to mag netoencephalography (MEG) studies on MI [Salmelin and Hari, 1994, Schnitzler et al., 1997,Kauhanen et al., 2004, Halme and Parkkonen, 2016, Halme and Parkko nen, 2018], which has the advantage of a higher spatial resolution and better resilience against artifacts as com pared to EEG, although pros of EEG, such as low cost and portability, are crucial for BCI development, but can be kept aside while understanding the fundamental activity underlying MI.

The aim of this study is to analyse MEG signals, es pecially in the alpha- and beta-frequency bands, asso ciated with MI in the SMR paradigm. We focus on the inhibitory mechanism to avoid overt action dur ing KI, that was previously investigated using other neuroimaging techniques, such as TMS. Subsequently, we perform various validation tests along the way us ing methods based on spectral power, coherence and ANNs, and suggest a model which explains empirical observations related to KI and real movements (overt actions).

2 Materials and Methods

The neurophysiological data were acquired using the Vectorview MEG system (Elekta AB) with 306 chan nels (102 magnetometers and 204 planar gradiometers) placed inside a magnetically shielded room (Vacuum Schmelze GmbH). Three fiducial points (nasion, left and right preauricular) were acquired for each subject. The experimental study consisted of ten (nine right handed, eight males) previously *untrained* volunteers between the age of 20 and 31. The subjects sat in a comfortable reclining chair with their legs straight, shoes off, and arms resting on an armrest in front of them. All of them provided a written informed-consent before the experiment commencement. The experi mental studies were performed in accordance with the Declaration of Helsinki.

Spatiotemporal signal space separation of [Taulu and Hari, 2009] was used to separate neuronal signals from nearby electromagnetic interference. The signals from bad MEG channels were replaced with spatially averaged signals of the nearby well-functioning MEG channels. The software used for this preprocessing task was MaxFilter that came along with the Elekta Neuromag machine. The sampling frequency was 1000 Hz and an online anti-alias [0.1–330] Hz bandpass fil ter was utilised.

(a) Order of presentation.

(b) MI trials for left hand.

Figure 1: Experimental protocol.

The experimental protocol was designed as shown in Fig.1. Resting-state recordings were performed at the start and end of each experiment with open eyes (OE) and closed eyes (CE), respectively. OE recordings were later discarded because all data during MI were recorded with closed eyes. The duration of CE record ings was different for each subject and ranged from 40 to 280 s.

MI recordings were divided into four series sets. Ev ery series contained the MEG data of MI of each of four limbs in a random order, i.e., left hand (LH), right hand (RH), left leg (LL), and right leg (RL). The order of presentation shown in Fig.1a represents one of such protocols, which was different for each subject. Before MI of each limb, a visual message was demonstrated to the subject to ask him/her to close eyes and imagine the movement of the indicated limb as soon as he/she hears a beep. The subsequent beeps were made every 6–8 s (the time interval was ordered randomly). Each imaginary movement between the beeps was counted as one trial. Figure 1b shows a model example of beep presentation for LH MI-trials. The number of trials for each limb was varied among subjects between 4 and 7 in each series. After every series, the subjects had a 40-s rest during which they listened a relaxing music.

The experiments were programmed using software provided by the Cogent 2000 team at the Functional Imaging Laboratory and the Institute of Cognitive Neu roscience and Cogent Graphics developed by John Ro maya at the Laboratory of Neurobiology at the Well come Department of Imaging Neuroscience. A MAT LAB code was used to produce all audio and visual commands (Cogent) as well as to log the time at the beginning of each MI-trial in a protocol file (in .txt for mat). The protocol file was later used to mark all events manually when analysing the MEG file (in .fif format). A part of the data analysis was performed with Brain storm [Tadel et al., 2011] documented and freely avail able for downloading under the GNU general public license (http://neuroimage.usc.edu/brainstorm). Once the events were marked at the beginning of each limb's MI using the protocol file, 5-s trials were extracted im mediately after these marks. Similarly, 10-s trials from CE-recordings were also marked and extracted as the background activity for every subject.

The time-frequency structure of the MEG signals was analysed with the help of a wavelet-based ap proach, well-known for the analysis of nonstationary time-series in medicine and biology [Iva, 1999]. For each limb, we used Morlet wavelets with f_0 = 1 Hz central frequency and a 3-s full width at half max imum (FWHM) to evaluate time-frequency spectro grams (TFSs) for all extracted 5-s MEG-trials of each limb, and then averaged the TFSs to all trials for that limb. Then, the TFS was also averaged over desired frequency ranges of delta (1–5 Hz) and mu (8–30 Hz). The same process was repeated for the background 10-s trials using the same parameters. To evaluate ERS/ERD, we took the difference between the spec trogram for the MI-trials and the averaged-over-time spectrogram of the background and then normalized it to the background. This normalized difference was as sumed to be positive for ERS and negative for ERD.

ANNs were used in the later stages for validation pur poses. Multilayer perceptron (MLP) was chosen as the network architecture to classify between LH and RH MI-trials. The input data for the ANN were taken from MEG time series from all 102 magnetometers, after bandpass filtering with a 10-Hz passing window. This passing window was varied from 5–60 Hz in steps of 5 Hz, i.e., (5–15), (10–20), (15–25), ..., and (50–60) Hz. The input layer containing 102 neurons was fol lowed by three hidden layers having 30, 15 and 5 neu rons, respectively. The output layer consisted of a sin gle neuron. A scaled conjugate gradient training algo rithm was used. The training stopped as soon as the batch training with all input data ran for at least 5000 times. To improve the efficiency of machine learn ing, we randomly mixed the input signal maintaining the correspondence to the MI-type, either LH or RH. Therefore, to classify MI of LH and RH, we mixed the MEG time series of all collected trials related to the LH and RH for each channel without losing their cor responding targets (0 for LH and 1 for RH) and time instance. The ANN classification was carried out in MATLAB (R2017a; Mathworks Inc., MA, USA) using Neural Network Toolbox.

3 Results and Discussion

Based on differential μ-activity of the cortex, we first segregated the subjects into two groups, six KI sub jects (Sub 1, 2, 4, 5, 9 and 10) and four VI subjects (Sub 3, 6, 7 and 8). The differentiation was performed according to ERD/ERS. Specifically, the KI subjects exhibited ERD in the aforementioned associated corti cal sites (Fig.2a), while the VI subjects showed ERS. Curiously, [Pfurtscheller and Lopes da Silva, 1999] re ported event-related desynchronisation (ERD) of mu rhythms in the sensorimotor cortex during MI in the SMR paradigm and ERS for resting. Although the sub jects in our study were instructed to perform KI, only some of them could successfully achieve this goal, be cause all participants were *untrained*.

The obtained results are in agreement with the previ ous study, where KI subjects (successful-SMR) exhib ited ERD in μ-band, while VI subjects (failed-SMR) showed ERS, similar to the resting state of SMR. In the δ-range, all KI subjects exhibited either ERS or ERD in the prefrontal cortex (PF) and insignificant activty in the posterior parts of the brain (Fig. 2b). In ad dition, the VI subjects exhibited the distributed non uniform activity without any preference for a particular region. The method used to evaluate ERS/ERD was as explained in section 2.

As discussed in section 1, KI and real movements share a common neuronal network, distinctly to KI which involves an additional mechanism for inhibiting overt movement that is likely to be situated in the IP. The coincidence of finding ERD for the KI subjects in μ-band at the same site as the one that is responsible for inhibitory control (i.e., IP) instils curiosity and deems to be further looked upon. In order to reveal the mech anism underlying this inhibitory control, we suppose that desynchronised activity of neurons near the IP dis rupts signal propagation that passes from IP to M1, as hinted by TMS studies.

The PF is also known to be involved in inhibition of movements [Krams et al., 1998], more specifically in choosing between brain responses [Duque et al., 2012]. [Sirigu et al., 1996] showed that when sub jects were asked to predict beforehand the time nec essary to perform motor tasks, the subjects with le sions in the posterior parietal cortex typically under estimated/overestimated the time. This strongly con trasted with subjects having dysfunctional motor re gions who exhibited impaired movements, but retained the ability to estimate motor performance times [Sirigu et al., 1995].

In order to predict motor performance times, a subject needs to simulate the entire repertoire of the act from long-term memory. This function is perhaps localised in the posterior parietal cortex. Conveniently, nearby

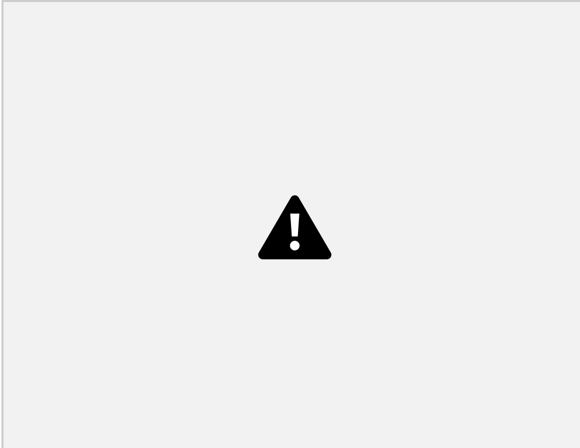

(d) ERS/ERD distribution for δ-frequency range averaged over all trials and trial time.

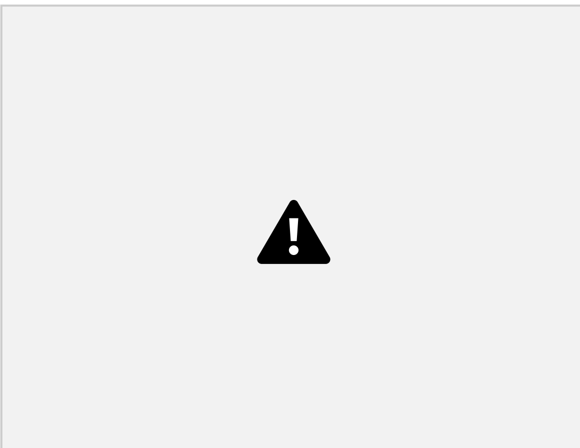

(c) ERS/ERD distribution for μ-frequency range averaged over all trials and trial time.

Figure 2: Event-related wavelet energy for subject-2 (KI).

temporal lobe has been implicated to play a role in long-term memory function, especially the medial tem poral lobe [for review see [Jeneson and Squire, 2012]]. Before the actual execution of motor commands by M1, aided by its associated areas like premotor cortex (PM) and supplementary motor area (SMA), passable responses are likely to be chosen at PF. As most of the conscious processing is performed in the frontal cor tex, PF being the point hosting this decision-making process is amenable.

We therefore propose the following neuronal pathway for motor signals (Fig. 3). Motor commands are gen erated in the posterior parietal cortex and need to travel to PF before being relayed to motor associated areas for final execution. ERD centred around IP disrupts the communication of motor commands from the posterior parietal cortex to PF in order to avoid any overt move ment during KI.

[Schwoebel et al., 2002] showed that bilateral lesions in the parietal cortex led to the execution of motor com mands during MI experiments without the patient real ising it. The patient with lesions at IP may not have

Figure 3: Neuronal pathway for KI. During KI, inhibi tion is manifested in the vicinity of IP in the form of ERD which prevents propagation of motor signal to wards PF. The rest of the neural circuitry remains the same for MI and actual execution of motor commands.

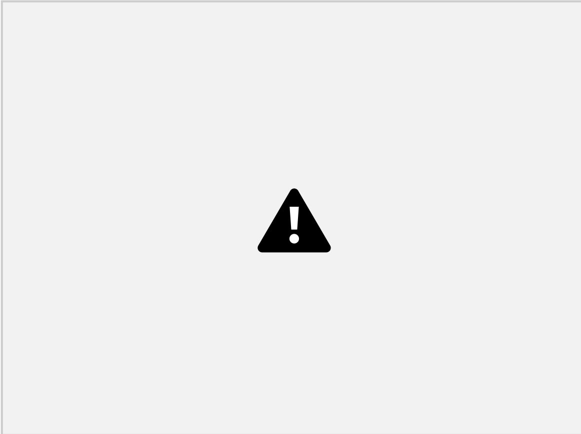

Figure 4: Connectivity between IP and PF for all 10 subjects. Mean squared coherence between MEG sig nals measured from channels situated at these loca tions. Peaks obtained at 10-Hz (mu), 32-Hz (gamma), 45-Hz (gamma), and 48-Hz (gamma). The thick red and blue line represent average connectivity of VI and KI subjects, respectively.

ERD in IP at μ-frequency and would pass the signal to the PF region, not expecting an input from IP dur ing KI and thus leading to actual execution without the subject's knowledge.

We used coherence as a measure of connectivity be tween two parts of the brain. The results indicate unin hibited communication in the μ-band between IP and PF for all VI subjects, whereas KI subjects show a clearly compromised connectivity between these areas. We plot the mean-squared coherence of the MEG sig nals collected from IP and PF versus frequency (in Hz). The strength of connectivity between these areas is in deed found to be suppressed for KI subjects than VI and showed peaks at 10 (μ), 32 (γ), 45 (γ), and 48 Hz (γ) for both groups of subjects (Fig.4).

[Lisman and Jensen, 2013] discussed about a theta gamma neural code for multi-message communication

during memory processes. They prescribed phase amplitude coupling between the phase of θ-waves and the amplitude of γ-waves and envisaged upon the ex tension of their model to sensory processes if θ-waves are replaced by α-waves. The studies of [Llinas and ´ Ribary, 1993, Mormann et al., 2005, Canolty et al., 2006, Demiralp et al., 2007, Sauseng et al., 2009, Ax macher et al., 2010, Voytek et al., 2010, Maris et al., 2011] provide evidences of this phase-amplitude cou pling in humans. During each γ-cycle, a set of neurons or neural ensemble fire concurrently, forming a spatial pattern on the cortex that corresponds to the object be ing represented by that γ-cycle. [Skaggs et al., 1996, Harris et al., 2003, Dragoi and Buzsaki, 2006, Gupta ´ et al., 2012] showed that a sequence of generated in formation in the form of gamma-cycles gets mapped to different phases of theta wave, maintaining the same order of information generation. [Voytek et al., 2010] have reported shifts in gamma phase-amplitude cou pling frequency from theta to alpha during visual tasks. Similarly, we expect a phase-amplitude coupling be tween γ-waves and α- / μ-waves for MI tasks.

We therefore propose that motor commands involve μ-waves as general carriers of motor related activ ity. These carrier waves carry γ-waves, containing specifics of motor activity from IP to PF, which acts as a relay junction and transfers the information to mo tor related areas such as M1, PM, and SMA. [Bressler, 1995,Varela et al., 2001,Fries, 2005,Siegel et al., 2012] also validate that coherence in γ-band between two points of the brain can be used to control neural com munication of information between them.

Our ANN classification study designed in an uncon ventional yet appropriate way, supports this hypothesis. The study was designed to find what frequency compo nent of the MEG signal generates higher ANN accu racy in order to gauge the kind of ANN classification task related information carried by that component. As discussed in section 2, bandpass filtering in windows of a 10-Hz width was used to pre-process MEG data be fore ANN classification of LH and RH MI. ANN clas sification accuracy was found to be largely independent of the KI or VI mode of MI. Figure 5 shows the ANN classification accuracy averaged over all subjects ver sus the bandpass frequency range. Each data point in this figure represents the centre of the corresponding bandpass frequency range. Thus, the points at the two local maxima represent 25–35 Hz and 45–55 Hz win dows, respectively, as marked in Fig. 5. Observing the two maxima in the frequency ranges which include the gamma signal frequencies shown in Fig. 4 validates our hypothesis that specifications of MI (e.g., hand motion) were encoded in the γ-band signals. On the other hand, the μ-band played a general role in this motor task and did not contribute as much in differentiating between two hands. The amplitude of intracellular spiking in γ band in the directionality-specific (LH or RH) neurons is codependent on the phase of the μ-band signal at 10 Hz which acts as an envelope for motor-related activity

Figure 5: ANN classification accuracy between LH and RH MI averaged for all subjects versus bandpass frequency range on the input MEG signal to the ANN. Each data point on the x-axis represents the centre of the bandpass-frequency range of a 10-Hz width. Two local maxima in the gamma range are found to be active during the coherence study.

between these regions.

In the very recent, systematic and extensive review, [Craik et al., 2019] described only eight studies that employed MLP for deep neural network classifica tion using EEG, three of which were focussed on MI. Only one of these MI studies utilised MEG time se ries as inputs for ANN [Sturm et al., 2016] with a 75% accuracy, whereas other two studies [Yohanan dan et al., 2018, She et al., 2019] used different forms of frequency transformations on the input signal and achieved up to 85% accuracy. The maximum accuracy obtained in our study, utilising MEG signals as input, was about 85% in the 40–50 Hz range.

4 Conclusions

In this work we identified the neuronal pathway for motor command propagation during both kinesthetic imagery and real movements. We also revealed parts of the encoding details and signal disruption to avoid overt action. During KI, desynschronised neurons pre vent brain activity in gamma (32-, 45-, and 48-Hz) car rying specifics of the movement to propagate from in ferior parietal lobe to the prefrontal cortex which can blindly relay the signal to the motor areas for execution. All motor related communications are performed in the mu (10-Hz) frequency regime using phase-amplitude coupling. Delta waves also participate in this circuit and definitely play an important role in the prefrontal cortex. We aspire that the identification of these mo tor related frequencies and the areas in which they are communicated through will turn out to be radical in de veloping BCIs henceforth. And, the insights about neu ral communication and inhibition may benefit research on controlling human inhibition towards harmful sub stances or preventing the propagation of undesirable sensations like pain.

Acknowledgements

This work was supported by the Spanish Min istry of Economy and Competitiveness under Project SAF2016-80240.

References

(1999). *Wavelets in Physics*, chapter Wavelets in medicine and physiology. Cambridge Univ. Press. (2006). *Encyclopedia of Biomedical Engineering*, vol ume 2, chapter EEG based brain–computer interface system, pages 1156–66. New Jersey: John Wiley and Sons, 1 edition.

Abiri, R., Borhani, S., Sellers, E. W., Jiang, Y., and Zhao, X. (2019). A comprehensive review of EEG based brain–computer interface paradigms. *Journal of Neural Engineering*, 16(1):011001.

Ang, K. K. and Guan, C. (2017). EEG-Based Strate gies to Detect Motor Imagery for Control and Reha bilitation. *IEEE Transactions on Neural Systems and Rehabilitation Engineering*, 25(4):392–401.

Axmacher, N., Henseler, M. M., Jensen, O., Weinreich, I., Elger, C. E., and Fell, J. (2010). Cross-frequency coupling supports multi-item working memory in the human hippocampus. *Proceedings of the National Academy of Sciences of the United States of America*, 107(7):3228–33.

Baxter, B. S., Decker, A., and He, B. (2013). Noninva sive control of a robotic arm in multiple dimensions using scalp electroencephalogram. In *2013 6th In ternational IEEE/EMBS Conference on Neural Engi neering (NER)*, pages 45–47. IEEE.

Bi, L., Fan, X.-A., and Liu, Y. (2013). EEG Based Brain-Controlled Mobile Robots: A Sur vey. *IEEE Transactions on Human-Machine Systems*, 43(2):161–176.

Birbaumer, N. (2006). Breaking the silence: Brain?computer interfaces (BCI) for communication and motor control. *Psychophysiology*, 43(6):517– 532.

Birbaumer, N. and Cohen, L. G. (2007). Brain computer interfaces: communication and restoration of movement in paralysis. *The Journal of Physiology*, 579(3):621–636.

Birbaumer, N., Ghanayim, N., Hinterberger, T., Iversen, I., Kotchoubey, B., Kubler, A., Perelmouter, ¨ J., Taub, E., and Flor, H. (1999). A spelling device for the paralysed. *Nature*, 398(6725):297–298.

Bressler, S. L. (1995). Large-scale cortical networks and cognition. *Brain Research Reviews*, 20(3):288– 304.

Canolty, R. T., Edwards, E., Dalal, S. S., Soltani, M., Nagarajan, S. S., Kirsch, H. E., Berger, M.

S., Barbaro, N. M., and Knight, R. T. (2006). High gamma power is phase-locked to theta oscillations in human neocortex. *Science (New York, N.Y.)*, 313(5793):1626–8.

Chen, C.-W., K. Lin, C.-C., and J Ming, S. (2008). Hand orthosis controlled using brain-computer inter face. *J of Med and Biol Eng*, 29:234–241.

Chholak, P., Niso, G., Maksimenko, V. A., Kurkin, S. A., Frolov, N. S., Pitsik, E. N., Hramov, A. E., and Pisarchik, A. N. (2019). Visual and kinesthetic modes affect motor imagery classification in untrained sub jects. *Scientific Reports 2019 9:1*, 9(1):9838.

Craik, A., He, Y., and Contreras-Vidal, J. L. (2019). Deep learning for electroencephalogram (EEG) clas sification tasks: a review. *Journal of Neural Engi neering*, 16(3):031001.

Daly, J. J. and Wolpaw, J. R. (2008). Brain–computer interfaces in neurological rehabilitation. *The Lancet Neurology*, 7(11):1032–1043.

Demiralp, T., Bayraktaroglu, Z., Lenz, D., Junge, S., Busch, N. A., Maess, B., Ergen, M., and Herrmann, C. S. (2007). Gamma amplitudes are coupled to theta phase in human EEG during visual perception. *Inter national Journal of Psychophysiology*, 64(1):24–30.

Dragoi, G. and Buzsaki, G. (2006). Temporal Encod- ´ ing of Place Sequences by Hippocampal Cell Assem blies. *Neuron*, 50(1):145–157.

Duque, J., Labruna, L., Verset, S., Olivier, E., and Ivry, R. B. (2012). Dissociating the role of prefrontal and premotor cortices in controlling inhibitory mech anisms during motor preparation. *The Journal of neu roscience : the official journal of the Society for Neu roscience*, 32(3):806–16.

Fries, P. (2005). A mechanism for cognitive dynam ics: neuronal communication through neuronal co herence. *Trends in Cognitive Sciences*, 9(10):474– 480.

Guillot, A., Collet, C., Nguyen, V. A., Malouin, F., Richards, C., and Doyon, J. (2009). Brain activity during visual versus kinesthetic imagery: An fMRI study. *Human Brain Mapping*, 30(7):2157–2172.

Guillot, A., Di Rienzo, F., Macintyre, T., Moran, A., and Collet, C. (2012). Imagining is Not Doing but In volves Specific Motor Commands: A Review of Ex perimental Data Related to Motor Inhibition. *Fron tiers in human neuroscience*, 6:247.

Gupta, A. S., van der Meer, M. A. A., Touretzky, D. S., and Redish, A. D. (2012). Segmentation of spatial experience by hippocampal θ sequences. *Nature neu roscience*, 15(7):1032–9.

Halme, H.-L. and Parkkonen, L. (2016). Comparing Features for Classification of MEG Responses to Mo tor Imagery. *PLoS ONE*, 11(12):e0168766.

Halme, H.-L. and Parkkonen, L. (2018). Across subject offline decoding of motor imagery from MEG and EEG. *Scientific Reports*, 8(1):10087.

Hanakawa, T., Dimyan, M. A., and Hallett, M. (2008). Motor Planning, Imagery, and Execution in the Dis tributed Motor Network: A Time-Course Study with Functional MRI. *Cerebral Cortex (New York, NY)*, 18(12):2775.

Harris, K. D., Csicsvari, J., Hirase, H., Dragoi, G., and Buzsaki, G. (2003). Organization of cell assemblies ´

in the hippocampus. *Nature*, 424(6948):552–556. Hwang, H.-J., Kim, S., Choi, S., and Im, C.-H. (2013). EEG-Based Brain-Computer Interfaces: A Thorough Literature Survey. *International Journal of Human Computer Interaction*, 29(12):814–826.

Jeneson, A. and Squire, L. R. (2012). Working mem ory, long-term memory, and medial temporal lobe function. *Learning & memory (Cold Spring Harbor, N.Y.)*, 19(1):15–25.

Kai Keng Ang, Cuntai Guan, Sui Geok Chua, K., Beng Ti Ang, Kuah, C., Chuanchu Wang, Kok Soon Phua, Zheng Yang Chin, and Haihong Zhang (2009). A clinical study of motor imagery-based brain-computer interface for upper limb robotic reha bilitation. In *2009 Annual International Conference of the IEEE Engineering in Medicine and Biology So ciety*, pages 5981–5984. IEEE.

Kauhanen, L., Rantanen, P., Lehtonen, J. A., Tarnanen, I., Alaranta, H., and Sams, M. (2004). ”sensorimo tor cortical activity of tetraplegics during attempted finger movements” intention and imagery. *Biomed. Tech.*, 49:59–60.

Krams, M., Rushworth, M. F. S., Deiber, M.-P., Frack owiak, R. S. J., and Passingham, R. E. (1998). The preparation, execution and suppression of copied movements in the human brain. *Experimental Brain Research*, 120(3):386–398.

LaFleur, K., Cassady, K., Doud, A., Shades, K., Ro gin, E., and He, B. (2013). Quadcopter control in three-dimensional space using a noninvasive motor imagery-based brain-computer interface. *Journal of neural engineering*, 10(4):046003.

Lebon, F., Byblow, W. D., Collet, C., Guillot, A., and Stinear, C. M. (2012). The modulation of motor cor tex excitability during motor imagery depends on im agery quality. *European Journal of Neuroscience*, 35:323–331.

Lisman, J. E. and Jensen, O. (2013). The θ-γ neural code. *Neuron*, 77(6):1002–16.

Llinas, R. and Ribary, U. (1993). Coherent 40-Hz os- ´ cillation characterizes dream state in humans. *Pro ceedings of the National Academy of Sciences of the United States of America*, 90(5):2078–81.

Lotte, F., Congedo, M., Lecuyer, A., Lamarche, F., and ´ Arnaldi, B. (2007). A review of classification al gorithms for EEG-based brain–computer interfaces. *Journal of Neural*

Engineering, 4(2):R1–R13.

Machado, S., Almada, L. F., and Annavarapu, R. N. (2013). Progress and Prospects in EEG-Based Brain Computer Interface: Clinical Applications in Neu rorehabilitation. *Journal of Rehabilitation Robotics*, 1(1):28–41.

Machado, S., Araujo, F., Paes, F., Velasques, B., ´ Cunha, M., Budde, H., Basile, L. F., Anghinah, R., Arias-Carrion, O., Cagy, M., Piedade, R., de Graaf, ´ T. A., Sack, A. T., and Ribeiro, P. (2010). EEG-based brain-computer interfaces: an overview of basic con cepts and clinical applications in neurorehabilitation. *Reviews in the neurosciences*, 21(6):451–68.

Maris, E., van Vugt, M., and Kahana, M. (2011). Spa tially distributed patterns of oscillatory coupling be tween high-frequency amplitudes and low-frequency phases in human iEEG. *NeuroImage*, 54(2):836–50.

McFarland, D. J., Sarnacki, W. A., and Wolpaw, J. R. (2010). Electroencephalographic (EEG) control of three-dimensional movement. *Journal of Neural En gineering*, 7(3):036007.

Meng, J., Zhang, S., Bekyo, A., Olsoe, J., Baxter, B., and He, B. (2016). Noninvasive Electroencephalo gram Based Control of a Robotic Arm for Reach and Grasp Tasks. *Scientific Reports*, 6(1):38565.

Moghimi, S., Kushki, A., Marie Guerguerian, A., and Chau, T. (2013). A Review of EEG-Based Brain Computer Interfaces as Access Pathways for Individ uals with Severe Disabilities. *Assistive Technology*, 25(2):99–110.

Morash, V., Bai, O., Furlani, S., Lin, P., and Hal lett, M. (2008). Classifying EEG signals preceding right hand, left hand, tongue, and right foot move ments and motor imageries. *Clinical Neurophysiol ogy*, 119(11):2570–2578.

Mormann, F., Fell, J., Axmacher, N., Weber, B., Lehn ertz, K., Elger, C. E., and Fernandez, G. (2005). ´ Phase/amplitude reset and theta-gamma interaction in the human medial temporal lobe during a continu ous word recognition memory task. *Hippocampus*, 15(7):890–900.

Muller-Putz, G. R., Scherer, R., Pfurtscheller, G., and ¨ Rupp, R. (2005). EEG-based neuroprosthesis con trol: A step towards clinical practice. *Neuroscience Letters*, 382(1-2):169–174.

Murguialday, A. R., Aggarwal, V., Chatterjee, A., Cho, Y., Rasmussen, R., O'Rourke, B., Acharya, S., and Thakor, N. V. (2007). Brain-Computer Interface for a Prosthetic Hand Using Local Machine Control and Haptic Feedback. In *2007 IEEE 10th International Conference on Rehabilitation Robotics*, pages 609– 613. IEEE.

Ono, T., Shindo, K., Kawashima, K., Ota, N., Ito, M., Ota, T., Mukaino, M., Fujiwara, T., Kimura, A., Liu, M., and Ushiba, J. (2014). Brain-computer interface with somatosensory feedback improves functional re covery from severe hemiplegia due to chronic stroke. *Frontiers in Neuroengineering*, 7:19.

Pfurtscheller, G. and Lopes da Silva, F. (1999). Event related EEG/MEG synchronization and desynchro nization: basic principles. *Clinical Neurophysiology*, 110(11):1842–1857.

Pfurtscheller, G. and Neuper, C. (1997). Motor im agery activates primary sensorimotor area in humans. *Neuroscience Letters*, 239(2-3):65–68.

Ramos-Murguialday, A., Broetz, D., Rea, M., Laer, ¨ L., Yilmaz, O., Brasil, F. L., Liberati, G., Curado, ¨ M. R., Garcia-Cossio, E., Vyziotis, A., Cho, W., Agostini, M., Soares, E., Soekadar, S., Caria, A., Cohen, L. G., and Birbaumer, N. (2013). Brain Machine-Interface in Chronic Stroke Rehabilitation: A Controlled Study. *Annals of neurology*, 74(1):100.

Rayegani, S. M., Raeissadat, S. A., Sedighipour, L., Mohammad Rezazadeh, I., Bahrami, M. H., Eliaspour, D., and Khosrawi, S. (2014). Effect of Neurofeedback and Electromyographic-Biofeedback Therapy on Improving Hand Function in Stroke Pa tients. *Topics in Stroke Rehabilitation*, 21(2):137– 151.

Salmelin, R. and Hari, R. (1994). Spatiotempo ral characteristics of sensorimotor neuromagnetic rhythms related to thumb movement. *Neuroscience*, 60(2):537–550.

Sarac, M., Koyas, E., Erdogan, A., Cetin, M., and Patoglu, V. (2013). Brain Computer Interface based robotic rehabilitation with online modification of task speed. In *2013 IEEE 13th International Confer ence on Rehabilitation Robotics (ICORR)*, pages 1–7. IEEE.

Sauseng, P., Klimesch, W., Heise, K. F., Gruber, W. R., Holz, E., Karim, A. A., Glennon, M., Gerloff, C., Bir baumer, N., and Hummel, F. C. (2009). Brain Oscil latory Substrates of Visual Short-Term Memory Ca pacity. *Current Biology*, 19(21):1846–1852.

Schnitzler, A., Salenius, S., Salmelin, R., Jousmaki, V., ¨ and Hari, R. (1997). Involvement of Primary Motor Cortex in Motor Imagery: A Neuromagnetic Study. *NeuroImage*, 6(3):201–208.

Schwoebel, J., Boronat, C. B., and Branch Coslett, H. (2002). The man who executed "imagined" move ments: evidence for dissociable components of the body schema. *Brain and Cognition*, 50:1–16.

She, Q., Hu, B., Luo, Z., Nguyen, T., and Zhang, Y. (2019). A hierarchical semi-supervised ex treme learning machine method for EEG recogni tion. *Medical & Biological Engineering & Comput ing*, 57(1):147–157.

Siegel, M., Donner, T. H., and Engel, A. K. (2012). Spectral fingerprints of large-scale neuronal interac tions. *Nature Reviews Neuroscience*, 13(2):121–134.

Sirigu, A., Cohen, L., Duhamel, J. R., Pillon, B., Dubois, B., Agid, Y., and Pierrot-Deseilligny, C. (1995). Congruent unilateral impairments for real and imagined hand movements. *NeuroReport*, 6:997– 1001.

Sirigu, A., Duhamel, J. R., Cohen, L., Pillon, B., Dubois, B., and Agid, Y. (1996). The mental rep resentation of hand movements after parietal cortex damage. *Science*, 273:1564–1568.

Skaggs, W. E., McNaughton, B. L., Wilson, M. A., and Barnes, C. A. (1996). Theta phase precession in hip pocampal neuronal populations and the compression of temporal sequences. *Hippocampus*, 6(2):149–172.

Solodkin, A., Hlustik, P., Chen, E. E., and Small, S. L. (2004). Fine Modulation in Network Activation dur ing Motor Execution and Motor Imagery. *Cerebral Cortex*, 14(11):1246–1255.

Sturm, I., Lapuschkin, S., Samek, W., and Muller, K.- ¨ R. (2016). Interpretable deep neural networks for single-trial EEG classification. *Journal of Neuro science Methods*, 274:141–145.

Tadel, F., Baillet, S., Mosher, J. C., Pantazis, D., and Leahy, R. M. (2011). Brainstorm: A user-friendly application for MEG/EEG analysis. *Computational Intelligence and Neuroscience*, 2011.

Taulu, S. and Hari, R. (2009). Removal of mag netoencephalographic artifacts with temporal signal space separation: Demonstration with single-trial auditory-evoked responses. *Human Brain Mapping*, 30(5):1524–1534.

Varela, F., Lachaux, J.-P., Rodriguez, E., and Mar tinerie, J. (2001). The brainweb: Phase synchroniza tion and large-scale integration. *Nature Reviews Neu roscience*, 2(4):229–239.

Vaughan, T., Wolpaw, J., and Donchin, E. (1996). EEG-based communication: prospects and problems. *IEEE Transactions on Rehabilitation Engineering*, 4(4):425–430.

Voytek, B., Canolty, R. T., Shestyuk, A., Crone, N. E., Parvizi, J., and Knight, R. T. (2010). Shifts in Gamma Phase–Amplitude Coupling Frequency from Theta to Alpha Over Posterior Cortex During Visual Tasks. *Frontiers in Human Neuroscience*, 4.

Wolpaw, J. R. and McFarland, D. J. (1994). Multi channel EEG-based brain-computer communication. *Electroencephalography and Clinical Neurophysiol ogy*, 90(6):444–449.

Wolpaw, J. R. and McFarland, D. J. (2004). Control of a two-dimensional movement signal by a noninvasive brain-computer interface in humans. *Proceedings of the National Academy of Sciences*, 101(51):17849– 17854.

Wolpaw, J. R., McFarland, D. J., Neat, G. W., and Forneris, C. A. (1991). An EEG-based brain-computer interface for cursor control. *Elec troencephalography and Clinical Neurophysiology*, 78(3):252–259.

Yohanandan, S. A., Kiral-Kornek, I., Tang, J., Mshford, B. S., Asif, U., and Harrer, S. (2018). A Robust Low Cost EEG Motor Imagery-Based Brain-Computer In terface. In *2018 40th Annual International Confer ence of the IEEE Engineering in Medicine and Biol ogy Society (EMBC)*, pages 5089–5092. IEEE.

EFFECT OF OPTICAL FEEDBACK ON MULTISTABILITY IN A MULTIMODE VCSEL

V. N. Chizhevsky
B.I. Stepanov Institute of Physics
National Academy of Sciences
Belarus
vnc@dragon.bas-net.by

S. A. Kavalenka
B.I. Stepanov Institute of Physics
National Academy of Sciences
Belarus
sopfykavalenka@gmail.com

Abstract

We present experimental study of the effect of isotropic optical feedback (OF) on the polarization dynamics of a multistable multimode vertical cavity surface-emitting laser (VCSEL). Without feedback, the VCSEL displays spatial multistability which shows up in the laser power

the OF and experimental schemes for its implemen and polarized-resolved measure ments of the laser intensity. The addition of OF shifts the boundaries of multistability and for a large enough strength OF can transforms multistability into bistabil ity. This effect is demonstrated with help of a hysteretic behavior of the polarization-resolved laser intensity de pending on the injection current and by the use of the method of vibrational resonance (VR). In the latter case the use of VR allows one to reveal hidden states which cannot be observed in the hysteretic behavior and gives a complete picture of coexisting states in a parameter space.

Key words

Vertical-cavity surface-emitting laser, multistability, optical feedback, vibrational resonance.

1 Introduction

The effect of optical feedback on the dynamics of vertical-cavity surface-emitting lasers was a subject of numerous experimental and theoretical investigations. This interest stems from the fact that such lasers widely used in different applications where they inevitably subjected to optical feedback of a different nature from environment. From the other hand the OF in semicon ductors lasers gives an opportunity to study a complex behavior in dynamical systems. Different schemes of OF were studied both experimentally and theoretically, in particular, such as isotropic [Ackemann, 2003; Valle, 2008], polarization-selective [Romanelli, 2005; Lin, 2010], frequency-selective [Romanelli, 2005; Chembo, 2009] OF. Many results were summarized in the pa pers [Panajotov, 2013]. Depending on the strength of

tation, the constant OF can lead to a decrease in the width of the bistability zone [Hong, 2005], suppression [Hong, 2004; Hong, 2005] and inducing [Sciamanna, 2003; Houlihan, 2004] polarization switchings. Po larization dynamics in a multitransverse mode VCSEL with isotropic optical feedback was also studied [Lin, 2008; Valle, 2008; Lin, 2015].

The subject of our interest here is to investigate the effect of isotropic OF on a multistability in a multi mode VCSEL. Multistability or, in other words, a co existence of several attractors for the same set of fixed parameters is a feature of nonlinear systems and can be found in different fields of physics, chemistry and biol ogy (see, for instance,[Pisarchik, 2014] and references therein). Among such systems one can note

VCSELs which for some range of parameters may display bista bility and multistability of polarization steady states. For instance, a coexistence of three [Barbay, 2003], four and five polarizations states were found in multi mode VCSELs [Chizhevsky, 2004]. It was also shown experimentally that the polarization bistability in a VC SEL can be associated with a coexistence of two dif ferent transverse structures where switching between them can activated by noise [Barbay, 2003]. It should be noted that the spatial multistability was observed in broad area single VCSELs or in a system of optically coupled VCSELs, where a coexistence of several spa tially localized solitons were observed [Genevet, 2011; Barbay, 2011].

We show here experimentally that for some range of the injection current a coexistence of two, three and four different spatial patterns of the laser beam can be clearly identify. Such a spatial multistability shows up as well in the hysteretic behavior of the total laser inten sity depending on the injection current and polarization resolved measurements. We show that isotropic OF leads to the shift of boundaries of existence domains of multistability.Finally, impact of OF of a strong enough strength results in the multistability suppression. These effects are demonstrated with the help of the hysteretic

behavior of the laser intensity with a change of the in jection current in the opposite directions and by the method of vibrational resonance. In the later case the method of VR gives a complete picture of coexisting states in a parameter space. It allowed us to find ”hid den” states which were not observed in hysteretic be havior.

2 Experimental setup

The experimental setup is shown in the Fig. 1. A com mercial 850 nm multimode proton-implanted VCSEL (Honeywell, HFE4080-321) is used in the free running mode. A threshold current for the solitary diode is ≈2.75 mA at 25 ˚C. The measurements are performed under controlled thermal fluctuations within to 0.01˚C. The laser radiation collimated with a lens with an anti reflective coating is directed to a 50/50 beam splitter.

3 Multistability in the multimode VCSEL output

At first, we characterize multistability which was ob served in our laser diode. We study the dependence of the integral laser intensity as a function of the injec tion current j_{dc} by its changing step-by-step with a step ≈0.029 mA. The results of these measurements of to tal intensity without polarization resolution are shown in Fig. 2(a) In what follows we denote this intensity as I_{np}. The results of the polarization-resolved mea

(a) (b) 50 40 75 80

I_{npr} (arb. units) 95 90 85

I_{pr} (arb. units)

The transmitted radiation is reflected from the mirror,

I

12 14 16 18 j_{dc}, mA

30 20

12 14 16 18 j_{dc}, mA

thus forming isotropic optical feedback. The length of the external cavity is ≈20 cm. The alignment of the external mirror is adjusted so that to minimize the laser threshold, increasing the feedback strength [?]. In the experiments we use the mirrors with the reflection co efficients *R*=0.2, 0.5 and 0.99 which induce the laser threshold shifts by 2.73, 5.06 and 10.1 percents of the laser threshold without OF, respectively. One of the beams is used for integral intensity measurements with out polarization selection performed with avalanche photo diode PD3 in the presence of the mirror M or PD2 in the absence of the mirror. Another beam is split into two polarization components by a half-wave plate and a Glan prism for polarization-resolved measure ments. One of the component was used for the anal

Figure 2. The integral laser intensity as a function of the dc current j_{dc} in the measurement (a) without and (b) with a polarization selec tion. Plots were obtained by a superimposition of the several scans of j_dc with different initial and final values. The intensities were ob tained by averaging over time series of the laser intensity recorded by USB oscilloscope for each value of j_{dc} changed step-by-step. The blue (thick) line corresponds to increasing j_{dc}, the red line (thin) corresponds to decreasing j_{dc}.

Osc

Osc

CCD

M

PD2

PC

NDF

BS G

PD3 PD1

Osc

L1

HWP

L2

PC

TC VCSEL CS

Figure 1. Experimental setup. VCSEL (Honeywell); TC, thermo controller (T200 Thorlabs), CS, current source; PD, avalanche pho todiode; M, mirror; G, Glan"s prism; HWP, halfwave plate; OSC, oscilloscope; BS, beam splitter, CCD, CCD camera; PC, computer.

ysis of the spatial intensity distribution. Another po larization beam was focused at PD1. The signals from avalanche photo diodes PD 1-3 were monitored by the digital oscilloscope with a 2 GHz sampling rate and a 300 MHz bandwidth.

surements are presented in Fig. 2(b). The intensity measured on the selected polarization we will denote as I_p. Plots on both figures were obtained by a super imposition of several scans of the injection current in the opposite directions with different initial and final values of j_{dc}. From the results presented in Fig. 2 for both intensities I_{np} and I_p it is clearly seen that as the injection current changes both dependencies dis

play the emergence of bi-, tri- and four-

stabilities in the range of large enough values of j_{dc}. The abrupt

changes in I_{np} and I_p appear for values of j_{dc} ≈12.46,

15.55, 15.69 16.03, 16.150, 17.37

mA, respectively. Accordingly, the widths of these zones are the fol

lowing: Δj_{dc} ≈ 3.09,

0.14, 0.34, 0.12, 1.22 mA. In fact, bistability and multistability are

observed in a

non-polarized measurements. However in order to observe such a picture in the polarization resolved measurements we should carefully choose the ration angle of the half-wave plate with respect to the selected polarization direction. Figure 3 gives an idea how the intensity in each polarization state depends on the rotation angle of the half-wave plate for the fixed value of j_{dc} in multistability domain. One can see that the clear differences between the polarization-resolved intensities for all four states are large enough only for rather narrow ranges of the rotation angle.

wide range of the pump current Δj_{dc} ≈4.91 mA. At the same time one can note that polarization-resolved measurement gives more clearly the picture of multi stability than

1

120

90

Similar regularities are observed in the

polarization resolved measurements [Figs.

5(e)-(h)]. However, the

60

the difference between

levels are larger as com pared to the previous pictures. For strong OF (*R*=0.99),

150

30

0.5

width of the bistable zones and the upper and lower bistable

bistable zone still remains in the range of the pump current values around j_{dc} ≈

180 0

an almost complete suppression of the multistability is observed, and only a narrow

210

270

330

300

15 mA. Thus,

polarization-resolved measurements give more exact picture on

240

the effect of optical feedback.

np (arb. units)
56
70
90

Figure 3. Polar plot showing the laser intensity with different po larization states depending on the rotation angle of the half-wave plate with respect to selected direction of polarization for fixed value of j_{dc}=15.61mA. Laser intensities are normalized by the maximal I value.

(a) (b) (c)

54
52

a consequence of

pr (arb. units)
60
12 14 16 18 j_{dc}, mA
65 60

60
12 14 16 18 j_{dc}, mA
80 70
40
12 14 16 18 j_{dc}, mA

In fact, this type of multistability is this

the spatial multistability which was observed in this laser. In Fig. 4 it is shown spatial distribution of the

(d) (e) (f)

40
100 0 100
I
20
0 50 100 50 100 0
$S_1 S_2 S_3 S_4$

40 20
30 20
12 14 16 18 j_{dc}, mA
12 14 16 18 j_{dc}, mA
12 14 16 18 j_{dc}, mA

Plots were obtained by a superimposition of the several scans of j_dc with differ ent initial and final values. The intensities I_{np} and I_p are obtained by averaging over time series by digital oscilloscope for each value of j_{dc} (T = 25°C). The blues line corresponds to increasing j_{dc}, the red one corresponds to decreasing j_{dc}.

Figure 4. Contour plots showing a coexistence of four spatial dis tributions of the polarization-resolved laser intensity for fixed value of j_{dc}=15.61mA.

laser intensity in each polarization state for the fixed value of j_{dc} = 15.61 mA corresponding to a zone of po larization multistability. One can see a rater big differ ence between spatial distributions. It should be noted that spatial multistability leads also to a strong local dependence of the hysteretic behavior in the laser in tensity depending on the injection current which is ob served in the experiments.

4 Effect of optical feedback on hysteretic behavior

The effect of optical feedback on the hysteresis behav ior is presented in Fig. 5 where the top row corresponds to measurements without polarization resolution while the bottom raw shows the results for polarization resolved measurements. Measurements without po larization resolution show that adding OF results in the disappearance of multistability which transformed into bistability for the case OF with R=0.2 and R=0.5 [Figs.5(a) and (b), respectively]. An another peculiar ity is the shift of the boundaries of bistable regions to wards the lower values of j_{dc}. For R=0.99 we observe a complete suppression of multistability in the the de pendence of I_{np} on the injection current [Fig. 5(c)].

Figure 5. The steady-state laser intensities I_{np} (the top row) and I_p (the bottom row) as a function of the dc current j_dc.

5 Investigation by the method of vibrational reso nance

In section above, it was shown by the hysteresis method that the OF may result in the suppression of multistability. However, the question is still re mained to be answered about existence of ”hidden” states which may not appear explicitly in the hystere sis behavior. In the Ref. [Chizhevsky, 2004] it was demonstrated that vibrational resonance can be used as an efficient tool for studying and revealing the ex istence domains of bistability and multistability in a multimode VCSEL. This approach was used here for investigations of the impact of OF on multistability and searching for ’hidden’ states.

In this study, two sinusoidal signals with frequencies f_L = 5 kHz and f_H = 100 kHz and amplitudes A_L and A_H, were added to the laser pumping current, respec tively. We studied the laser response R_L at the fre quency f_L with a fixed amplitude A_L = 0.025 mV de pending on the amplitude A_H in a wide range of the pump current. The response amplitude R_L was esti mated as the height of a peak in spectra of the Fourier transformed time series of the laser intensity at the fre quency f_L with and without polarization selection. The measurements were carried out at the same experimen tal conditions as in the section above.

In Fig. 6 it is shown the response amplitude R_L de pending on the the amplitude A_H for three fixed val ues of j_{dc} in the zone of multistability for the case of polarization-resolved measurements. It is seen an ap pearance of nonlinear resonances in the response am plitude R_L as amplitude A_H increases. Such a behav ior is a manifestation of the phenomenon of vibrational resonances in multistable systems [Chizhevsky, 2004]. These resonances indicate on the number of coexist

5(a)

0

R p (arb.uits)(b) R p

(arb.uits)(b) R p

(arb.uits)(b) R p

(arb.uits)(b)

10
10
10
10

5
5
5
5

0
0
0

H (V) A

H (V) A

0.4 0.3 0.2 0.1 0

0.4 0.3 0.2 0.1 0

20 40 60

(a)

13 14 15 16 17 j_{dc} (mA)

20 40 60 80 (c)

13 14 15 16 17 j_{dc} (mA)

20 40 60 80 100 (b)

13 14 15 16 17 j_{dc} (mA)

10 20 30 40 (d)

13 14 15 16 17 j_{dc} (mA)

0
20 20 20 20

10 10 10 10

0
0
0
0

(c)
(c)

(c)
(c)

0 0.1 0.2 0.3 0.4 0 0.1 0.2 0.3 0.4

0 0.1 0.2 0.3 0.4

0 0.1 0.2 0.3 0.4 A_H (V)

A_H (V)

A_H (V)

A_H (V)

Figure 7. Contour plots for the polarization-resolved laser response amplitudes R_L as a function of dc current j_{dc} and the modulation amplitude A_H, shown for different values of the OF strength. (a) Without OF, (b) R=0.2, (c) R=0.5, (d) R=0.99.

Figure 6. Low-frequency response amplitude R_L as a function of the amplitude of the control signal A_H shown for different values of the injection current j_{dc} = 14.67, 15.33, 16.11 mA in the absent of optical feedback.

ing states. For fixed value of A_L as the amplitude A_H reaches some critical value for the switching thresh old two neighboring coexisting states are involved into the periodical switching dynamics giving rise to one nonlinear resonance at the frequency f_L. Further in crease A_H results in the appearance of the next nonlin ear resonance and so on. Such a picture is seen in the Fig.?? where two [Fig.6(a)], four [Fig.6(b)] and three [Fig.6(c)] nonlinear resonances appear, which corre spond to a coexistence of thee, five and four polariza tion states, respectively. In a general case, the number of coexisting states is larger by one than the number of nonlinear resonances. However, the number of reso nances, observed in the experiment, may depend on the initial conditions [Chizhevsky, 2004]. Therefore, this method gives a lower bound on the number of coexist ing states.

In Fig. 7 we present the results of the systematic study of "hidden" states by the method of vibrational reso nance for polarization- resolved measurements. In par ticular, the contour plot in Fig. 7(a) corresponds to measurements without optical feedback. Every dark straight line in the contour plot is a branch of the non linear resonance. One can see the presence of two closely spaced resonant branches of vibrational reso nance in the range of pump currents from ≈13 to ≈17 mA. This corresponds to two bistability zones. In the region of pump currents near 14 mA, the coexistence of two resonant branches is observed, which means the presence of tri-stability. With OF, this pattern of dis tribution of resonances changes significantly as seen in Figs. 7(b) and 7 (c). At moderate level of the OF (R = 0.5) [Fig. 7(b)], both resonant branches shift towards smaller values of pump currents with increasing dis tance between them, while the tri-stability almost dis appears. With strong feedback (R = 0.99) [Fig.

7(d)], one resonant branch disappears and only one branch remains, which corresponds to bistability. It should be noted that the shift of resonance curves is quite large, more than two milliamperes in the direction of smaller values. These results are in agreement with the results of the study of the hysteretic behavior shown above. However, in this case, the VR method provides a more complete and detailed picture of the current ranges for which bistability and multistability can be observed. Analogous measurements were performed without po larization resolution. In this case we observed similar regularities but these effects were less pronounced.

55

6 Conclusion

To conclude, we have experimentally shown that isotropic optical feedback in multimode VCSELs can lead to the suppression of multistability which was observed both in the polarization-resolved measure ments and without ploarization selection. The nonlin ear VR method revealed the presence of hidden bista bility, which does not manifest itself explicitly in the hysteresis behavior of the lasing intensity.

Acknowledgements

The authors thank BRFFI for the financial support of the project F18KI-019.

References

Ackemann, T., Sondermann, M., Naumenko, A., and Loiko, N. A. (2003) *Polarization dynamics and low-frequency fluctuations in vertical-cavity surface emitting lasers subjected to optical feedback*, Appl. Phys. B 77, pp. 739-746.

Valle, A., Lin, H., Lapin, Z. J., and Malla, B. (2008) *Analysis of the polarization dynamics in a multitransverse-mode vertical-cavity surface emitting laser with isotropic optical feedback* Phys. Rev. A 78, 033828.

Romanelli, M., Hermier, J.-P., Giacobino, E., and Bra mati, A. (2005) *Demonstration of single mode opera tion of a vertical-cavity surface-emitting laser with optical feedback: the intensity-noise-measurement approach* J. Opt. Soc. Am. B 22, pp.2596-2600.

Lin, H., HoShue, J., Lapin, Z.-J., and Valle, A. (2010) *Polarization instabilities in a multi-transversemode vertical-cavity surface-emitting laser with polar ized optical feedback* Optics Communications 283, pp.1424-1433.

Chembo, Y. K., Mandre, A. K., Fischer, I., Elsasser, W., and Colet, P. (2009) *Controlling the emission properties of multimode vertical-cavity surfaceemit ting lasers via polarization- and frequency-selective feedback* Phys. Rev. A 79, 013817.

Panajotov, K., Sciamanna, M., Arteaga, M. A. and Thienpont, H. (2013)*Optical feedback in vertical cavity surface-emitting lasers* IEEE J. of Selected Topics in Quant. Electron. 19, 1700312.

Hong,Y., Ju, R., Spencer, P. S., and Shore,K. A. (2005) *Investigation of polarization bistability in vertical cavity surface-emitting lasers subjected to optical feedback*IEEE J. of Quant. Electron. 41, pp.619-624.

Hong,Y., Ju, R., Spencer, P. S., and Shore,K. A. *up pression of polarization switching in vertical-cavity surface-emitting lasers by use of optical feedback* Opt. Lett. 29 pp.2151-2153.

Sciamanna, M., Panajotov, K., Thienpont, H., Vereten nicoff, I., Megret, P. and Blondel, M. (2003) *Opti cal feedback induces polarization mode hopping in vertical-cavity surface-emitting lasers* Opt. Lett. 28 pp.15431545

J. Houlihan, L. Lewis, and G. Huyet, (2004) *Feedback induced polarisation switching in vertical cavity sur face emitting lasers* Opt. Commun. 232, pp.391–397. Lin, H., Lin, H., Lapin, Z. J., Malla, B., and Valle A. (2008) *Polarization dynamics in a multi-transverse mode vertical-cavity surface-emitting laser subject to optical feedback* Phys. Rev. A 77, 033813.

Lin, H., Khurram, A., Black-Ingersoll, M. D. and Valle, A. (2015) *Polarization and modal dynamics of mul timode vertical-cavity surface-emitting lasers sub ject to optical feedback and current modulation* Opt. Commun. 350, pp. 178-188.

Pisarchik, A. N. and Feudel, U. (2014). Control of mul tistability, Phys. Rep. 540, pp.167-218.

Barbay, S., Giacomelli, G., Lepri, S., Marin, F., Rab biosi, I., and Zavatta, A. (2003). *Experimental in vestigation of stochastic processes in vertical-cavity lasers, Physica A: Statistical Mechanics and its Ap plications* 327, pp. 120-123.).

Chizhevsky, V. N. (2014) *Experimental evidence of vibrational resonance in a multistable system* Phys. Rev. E 89, 062914.

Genevet, P., Barland, S., Giudici, M., and Tredicce, J.R. (2011) *Cavity soliton laser based on coupled micro-resonators* in Localized States in Physics: Solitons and Patterns, edited by O. Descalzi, M. Clerc, S. Residori, and G. Assanto (Springer Berlin Heidelberg, Berlin, Heidelberg, pp. 169186.

Barbay, S., Kuszelewicz, R., and Tredicce, J. R. (2011). *Cavity solitons in VCSEL devices* Advances in Opti cal Technologies, Article ID 628761.

Soriano, M. C., Yousefi, M., Danckaert, J., Barland, S., Romanelli, M., Giacomelli, G., and Marin, F. (2004) *Low-frequency fluctuations in vertical-cavity surface-emitting lasers with polarization selective feedback: experimentand theory* IEEE J. of Selected Topics in Quant. Electron. 10, pp.9981005.

PHYSCON 2019, Innopolis, Russia, 8–11 September, 2019

MODE HOPPING IN A PULSE-COUPLED OSCILLATOR WITH DELAYED FEEDBACK

Otti D'Huys
Department of Mathematics
Aston University
Birmingham, United Kingdom
o.dhuys@aston.ac.uk

Vladimir V. Klinshov
Nonlinear Dynamics Research Group
Institute of Applied Physics
Nizhny Novgorod, Russia
klinshov@gmail.com

Abstract

Most interacting elements, including neurons, exhibit

We consider a spiking phase oscillator with delayed feedback and internal noise. As in any typical oscillator system with delayed feedback, multiple stable periodic orbits coexist. When taking noise in the oscillator into account, one observes mode hopping between these co existing orbits. Here, we analyse the characteristics of mode hopping. We find that, in the limit of weak cou pling, the results are well approximated by those of a continuously coupled system. However, with increas ing coupling strength, the noise breaks the symmetry and induces a shift towards faster cycles in the distribu tion of of interspike intervals, and a longer lifetime for solutions with a shorter interspike interval. Moreover, while for weak coupling the average lifetime scales ex ponentially with the coupling strength, it saturates and decreases for strong coupling.

Key words
delay, pulse-coupled oscillators, mode hopping, stochastic delay

1 Introduction

Pulse coupled phase oscillators are a popular model for coupled spiking neurons and other biological oscil lators such as cardiac, respiratory or circadian rhythms [1; 2; 3; 4]. Beyond biology, they have been used to model, between others, wireless networks [5] and opti cal systems [6]. Rather than being coupled at all times, such oscillators transmit pulses or spikes. Defining the phase based on the spike timings, the oscillators emit a pulse at the moment that they complete an oscillatory cycle. As an oscillator receives a spike, its phase is shifted by an amount that depends on the timing of the spike. This change in phase of the oscillator is called the phase-response curve (PRC) [7]. PRCs are popular among experimentalists as they provide a straightfor ward way to quantify the behavior of the system. More over, they can be built experimentally in an electronic setup.

a coupling delay, accounting for the travelling time of a signal. A typical effect of such a coupling delay in oscillatory systems is to induce multiple periodic states with a different period [8; 9]. Here, we study the ef fect of noise, which is present in any real life system, on such pulse-coupled oscillator networks with delay. As in any multistable system, noise can be expected to induce switching between the coexistent stable states [10]. These switching characteristics due to stochastic perturbations determine the effective dynamics and the memory storage capacities. In the present work, we in vestigate the mode hopping dynamics in the simplest pulse coupled system: a phase oscillator with delayed feedback.

2 Stochastic switching between coexistent states

We consider a single pulse-coupled oscillator with de lay, modelled as

$$\dot{\varphi}(t) = 1 + \sum_s Z(\varphi(t))\delta(t - t_s - \tau) + \sigma\xi(t), \quad (1)$$

where $\xi(t)$ is standard white gaussian noise, and σ is the noise strength. The coupling is characterised by the phase response curve $Z(\varphi)$, the coupling strength and the coupling delay τ. When $\varphi(t) = 1$, the oscillator emits a spike and the phase is reset to zero; the time that these spikes are emitted are denoted t_s.

Without noise, the system has multiple coexisting sta ble solutions with a constant interspike intervals (ISI) T_C, characterised by

$$\psi^*_C = \tau - CT_C \quad (2)$$

$$T_C = 1 - Z(\psi^*_C). \quad (3)$$

The integer number $C \in \mathbb{N}$ is the number of interspike intervals within a time delay interval, and we refer to it

as the 'capacity' of the solution. The phase ψ^*_C is the phase of the oscillator when the spike is received within this solution. Solutions are stable if $1/C < Z(\psi^*_C) < -1$ [11].

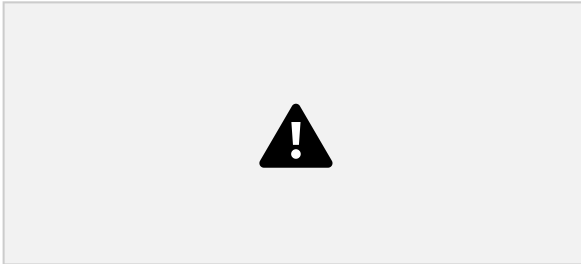

Figure 1. Panel (a): distribution of ISIs for a single pulse-coupled oscillator with delayed feedback and noise, described by Eqs. (1) and (4). The full red lines indicate the minimal and maximal ISI of the deterministic solutions, the dashdotted line indicates the central solution with $T = 1$. For our parameter choice, there are 20 co existing stable states. Panel (b): same distribution of the ISIs, after applying a moving average filter with a width of 63. The different peaks correspond to the ISIs of coexisting stable periodic states, in dicated by dashdotted lines. Panel (c): time trace of the consecutive ISIs after applying a moving average filter. The mode hopping is clearly visible. The dashdotted lines are the ISI of the stable periodic states. Parameters are $= 0.3$, $\sigma = 0.07$ and $\tau = 62.5$.

Adding noise leads to the smearing of the inter-spike intervals. In Figure 1 we illustrate the dynamics of the system Eq. (1), with a phase response curve given by

$$Z(\varphi) = \frac{1}{2}\sin(2\pi\varphi) \quad (4)$$

and the noise strength $\sigma = 0.07$. We observe a distribu tion of ISIs that spans the whole range of solutions, as indicated in Fig. 1(a). However, when applying a mov ing average filter, with a width broadly corresponding to the delay time (Fig 1.(b)) the distribution narrows and we observe a clear structure of 4 peaks, centred around the solutions with different capacity (indicated by red dashdotted lines) .Looking at the series of the

Renaming the variable $x(t) = \varphi(t) - \varphi(t - \tau)$ and making the assumption $\dot{\varphi}(t - \tau) = \frac{x}{\tau} + \sigma\xi(t - \tau)$, the system (5) can written as

$$\dot{x}(t) = -\frac{dV(x)}{dx} + \sqrt{2}\sigma(\tilde{\xi}(t)),$$

with $V(x) = \frac{1}{2\tau}(x - \tau)^2 - Z(x)dx$ and $\tilde{\xi}(t) = 1/\sqrt{2}(\xi(t) - \xi(t - \tau))$ standard white gaussian noise (in a good approximation) [13].

The equilibrium distribution of x can easily be derived as

$$f(x) \propto e^{-\frac{V(x)}{\sigma^2}}, \quad (6)$$

which results in a distribution with a gaussian envelope $f(x) \propto e^{-(x-\tau)^2}$ $2\tau\sigma^2$. The coupling function $Z(x)dx$ determines the location of the maxima, while the cou pling strength determines how pronounced these peaks are. The average lifetimes are approximated by the Kramers rate [10]. Consequently, the number of peaks (i.e. attended periodic solutions) scales with $\sigma\sqrt{\tau}$ and does not depend on the coupling strength . On the other hand, the average lifetime depends mainly on the difference between minima and maxima of the potential, and thus scales approximately exponentially with $/\sigma^2$.

We compare the frequency distributions and lifetimes in the continuous coupling theoretical approximation to the phase oscillator with pulse coupling. We consider the phase response function Eq. (4). The weak cou pling potential is then given by

$$V(x) = \frac{1}{2\tau}(x-\tau)^2 + \frac{}{4\pi}\cos(2\pi x).$$

In the limit of long delays, the different stable states are located at $x = k \in \mathbb{Z} + \frac{1}{2}$, with the most stable state closest to $x = \tau$.

In the long delay limit, the lifetimes can be approx $e^{2\pi\sigma 2 + 1}$

4 Numerical results

smoothed consecutive ISI's in Fig. These 1(c) we observe clear jumps from one stable solution to another.

imated as $T \approx \sqrt{\frac{\pi}{8\tau\sigma^2}}\,\pi^{22}-1/\tau^2$ 2τ), and hence $\cosh(\frac{x}{C-\tau}$

jumps roughly coincide with a change of the capacity C, i.e. the events when the number of pulses stored in the delay line increases or decreases by one.

3 Analytic theory for weak coupling

Assuming weak noise and weak coupling, the system (1) can be approximated by the continuously coupled system [12]

$$\dot{\varphi}(t) = 1 + Z(\varphi(t) - \varphi(t-\tau)) + \sigma\xi(t), \quad (5)$$

scale approximately exponentially with $\sigma 2$. The variable $x(t) = \varphi(t) - \varphi(t-\tau)$ in the weak cou pling approximation equals $\psi^* + C$ at the moment of the arrival of the spike, in the pulse-coupled system. As shown in Fig. 2(a), for weak coupling (= 0.05) un surprisingly the weak coupling theory provides a good approximation. As the coupling increases, this approx imation becomes worse, as the distribution shifts to wards solutions with shorter ISI and higher frequency. For strong coupling (= 0.3), as is illustrated in Fig. 2(b), the distribution becomes wider, and the mean is shifted towards solutions with higher capacity.

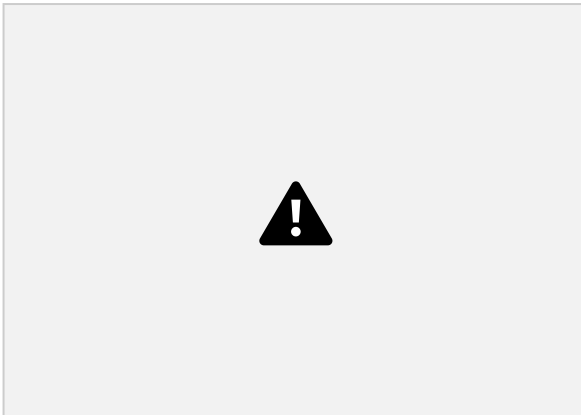

Figure 2. Distribution of $\psi^* + C$ (grey), together with their weak coupling theoretical approximations (full red line). Parameters are $\sigma = 0.07$, $\tau = 62.5$, $= 0.05$ (a) and $= 0.3$ (b).

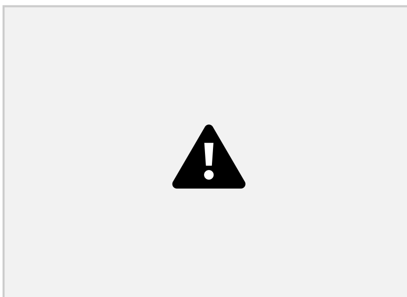

Figure 3. Average lifetime of the solution with stable ISI $T_C = 1$ for increasing coupling strength (blue diamonds connected by a full black line). The red dot-dashed line is the weak coupling theoretical approximation. Parameters are $\sigma = 0.07$ and $\tau = 62.5$

We find a similar behaviour for the lifetimes. As shown in Fig. 3, the analytical weak coupling theory, which predicts an exponential scaling of the average lifetime with the coupling strength is indeed valid for weak coupling. However, in contrast to continuously coupled phase oscillators, we find that for pulsed cou pling, the lifetimes saturate and eventually decrease.

These two trends, the shift towards smaller ISIs and the saturation and decrease of the lifetime with high coupling strength, are general for pulse-coupled oscil lators. However, the magnitude of the shift towards so lutions with smaller ISIs, and the coupling strength for which the central solution is maximally stable, do de pend on the shape of the PRC.

5 Conclusion

We have studied the stochastic switching behaviour between solutions with different interspike intervals in a pulse-coupled phase oscillator with delayed feed back. While in the limit of weak coupling, the approx imation with a continuously coupled phase oscillator is good, this approximation deteriorates as the coupling becomes stronger: the ISI distribution shifts towards solutions with higher capacities (i.e. shorter interspike intervals). The average lifetimes scale exponentially with the coupling strength for small coupling, but sat urate and decrease as the coupling increases further. This feature suggests the existence of the optimal in termediate coupling strength corresponding to maximal resilience with respect to noise.

Acknowledgements

This project is jointly funded by The Royal Society and The Russian Foundation for Basic Research (grant agreements IEC\R2\181113 for O.D. and RFBR grant 19-52-10004 for V.K.) O.D. also acknowledges fund ing from the European Union's Horizon 2020 re search and innovation programme under the Marie Sklodowska-Curie grant agreement No 713694.

References

Winfree A.T.: The geometry of biological time. Springer (2001)

Yuste R., MacLean J.N., Smith J., Lansner A.: The cor tex as a central pattern generator, Nat Rev Neurosci 6, pp. 477–483 (2005)

Peskin C.S.: Mathematical Aspects of Heart Physiol ogy New York: Courant Institute of Mathematical Sciences, New York University (1975)

Lewis J. E., Glass L., Bachoo M. and Polosa C.: Phase resetting and fixed-delay stimulation of a sim ple model of respiratory rhythm generation. Journal of Theoretical Biology, 159(4), pp. 491 – 506 (1992)

Pagliari, R., and Scaglione, A. (2010). Scalable net work synchronization with pulse-coupled oscillators. IEEE Transactions on Mobile Computing, 10(3), 392-405.

Colet P. and Roy R.: Digital communication with synchronized chaotic lasers. Opt. Lett., 19(24), pp. 2056–2058 (1994)

Canavier C.C., Achuthan S.: Pulse coupled oscilla tors and the phase resetting curve. Mathematical bio sciences, 226(2), pp. 77–96 (2010)

Yanchuk S.,Perlikowski P.: Delay and periodicity. Phys. Rev. E, 79(4) 046221 (2009)

Foss J., Milton J.: Multistability in recurrent neural loops arising from delay, J Neurophysiol 84, pp. 975– 985 (2000)

Kramers, H. A. (1940). Brownian motion in a field of force and the diffusion model of chemical reactions. Physica, 7(4), 284-304.

Klinshov V., Lucken L., Shchapin D., Nekorkin V., ¨ Yanchuk S.: Multistable jittering in oscillators with pulsatile delayed feedback. Phys. Rev. Lett., 114 178103 (2015)

Goel P. and Ermentrout B., Synchrony, stability, and firing patterns in pulse-coupled oscillators. Physica D 163 191–216 (2002)

D'Huys, O., Jungling T. and Kinzel W.: Stochastic ¨ switching in networks of delay-coupled oscillators. Phys. Rev. E 90, 032918 (2014)

PHYSCON 2019, Innopolis, Russia, 8–11 September, 2019

ARDUINO-BASED INVESTIGATION OF HYSTERESIS IN POLYMER FLEX SENSOR

Maxim Demenkov
Institute of Control Sciences
Russian Federation
max.demenkov@gmail.com

Abstract

We consider flex (or bending) polymer-based soft sen

sor that measures its own bending in terms of electrical resistance. When it is used for precise positioning as a part of fast control feedback, e.g. in soft robotic ma nipulators, sensor measurements show hysteresis-like rate-dependent behaviour typical for viscoelastic mate rials. We have constructed a simple electromechanical device for its investigation.

Key words
Soft robotics, nonlinear dynamics, hysteresis.

1 Introduction

Various devices using resistive flex sensors [Saggio et al., 2016] have been made available in different ar eas such as biometric measurements for medical pur poses or interfacing virtual reality. Nevertheless, these are slow-motion, imprecise applications. The advance ments in soft robotics [Elgeneidy, Lohse and Jackson, 2018; Zhang et al., 2017], where such sensors could be printed directly on a robot body or used in other ca pacity as a part of control feedback, poses a serious question about reliability of their readings. Since the sensors are made of polymers, it is natural to assume that the well-known viscoelastic behaviour of polymers (see e.g. [Wineman and Rajagopal, 2000; Banks, 2008; Bles, Nowacki and Tourabi, 2009]), including rate dependent hysteresis, can affect the sensor readings.

Nonlinear rate-dependent hysteresis was not exten sively studied from the mathematical viewpoint, and so far only a few publications (see e.g. [Anderssen, Gotz ̈ and Hoffmann, 1998]) are available on the subject. Well-known classical models of hysteresis, such as the Prandtl-Ishlinskii and Krasnoselskii-Pokrovskii model, do not incorporate rate dependence [Krasnosel'skii and Pokrovskii,1989; Visintin, 1994]. Even the application of the term "hysteresis" in a rate-dependent setting is questionable for some researchers in mathematics. It is therefore important to create a simple and cheap device

E_0 E_1

η

Figure 1. Linear viscoelastic model.

to analyse such behaviour in a typical university envi ronment without complex laboratory setup, to facilitate the development of its mathematical models.

The viscoelastic materials have a relationship between stress and strain that depends on time or frequency. In engineering, linear viscoelastic material models can be represented by an arbitrary composition of linear springs and dampers (see Fig.1). The simplest model for solids that is able to show all phenomena related to viscoelasticity is the following three-parameter model (also called the standard linear solid or the Zener model, see e.g. [Wineman and Rajagopal, 2000]):

$$\sigma + \frac{\eta}{E_1}\dot{\sigma} = E_0\varepsilon + \eta\frac{E_0 + E_1}{E_1}\dot{\varepsilon},$$

where σ is stress, ε is strain, η is viscosity, E_0 and E_1 are Young's modulus and the parameters of the relax ation function:

$$E(t) = E_0 + E_1 \exp(-t/\tau_R),\ t > 0,$$

and $\tau_R = \eta/E_1$ denotes the relaxation time. In the nonlinear case, no "standard" model is available.

2 Experimental results

In our experimental device, a small oval-shaped plas tic arm is attached to an Arduino-controlled servomotor

and is kinematically linked with the Flex Sensor®4.5" available from Spectra Symbol, which is connected to the same Arduino module as the servomotor. Arduino is a popular robotics hobbyist platform, which can be also used for data aquisition in experiments. One side of the sensor is printed with a polymer ink that has con ductive particles embedded in it. When the sensor is bent away from the ink, the conductive particles move further apart, increasing its resistance.

Flex sensor Mount

Servo motor

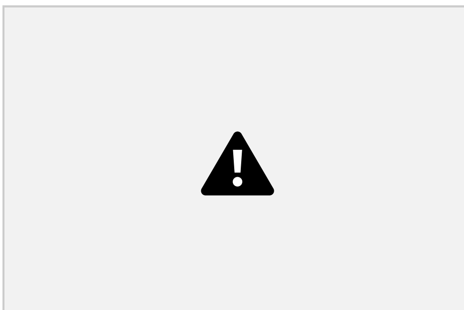

Figure 2. Scheme of our device and its actual implementation.

The positional servomotor SG90 can approximate a trajectory of its angular motion using a number of ref erence points. The delay before setting the next refer ence point is related to its angular speed (maximum is 500 deg/sec). Angular speed for the sensor tip is lin early related to the angular speed of the motor, which is 6 times higher.

This device (see Fig. 2) is a modification (simply the replacement of a fan with servomotor) of Flexy [Kaluz, ´ Cirka and Fikar,2018], initially created at the Slovak ˇ University of Technology in Bratislava for teaching students the basics of automatic control. Its electri cal schemes and blueprints for laser cutting are freely available [Kaluz, 2018]. ´

To test the hypothesis of sensor viscoelastic be haviour, we have conducted a number of experiments with different piecewise-linear angular inputs (Fig. 3). In each case, we vary the sensor tip angle from 5 to 20 degrees (measured by a protractor). We divide the whole angle interval into 40 reference points and then vary the delay before setting a new reference point for the servo. As a result, with decreasing of the delay we have obtained different curves for loading (angle increasing) and unloading (angle decreasing), see Fig. 3. In the fastest case depicted in Fig. 4, a possible error in sensor readings can be as large as 60–70%.

As one can see, under slow angular motion (blue in Fig. 3) the hysteresis curve (also blue in Fig. 4) can cross itself. It is also not a loop: probably due to the viscosity of the sensor, it never returns exactly to the same reading as started, but it can get there after some time if unloaded. It appears that the hysteresis curve is asymmetrical and its width increases with increasing of the angular speed.

20

15

10

5

0 0.5 1 1.5 2 2.5 3 3.5 4 Time, sec

Figure 3. Piecewise-linear angular input (blue color corresponds to the motor speed of 45 deg/sec, green – 90 deg/sec, magenta – 450 deg/sec).

630

620

610

600

590

580

570

5 10 15 20 Tip angle, grad

Figure 4. Sensor readings under piecewise-linear angular input (magenta color corresponds to the fastest motion with circles rep resenting the reference points).

3 Conclusion

We have developed a simple electromechanical device based on freely available design, which can be used for investigation of rate-dependent viscoelastic hysteresis. At the present time, the results are inconclusive: ac cording to some reviewers, the servomotor cannot be used for correct system identification due to the fact that it has no positional feedback. Our future goals is to improve our device to make it more precise and to derive a mathematical model of the sensor.

References

Saggio, G., Riillo, F., Sbernini, L., Quitadamo, L.R. (2016) Resistive flex sensors: a survey. *Smart Mater Struct*, 25, pp. 1–30.

Elgeneidy, K., Lohse, N., Jackson, M. (2018) Bending angle prediction and control of soft pneumatic actua tors with embedded flex sensors — a data-driven ap proach. *Mechatronics*, 50, pp. 234–247.

Zhang, J., Iyer, K., Simeonov, A., Yip, M.C. (2017) Modeling and inverse compensation of hysteresis in supercoiled polymer artificial muscles. *IEEE Robot. Autom. Lett.*, 2(2), pp. 773–780.

Wineman, A.S., Rajagopal, K.R. (2000)

Mechanical response of polymers. Cambridge University Press, Cambridge.
Banks, H.T. (2008) A brief review of some approaches to hysteresis in viscoelastic polymers. *Nonlinear Anal.*, 69(3), pp. 807–815.
Bles, G., Nowacki, W.K., Tourabi, A. (2009) Exper imental study of the cyclic visco-elasto-plastic be haviour of a polyamide fibre strap. *Int. J. Solids Struct.*, 46, pp. 2693–2705.
Anderssen, R.S., Gotz, I.G., Hoffmann, K.H. (1998) ¨ The global behavior of elastoplastic and viscoelastic materials with hysteresis-type state equations. *SIAM J. Appl. Math.*, 58(2), pp. 703–723.
Krasnosel'skii, M.A., Pokrovskii, A.V. (1989) *Systems with hysteresis*. Springer-Verlag, Berlin.
Visintin, A. (1994) *Differential models of hysteresis*. Springer-Verlag, Berlin.
Kaluz, M., ´ Cirka, L., Fikar, M. (2018) Flexy: an ˇ open-source device for control education. *Proc. 13th APCA International Conference on Control and Soft Computing (CONTROLO)*, Univesrity of the Azores, Ponta Delgada, Portugal, 4-6 June.
Kaluz, M. (2018) Flexy. ´ *https://www.uiam.sk/˜kaluz/ opensourceprojects/contents/flexy.html*. Accessed 6 Sept. 2018.

SEISMIC-ACOUSTIC SIGNAL GENERATION MODEL FROM FIBER OPTICAL MEASURING LINES FOR NEURAL-LIKE CLASSIFIER

Igor Denisov
Baltic Federal University
Russia
igordenisov@inbox.ru

Alexander Sonin
Baltic Federal University
Russia

Abstract

dale_15@mail.ru

indirectly carries the information about of

In this article the principles of signal generation model of seismic-acoustic tomography detection via fiber optical measuring lines are described. The neural-like classifier method of the solution of the tomography problem of the physical fields reconstruction is considered. As the tomography integrated data coming from the fiber-optical measuring lines stacked on fiber-optical measuring network of researched underground area were used. Principles of fiber optical real time information gathering and processing for wide perimeter security system are made.

Key words

signaling security system, fiber-optical measuring network, measuring line, informational measuring system, fiber-optical reconstructive tomography.

1 Introduction

At the present time the researches of natural and artificial physical, technical and technological objects and fields need application of the informational measuring systems. Data gathering in such systems is carried out with use of the distributed measuring networks. The most perspective type of measuring networks is fiber-optical measuring networks [Kulchin, 2001]. This fiber-optical measuring networks (FOMN) have a whole series of exclusive advantages. It is connected with widely known features of fiber-optical element base in comparison with devices on the basis of other element bases. It is the wide bandwidth of optical fiber, its insensitivity to electromagnetic noises and small weight, complexity of realization of the illegal access to optical information and other characteristics of fiber [Sterling, 1993]. FOMN represent the set of the distributed fiber-optical measuring lines (FOML). Such lines are stacked underground via the required scanning scheme on the researched areas. Sensitive areas detect the external physical influences on the measuring network. Physical influence on the area of FOMN results to change of light intensity on output of FOML proportionally to this influence. Optical radiation

characteristics of the technical objects and also structures of the researched natural and artificial physical fields distributed on some area [Denisov, Rybalchenko, Sedov, 2006].

With regard to security system such applications are extended objects and the perimeters of especially important objects [Kryukov, Denisov, Kiper, 2017]. In order to increase of the false alarm average time, as well as expanding of the information signs about the detection object, it is necessary to extract as much as possible all information from streaming data of the fiber-optic linear part. In the case of signaling security system based on FOML all frequency components come from here in addition to seismic signals, including acoustic signals.

2 Introductions

The signal on output of FOML $g\ (p, \varphi)$ represents linear integral from distribution function of the researched parameter of physical field $f\ (x, y)$. Here p, φ – the polar coordinates specifying position of rectilinear contours, i.e. p – distance from the coordinate origin up to straight line L, φ – the angle between p and abscissa axis.

Mathematically the problem of signals processing from FOMN come to reconstruction of initial function $f\ (x, y)$ on values $g\ (p, \varphi)$, i.e. to realization of return transformation of Radon [Helgason, 1983]: $f\ (x, y) = \mathbf{R}^{-1}\,[g\ (p, \varphi)]$. This problem is fiber-optical tomography problem [Denisov, Sonin, 2018].

Fiber-optical reconstructive tomography is not adequately explored problem for distributed researched fields when the number of information FOML is less than number of unknown parameters of the physical fields. Mathematically this implied that the number of the equations is less than number of unknown variables. The condition of uniqueness and stability (by Adamar) the solution of this problem did not satisfy [Tikhonov, Arsenin, 1977]. For the solution of the given incorrect problem is required of application of special methods of information processing (iterative or neural network) [Denisov, Kamenev, Kim, Kulchin, Panov, 2003].

In our case for extended objects and the perimeters most promising to apply neural-like classifier method of the solution of the tomography problem of the physical fields [Denisov, Kulchin, Panov, 2005]. However, for building of its structure requires the signal generation knowing. Depending on this, the internal structure of this classifier, data gathering and their interpretation will be built.

3 The informational-measuring system The fiber-optical information-measuring security system (fig. 1) consists of the fiber-optical seismic acoustic detection means and the seismic-acoustic data gathering and primary information processing system (SAIS). The sensitive fiber-optical underground sensor of seismic-acoustic detection tool is built on the basis of FOML. Set of such lines detects the external physical effect in the seismic and acoustic frequency range. The SAIS consists of typical photodetector, integrated with fiber-optical cable of FOML, as well as the ADC and the information post-processing system (IPS).

sound power. Four implementations of signals from moving intruder without voice and with voice are presented in Figures 2 and 3, respectively.

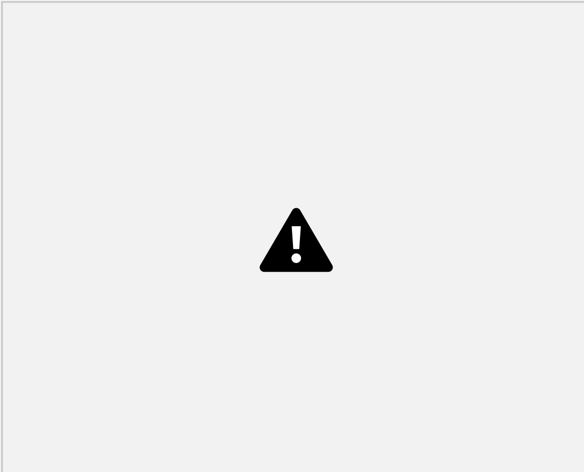

Figure 1. Block diagram of the fiber-optical information-measuring system.

On the way of development of seismic-acoustic security detecting systems of moving intruder the great importance have an effectiveness of legitimate signal extracting algorithm on the background numerous artificial and natural noise signals. The difficulty of implementing of effective classification algorithm is due to nonstationarity of seismic signals recorded under the same conditions. Therefore the optimization of such algorithm should be based on the results of analysis of the structure processed signals. By decomposing of the signals into components it can be find the features of this signals and can be signal separate into legitimate and noise signals.

4 Signal generation model

For information capability assessment of the acoustic signals in addition to seismic signals experiments were performed. Signals were received from single moving intruder. He is crossing with constant-speed transverse sensing zone based on underground FOMN. During recordings of realizations, the moving intruder passages without of voice and with voice. In the latter case the moving intruder pronounced the strictly defined sequence of words with the same

Figure 2. Seismic-acoustic signal from moving intruder without of voice.

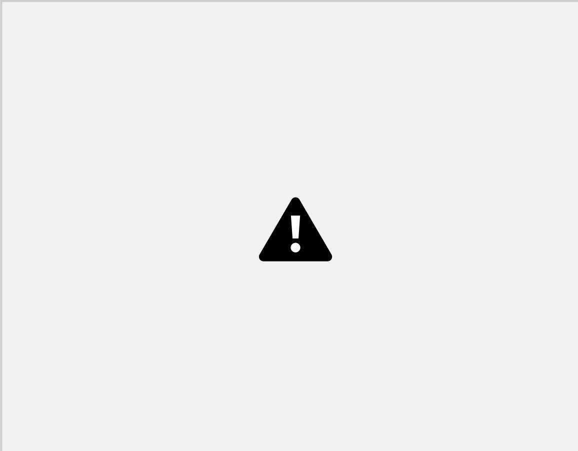

Figure 3. Seismic-acoustic signal from moving intruder with voice.

From figures 2 and 3 it can be seen that the received signals are completely different both from each other and from the type of impact: seismic (without of voice) and seismic acoustic (with voice). This difference is due to the nonstationarity of the shock ground excitation by walking, including the conversion of sound from air to ground, as well as the specifics of the distribution of elastic vibrations in the ground. The essential feature of both signals is their fading pseudoharmonic type. This process is most adequately described by function of elastic oscillations damping with time *t* and frequency *ω*:

(1)

where – attenuation coefficient, which depends on the ground properties; – initial oscillation amplitude, which depends on the signal formation model, i.e. on the parameters of disturbing influence by moving intruder to the ground.

To obtain of the expression of damped oscillations process from moving intruder to the ground it is necessary to consider of the generating signals process. Let the ground as horizontal layered elastic half-space, excited by pulsed shocks on its free surface by average force *F* :

(2)

where – weight of intruder, *kg*; – speed of moving intruder, *m/s*; – height at which the limb falls to the ground, *m*; – step angle or foot angle, *rad*.

Let that the ground layers performs the function of elastic oscillations waveguides [Glikman, 2005]. Let that each such waveguide will be excited by own resonance frequency and move the elastic oscillations energy to seismic-acoustic receiver. Using this signal generation model of seismic-acoustic tomography detection via FOML, you can get information about of ground structure and more complete picture of our signals [Denisov, Kulchin, Kirichenko, 2003].

Numerical simulation via experimental data set for one periodic harmonic damped oscillation gave:

(3)

where – the frequency of these oscillations, which depends on both the pulse duration , so the duration of its front . This expression is seismic-acoustic signal generation model. The differences between signals with and without voice will be concluded in the changing parameters . Moreover, for signals with voice, the values of all parameters are higher in magnitude.

5 Conclusion

Further information processing of such signals into IPS gives the characteristic features, by the space of which the recognition model is built. Moreover, the other feature is that the attribute space receives the additional information by adding of voice components in the signals from the FOMN. Thus, the information measuring security system developed on the basis of fiber-optical seismic-acoustic detection tool allows expanding the attribute space of detection objects. Further research consists in forming of neural-like classifier for solution of the fiber-optical tomography problem of the physical fields reconstruction.

References

Denisov, I.V., Kamenev, O.T., Kim, A.Yu., Kulchin, Yu.N., Panov, A.V. (2003). Neural data processing method for fiber-optic distributed measuring systems. Optical Memory & Neural Networks, vol. 12, no. 3, pp. 165-172.

Denisov, I., Kulchin, Y., Kirichenko O. et.al. (2003). Model of optoelectronic measuring intelligent system. Physics and Control: General problems and applications – PhusCon. Proc. of IEEE. – V. 1. – P. 172-175.

Denisov, I.V., Kulchin, Yu.N., Panov A.V. et.al. (2005). Neural network methods of reconstruction tomography problem solutions. Optical Memory & Neural Networks (Information Optics). Allerton Press, Inc. – Vol. 14. – No. 1, – P. 3-29.

Denisov, I.V., Rybalchenko, N.A., Sedov, V.A. Fiber optical phase sensitive surface. Laser Sensing, Imaging, and Information Technologies. Proc. SPIE. – V. 6162. – P. 127-136.

Denisov, I.V., Sonin, A.E. (2018). Staging fiber optical reconstructive tomography of extended physical fields. Radio Engineering. – № 2. – p. 49- 51.

Glikman, A.G. (2005). Spectral seismic prospecting - sources and consequences. – 247 p.

Helgason, S. (1983). Transformation of Radon, Mir Press, Moscow (in Russian).

Kryukov, I.N., Denisov, I.V., Kiper, A.V. (2017). Application of fiber-optic measuring networks for monitoring extended deformation fields when building geographically distributed security systems. Radio engineering. – № 1. – p. 5-11.

Kulchin, Yu.N. (2001). Distributed fiber-optical measuring systems, Science Press, Moscow (in Russian).

Sterling, Donald J. Jr. (1993) Technician's guide to fiber optics, Delmar Publishers Inc. (in Russian).

Tikhonov, A.V., Arsenin, V.Y. (1977). Solution of Ill posed Problems, Winston, Washington, DC.

PHYSCON 2019, Innopolis, Russia, 8–11 September, 2019

STRUCTURAL STABILITY OF CHIMERA STATES CLONING IN A LARGE NON-STATIONARY COUPLED TWO-LAYER MULTIPLEX NETWORK OF BISTABLE RELAXATION OSCILLATORS

Aleksei Dmitrichev
Nonlinear Dynamics Department
Institute of Applied Physics RAS
Russia
admitry@appl.sci-nnov.ru

Vladimir Nekorkin
Nonlinear Dynamics Department
Institute of Applied Physics RAS
Russia
vnekorkin@appl.sci-nnov.ru

Abstract

We continue to study the cloning of chimera states, which is a recently discovered effect caused by inter action between chimera states in a multiplex network. The effect is observed when two ensembles of locally and linearly coupled two-frequency (bistable) relax ation oscillators, for some time, are joined into the mul tiplex network. Then for certain values of strength and time of multiplex interaction, a clone of the chimera state is formed in the initially disordered ensemble. We show that under certain parameters of multiplex inter action, as in the case of small networks, the cloning of chimera states is also independent of the initial condi tions in large networks.

Key words

Dynamical systems, Multiplex networks, Bistable os cillators, Chimera states, Cloning

1 Introduction

One of the striking phenomena has been found in many nonequilibrium oscillatory systems is the forma tion of chimera states [Abrams and Strogatz, 2004], i.e., hybrid spatial-temporal regimes consisting of os cillators with coherent and incoherent behavior. For ex ample, such states exist in mechanical [Martens et al., 2013; Kapitaniak et al., 2014; Dudkowski et al., 2016; Wojewoda et al., 2016], optical [Hagerstrom et al., 2012; Larger et al., 2015], chemical [Smart, 2012; Tinsley et al., 2012; Wickramasinghe and Kiss, 2013; Schmidt et al., 2014; Wickramasinghe and Kiss, 2014], radiotechnical [Larger et al., 2013; Gambuzza et al., 2014; Hizanidis et al., 2016] and neural

2004; Abrams et al., 2008; Bordyugov et al., 2010;

[Mukhame tov et al., 1977; Lyamin et al., 2008] systems. To date significant progress has been achieved in studies of mechanisms and conditions of formation of chimera states [Nekorkin et al., 1999; Kuramoto and Battog tokh, 2002; Kuramoto, 2003; Abrams and Strogatz,

Martens, 2010; Omelchenko et al., 2011; Sethia et al., 2013; Yeldesbay et al., 2014; Zakharova et al., 2014; Laing, 2015; Loos et al., 2016; Sch¨oll, 2016; Semen ova et al., 2016; Maistrenko et al., 2017; Semenova et al., 2017; Shepelev et al., 2017]. For a long time the formation was attributed to a complex nonlocal or non linear character of couplings between oscillators and to a large size of systems. However, it was recently established theoretically and experimentally [Shchapin et al., 2017] that chimera states can exist in systems with local and even linear couplings containing from several to hundreds of thousands oscillators.

At present, great attention is paid to studying of inter action of chimera states [Andrzejak et al., 2017; Tian et al., 2017; Majhi et al., 2017; Kasatkin and Neko rkin, 2018; Hizanidis et al., 2016; Ujjwal et al., 2016; Maksimenko et al., 2016]. Note however that in all these works the interaction of chimera states led to the formation of new chimera states (in some cases with synchronous coherent parts) that are different from the pre-existing chimera state. Recently we presented an example [Dmitrichev et al., 2018; **?**] of a two-layer multiplex network which allows one to receive in one of its layers a clone of the chimera state existing ini tially in another layer. The cloned chimera has the same average frequency and amplitude distributions, as well as an identical phase distribution in coherent part as in the original one. We called this effect the chimera states cloning. We studied the effect in detail for the case of a small network and showed that it is observed for a par ticular initial condition in a network with large number of oscillators. Here we show that under certain param eters of multiplex interaction, the cloning of chimera states is also independent of the initial conditions in large networks.